INFORMATION TO USERS

This manuscript has been reproduced from the microfilm master. UMI films the text directly from the original or copy submitted. Thus, some thesis and dissertation copies are in typewriter face, while others may be from any type of computer printer.

The quality of this reproduction is dependent upon the quality of the copy submitted. Broken or indistinct print, colored or poor quality illustrations and photographs, print bleedthrough, substandard margins, and improper alignment can adversely affect reproduction.

In the unlikely event that the author did not send UMI a complete manuscript and there are missing pages, these will be noted. Also, if unauthorized copyright material had to be removed, a note will indicate the deletion.

Oversize materials (e.g., maps, drawings, charts) are reproduced by sectioning the original, beginning at the upper left-hand corner and continuing from left to right in equal sections with small overlaps.

Photographs included in the original manuscript have been reproduced xerographically in this copy. Higher quality 6" x 9" black and white photographic prints are available for any photographs or illustrations appearing in this copy for an additional charge. Contact UMI directly to order.

ProQuest Information and Learning
300 North Zeeb Road, Ann Arbor, MI 48106-1346 USA
800-521-0600

1985

Data Integration in 3-D Geostatistical Porosity Modeling of Hanifa Reservoir in Berri Field, Saudi Arabia

BY

Mohammad Ahmad Hasan Al-Khalifa

A Thesis Presented to the

DEANSHIP OF GRADUATE STUDIES

KING FAHD UNIVERSITY OF PETROLEUM & MINERALS

DHAHRAN, SAUDI ARABIA

In Partial Fulfillment of the

Requirements for the Degree of

MASTER OF SCIENCE

In

GEOLOGY

MAY 2001

KING FAHD UNIVERSITY OF PETROLEUM AND MINERALS
DHAHRAN, SAUDI ARABIA

DEANSHIP OF GRADUATE STUDIES

This thesis, written by **Mohammad Ahmad Al-Khalifa** under the direction of his Thesis advisor and approved by his Thesis committee, has been presented to and accepted by the Dean of Graduate Studies, in partial fulfillment of the requirements for the degree of **MASTER OF SCIENCE IN GEOLOGY**.

Thesis Committee

29/8/2001

Chairman (Dr. Gabor Korvin)

Co-Chairman (Dr. M. Makkawi)

Member (Dr. Badrul Imam)

Department Chairman

Dean of Graduate Studies

29/8/2001

Date

عمادة الدراسات العليا
DEANSHIP OF GRADUATE STUDIES

Dedication

I would like to dedicate my thesis to Kathem Ali Al-Khalifah for his moral encouragement during my master study and thesis work and to my wife and two daughters for their patience and support during my studies.

ACKNOWLEDGMENTS

Acknowledgments are due to the King Fahd University of Petroleum and Minerals for support of this research, and Saudi Aramco and the Ministry of Petroleum and Mineral Resources for permission to publish this thesis.

I would like to express my profound gratitude and appreciation to my thesis chairman, Dr. Gabor Korvin, for his guidance and for his critical review of the manuscript. Sincere thanks are also due to my thesis co-chairman, Dr. Mohammad Makkawi, for his excellent advice and comments during this time, and to my thesis committee member, Dr. Badrul Imam, for his contributions to this work.

Appreciation and thanks are due to Chairman Dr. Mustafa Al-Hariri and other faculty and colleagues of the Earth Sciences Department for their support during my association with them.

I would like to thank the management of Saudi Aramco for providing the facilities and data used in this study. Of these, I am especially grateful to Mr. Mahmoud Abdul-Baqi, Vice President of Exploration; Dr. AbulJaleel Al-Khalifa, Manager of Reservoir Characterization; Mr. Adnan Al-Sharif, Chief Geologist of the Northern Fields Characterization; Mr. Hesham Al-Qassab, Group Leader of Geological Modeling; and Mr. Adnan Al-Bagshi, Team Leader of the Qatif Team.

Finally, my sincere thanks are extended to my family and friends for their support and encouragement during this period of study.

TABLE OF CONTENTS

LIST OF TABLES

LIST OF FIGURES

THESIS ABSTRACT

Name: Mohammad Ahamad Hasan Al-Khalifa
Title: Data Integration in 3-D Geostatistical Porosity Modeling of Hanifa, Reservoir in Berri Field, Saudi Arabia
Major Field: Geology
Date: May 2001

Understanding the spatial distribution of reservoir properties such as lithology and porosity is essential for development drilling, reserve estimation and fluid flow simulation. Data come from various sources at various scales with varying degrees of reliability. Data from wells alone have limitations and they are not enough to produce an accurate view of the reservoir. Geostatistics provides a toolbox for geologists and engineers to use in analyzing data and transferring such analysis and interpretations to the task of reservoir modeling and forecasting.

The objective of this thesis is to evaluate the added value of integrating different data types such as facies and seismic impedance in 3-D geostatistical porosity models. To achieve this goal four porosity models were built. The first porosity model was generated based on porosity logs from wells only. The other three porosity models were generated by different combination of porosity logs, facies and seismic impedance. These models have been evaluated by using qualitative and quantitative methods.

The results of this study showed that facies-based porosity models yield better definition of porosity in vertical and lateral directions than other models. This is due to the use of the facies model as constraint for porosity distribution. The accuracy of the seismic controlled model was better than all other models. This is due to the fact that seismic has a more dense spatial samples density than wells. Porosity from the wells-only model has the lowest accuracy compared to the other models, which shows the importance of introducing other type of data in porosity modeling.

Master of Science Degree

King Fahd University of Petroleum and Minerals
Dhahran, Saudi Arabia

May 2001

ملخص الرسالة

الاسم : محمد احمد حسن الخليفة

العنوان : تكامل المعلومات في النماذج المسامية الثلاثية الأبعاد لمكمن الحنيفة في حقل البري،المملكة العربية السعودية

التخصص : علم طبقات الأرض

التّاريخ : مايو 2001

يعتبر فهم توزيع خصائص المكمن مثل نوعية الصخور ومساميتها أساسيةً لحفر الآبار و تَطوّر الحقول النفطية وتقدير احتياطي ومحاكة المكمن. البيانات تَجيء من مصادر متعدّدة وفي وحدات قياس مختلفة و بدرجات ثقة متفاوتة. البيانات من الآبار لوحدها ليست كافية لكي تنتج صورة دقيقة للمكمن. الجيولوجيا الإحصائية تساعد الجيولوجيين ومهندسي البترول في تَحليل بيانات مختلفة و دمجها ومن ثم استخدمها في إنتاج نماذج ثلاثية الأبعاد ذات دقة عالية.

هدف هذه الرسالة أن تقيم إضافة أنواع البيانات من مصادر مختلفة مثل الجيولوجية و الجيوفيزياية في إنتاج نماذج مسامية ثلاثية الأبعاد. لإنجاز هذا الهدف أربعة نماذج مسامية قد بنيت بطرق مختلفة. النموذج الأول قد بني معتمدا على معلومات من سجلات الآبار فقط. الثّلاثة نماذج الأخرى قد بنيت بمزج معلومات من سجلات الآبار و معلومات جيولوجية و جيوفيزياية. وقد تم تقيم هذه النّماذج باستعمال طرق نوعية وكمّية.

أظهرت هذه الدّراسة إن النماذج المسامية التي بنيت على معلومات جيولوجية أفضل في محاكاة المسامات في الجهات العمودية والجانبية من النّماذج الأخرى. بينما النماذج المسامية التي بنيت على معلومات جيوفيزياية كانت أفضل من كل النّماذج من حيث الدقة. هذه بسبب أن المعلومات الجيوفيزياية ذات كثافة عينات أكثر من سجلات الآبار. المعلومات من سجلات الآبار فقط أنتجت نماذج مسامية ذات دقة منخفضة بالمقارنة مع النّماذج الأخرى. هذا يوضح أهمية استعمال جميع البينات المتوفرة في إنتاج النماذج المسامية.

درجة الماجستير في العلوم
جامعة الملك فهد للبترول والمعادن
الظهران، العربية السعودية
مايو 2001

CHAPTER 1

INTRODUCTION

1.1 Geostatistics and Data Integration

Understanding the spatial distribution of reservoir properties like lithology and porosity is essential for development drilling, reserve estimation and fluid flow simulation. Data come from various sources at various scales with varying degrees of reliability. Data from wells alone have limitations and they are not enough to produce an accurate view of the reservoir. Geostatistics provides a toolbox for geologists and engineers to use in analyzing data and transferring such analysis and interpretations to the task of reservoir modeling and forecasting.

One of the most important challenges in reservoir modeling is data integration. Geostatistics offers tools for integrating data at different scales of different types and different reliability. For example, combining the high spatial continuity of the seismic data with the high vertical resolution of the well data to come up with better 3-D reservoir models (Wolf et al, 1994).

The first challenge for geostatistics in data integration was to come up with petrophysical models (e.g. porosity) that have a geological signature. This task is accomplished by honoring the distribution of petrophysical property within each facies at the modeling stage.

Seismic data are routinely and effectively used to delineate the structures of a reservoir. However, there has been limited application for using seismic data to help directly map reservoir properties such as porosity. This limitation is caused by the difference in scale of measurements for well data (e.g. core and log) and the seismic data. While the well data have a high vertical and a low horizontal resolution and are measured in depth, the seismic data have a high horizontal and low vertical resolution and they are measured in time.

Advances in geostatistics and seismic inversion have created new frontiers for 3-D seismic such as improving reservoir characterization by allowing the integration of seismic and well data. Seismic data have been successfully used to predict spatial variations in lithologies and porosity using geostatistical techniques. A proper integration of 3-D seismic data with core and log data greatly improves the spatial description of the reservoir (Al-Qassab et al, 2000; Xu et al, 1992).

1.2 Objectives

The objective of this Thesis is to evaluate the importance of integrating different data types in 3-D geostatistical porosity modeling. To achieve this, four porosity models will be built. The first model will be based on well data only and the other three will be different combinations of well porosity logs, facies and seismic data. Then these models will be evaluated to investigate the impact of data integration on reservoir characterization.

1.3 Dataset Description

A sector area from Hanifa Reservoir in the offshore Berri Field has been selected for this project, Figure 1.1. This area has 97 wells drilled in the Hanifa Reservoir and a recent 3-D seismic survey that had already been inverted to impedance. The wells are a mixture of vertical, deviated and horizontal. All have porosity logs and 22 wells have impedance log derived from sonic and density logs. The logs dates stem from the late 1960s to late 1990s. All wells have facies logs described by the Saudi Aramco geologists.

The acoustic impedance 3D model was generated by using stochastic inversion algorithms. This impedance model was converted to depth by converting the markers from time domain to depth domain.

1.4 Methodology

The first step will be studying the statistical distributions of porosity and facies. Then the distribution of porosity within different facies will be examined. Porosity-impedance and facies-impedance cross-plots will be constructed to establish a relationship

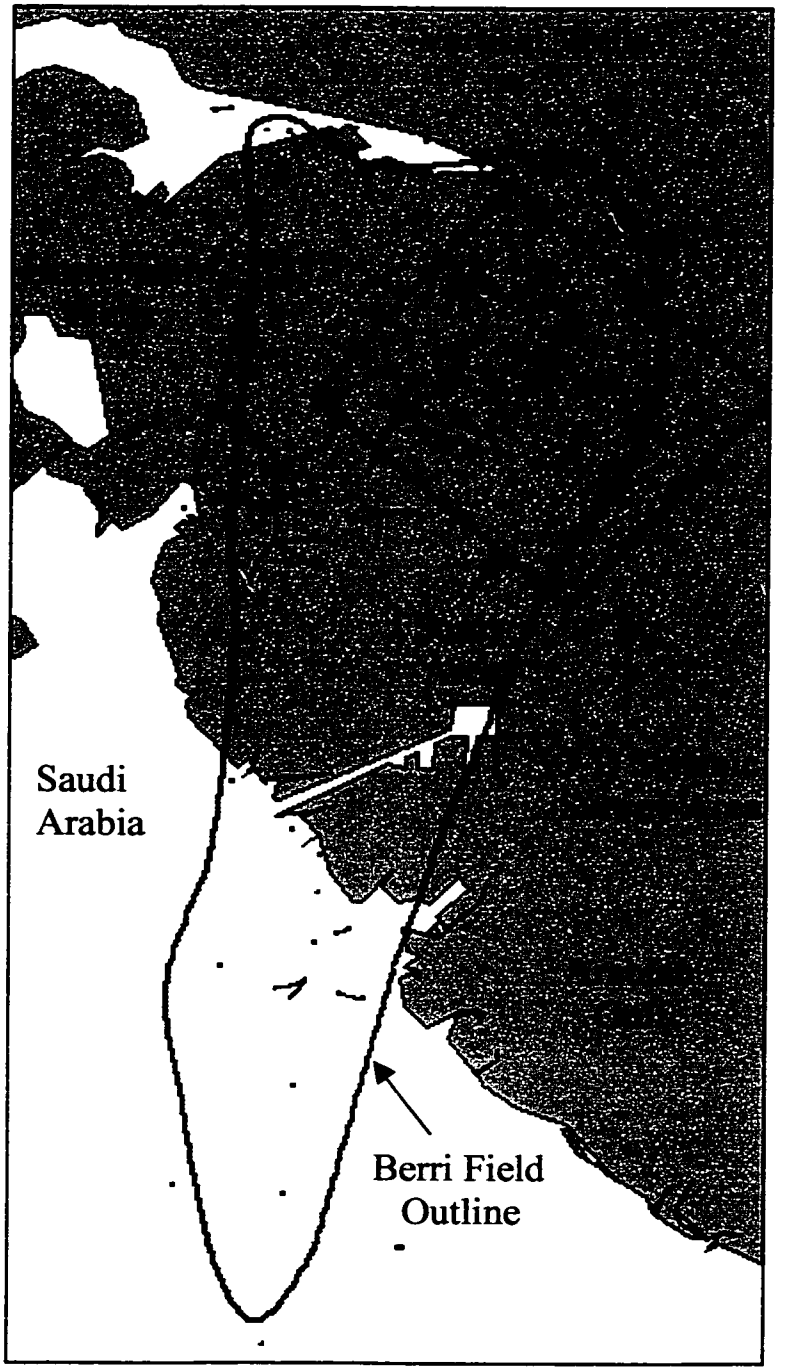

Figure 1.1: Location of the study area within the Berri Field

between well log porosity and well log impedance or between facies and impedance. This relationship, if existing, will be used in integrating the seismic impedance in the porosity and facies models

The second step will be calculating semi-variograms to quantify the spatial correlation of porosity and facies from well logs. Both omnidirectional and directional semi-variograms will be calculated to check the directionality of the data. These semi-variograms will also be used later on in the geostatistical modeling of porosity and facies.

The third step will be modeling porosity distribution in the reservoir. The first porosity model will be built based on wells using only Sequential Gaussian Simulation. The second porosity model will be built based on facies. Porosity histograms for each facies group will be created and used in the facies-based porosity model. This should help to constrain the porosity distribution within each facies. Sequential Gaussian simulation facies-based algorithm will be used in this step.

The third porosity model will be built by integrating the seismic impedance and porosity logs from wells and by utilizing the porosity and seismic impedance relationship. This should improve the accuracy of the generated porosity model by utilizing the high spatial sampling density of the seismic impedance. Sequential Guassian simulation with co-kriging algorithm will be used in this phase.

The final porosity model will be obtained by integrating the porosity from logs with facies and impedance from seismic. Sequential Gaussian simulation with collocated co-kriging algorithm will be used in this step. In all steps several realizations will be created for each model.

Model validation will be done by two methods, quantitative and qualitative. In the qualitative method, histograms of the simulate porosity values will be compared to that of the input porosity. Also, several porosity maps and cross sections will be constructed for each model and compared to observe the spatial and vertical porosity distribution. In the quantitative method simulated porosity traces will be compared to the true porosity traces for ten wells that have not been used in the models. The best model will be the one that gives the closest porosity estimation.

1.5 Facilities

Saudi Aramco will provide data, hardware and software to conduct this study. This work is carried out using unix based Silicon Graphics Octane workstation dual screen with 250 MHZ IP30 processor, memory size of 1536 Mbytes and hard disk size of 13 Gbytes.

Geostatistical modeling package from Reservoir Characterization Research and Consulting, Inc. (RC^2) will be used in this study. Four tools from that package will be used, which are ResPrep, ResGram, ResMod, ResCalc and ResScape.

ResPrep is used to prepare the well logs for subsequent statistical and modeling steps. ResGram is used to compute and model experimental semi-variograms. ResMod is the geostatistical-modeling program. It has large number of estimation and simulation algorithms to generate 3-D models. ResCalc program is used to do model operations and uncertainty assessment. ResScape is a 3-D visualization tool and enables the rotation of models.

CHAPTER 2

LITERATURE REVIEW

2.1 Porosity

2.1.1 Definition

Porosity is one of the essential attributes of an oil reservoir. Pore spaces within a rock are generally filled with connate water, but may contain oil or gas. Porosity is the pore volume per unit volume of formation and is expressed as percentage:

$$\text{Porosity } (\%) = \frac{\text{Volume of Voids}}{\text{Total Volume of rock}} \times 100$$

Measured porosity can be of two types, total and effective. Total porosity is defined as the ratio of the volume of all the pores to the bulk volume of a material, regardless of

whether or not all of the pores are interconnected. Effective porosity is defined as the ratio of the interconnected pore volume to the bulk volume of a material.

Porosities of subsurface formation can vary widely. Dense carbonates (limestones and dolomites) and evaporites (salt, anhydrite) may show practically zero porosity; well-consolidated sandstone mat have 10 to 15% porosity, unconsolidated sands my have 30% or more porosity. Shales or clays may contain more than 40% water-filled porosity, but the individual pores are usually so small that the rock is impervious to the flow of fluids.

Porosity is one of the important factors in defining commercial hydrocarbon reservoirs. Usually the more the porosity the more hydrocarbons one can have and vice versa. However, a carbonate oil reservoir with 20% intragranular porosity may not produce oil at the same rate as a 20% intergranular porosity reservoir, keeping all other reservoir properties the same. Classification and measuring carbonate porosity is an important and by no means easy task (Selley, 1985).

2.1.2 Carbonate Porosity Classification

The world of carbonate is much more complex. The simple primary intergranular porosity that characterizes sandstone reservoirs is rarely found in carbonates. Almost all carbonate pore systems have been altered by postdepositional processes that fall under the general term diagenesis. The degree of diagenetic alteration can vary from a modest loss of primary intergranular porosity by pore filling cement to a complete and pervasive reorganization of the pore network.

Carbonate porosity can be described as being of either primary or secondary origin, but the precise difference is not always clear. Primary porosity is the one that existed at

the time of deposition: for example the intergranular porosity of a clean oolitic grainstone. Some diagenetic process on the rock or sediment usually produces secondary porosity. (Selley, 1985)

In the real world of carbonate rocks, such a division is much too simple and often misleading. Rocks containing only primary porosity are very rare. Secondary porosity is more accurately described as rearrangement or reconstruction of the original pore networks rather than creation of new porosity. For example, the dolomitization of porous lime mud does not create porosity, but reorganizes it and helps to preserve the porosity that was already present. (Choquette and Pray, 1970)

The most useful classification of carbonate pore types is that published by Choquette and Pray (1970). They recognized two basic categories: fabric selective and not fabric selective (Figure 2.1). (Choquette and Pray, 1970)

Fabric Selective

Fabric selective elements of porosity are those that are related to the depositional fabric of the rock. The first four of the fabric selective pore types are the most important and constitute more than 90% of the fabric selective porosity in the subsurface. The most common types are Interparticle, Intraparticle, Intercrystalline and Moldic, figure 2.1. Most of the Hanifa Reservoir porosity is classified as interparticle. (Saudi Aramco, 1991)

Not Fabric Selective

Not fabric selective pore types are secondary in that new porosity is created and added to the rock. These types include fracture, vug, cavern channel. (Choquette and Pray, 1970)

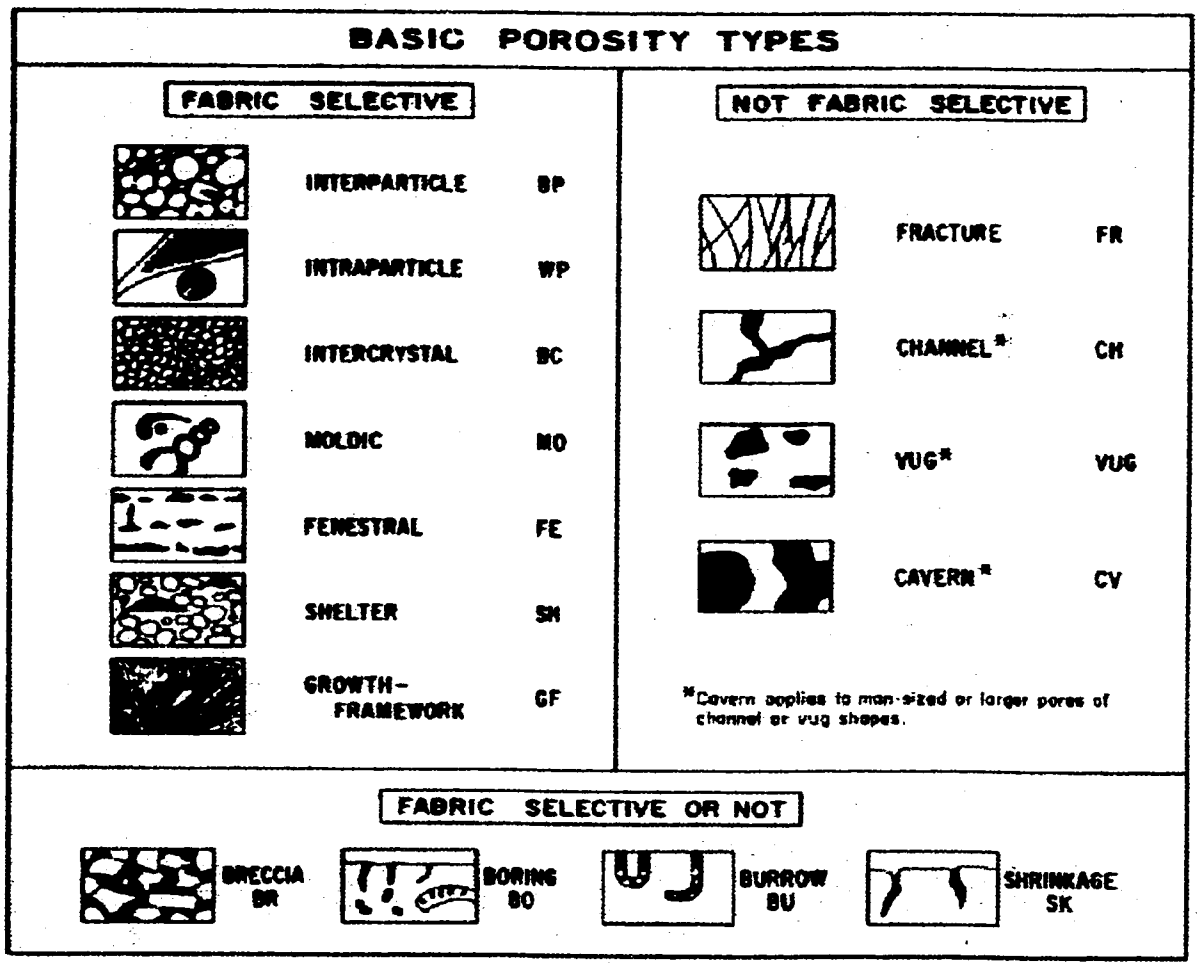

Figure 2.1: Geologic classifications of porosity in carbonate rocks. (From Choquette and Pray, 1970)

2.1.3 Methods of Measurement

Porosity is measured by two main methods: directly from cores or indirectly from geophysical well logs. Both methods will be described briefly with their advantages and disadvantages.

Porosity from Cores

A core is a cylindrical shape rock sample with a diameter between 2 ½ inches and 4 inches that is taken from the formation and brought to the surface by special drilling tools. Core information includes detailed lithology, macroscopic features and petrophysical properties of the reservoir rocks such as porosity and permeability. The porosity of a core sample is usually measured in the laboratory using several methods: the most common Boyle's law, summations of fluids and bulk volume determination. (Blackbourn, 1990 and Whittaker, 1985)

Porosity from cores has the advantage of being the only way to measure effective porosity and know the correct classification of such porosity. Although cores provide very important information, they are very expensive and only a few selected wells are cored. Even then, no 100% recovery of the formation cored is retrieved. Usually most porosity measurements are preformed at room temperature and pressure that are different from the reservoir temperature and pressure. These differences may introduce some error in the measurements. So, these reading are scaled by factor to compensate for such differences. (EPS, 1998)

In core samples, porosity is usually determined on 1-inch diameter plugs, however in special cases a full diameter core may be used. These plug measurements represent porosity value at a small volume, which may not represent the real porosity distribution.

In carbonate rocks, it is very difficult to estimate the fracture porosity from core plugs and even full core samples. Moreover, during a core cutting process, the rock fabric may change due to the drilling mud, drilling bit type and the experience of the driller (Whittaker, 1985).

Porosity from Geophysical Well Logs

Geophysical well logs are electrical tools that are lowered in the borehole and measurements are taken from the bottom to the top or at selected interval in the well. At present time, it has become a standard procedure to run well logs in every new well drilled. The logging operations are much cheaper than the cost of coring. Well logs can be used to obtain petrophysical reservoir properties such as porosity, water saturation and lithology identification (Western Atlas, 1992; Schlumberger, 1989).

Porosity can be obtained from different well logs such as sonic, density or neutron logs. Log measurements are done in the field at the reservoir temperature and pressure. All three logging techniques respond to the characteristics of the rock immediately adjacent to the borehole. The lateral depth of investigation for these tools is very shallow, only a few inches or less. The sampling rate is one sample every ½ foot. However, these log measurements are influenced by rock volumes that are larger than 1-inch core plugs. This increases the chance for finding real porosity distribution. (EPS, 1998)

Porosity logs have the advantage of being available at most wells. They, also, are considered to be more representative for porosity over core. However, they need correction for bottom hole conditions such as drilling mud and drilling hole size. Usually porosity logs respond to total porosity, unlike cores that give effective porosity. It is very

difficult, if not impossible, to classify porosity types based on logs response. (Schlumberger, 1989)

Logs cannot replace cores, nor can cores replace logs. Both data are needed for any field development. The current practice in the oil industry is to use porosity logs as the base for porosity modeling. This thesis will follow the current industry practices and use log porosity to generate porosity models by using different geostatistical techniques and integrating geological and geophysical data.

2.2 GEOLOGICAL REVIEW

2.2.1 Background

Hanifa Reservoir forms the upper part of Hanifa Formation. Among other formations, Hanifa Formation is part of the upper Jurassic section in Saudi Arabia (Figure 2.2). This Jurassic section is by far the largest hydrocarbon reservoirs in the history of the world oil industry. About 17% of the world's and 67% Saudi Arabia's oil are located in this section (Saudi Aramco, 1990). Most of the major oil wells in Saudi Arabia are producing form this section, Ghawar being the largest oil field in the world, and then Berri Field.

The Saudi Jurassic section has been divided into seven Formations, figure 2.2. They are from oldest too youngest: Marrat, Dhruma, Tuwaiq Mountain, Hanifa, Jubaila, Arab and Hith Formations. In each of these formations there is at least one oil reservoir. In Berri Field commercial oil reservoirs have been discovered in the Arab, Hanifa, Tuwaiq Mountain and Dhruma Formation.

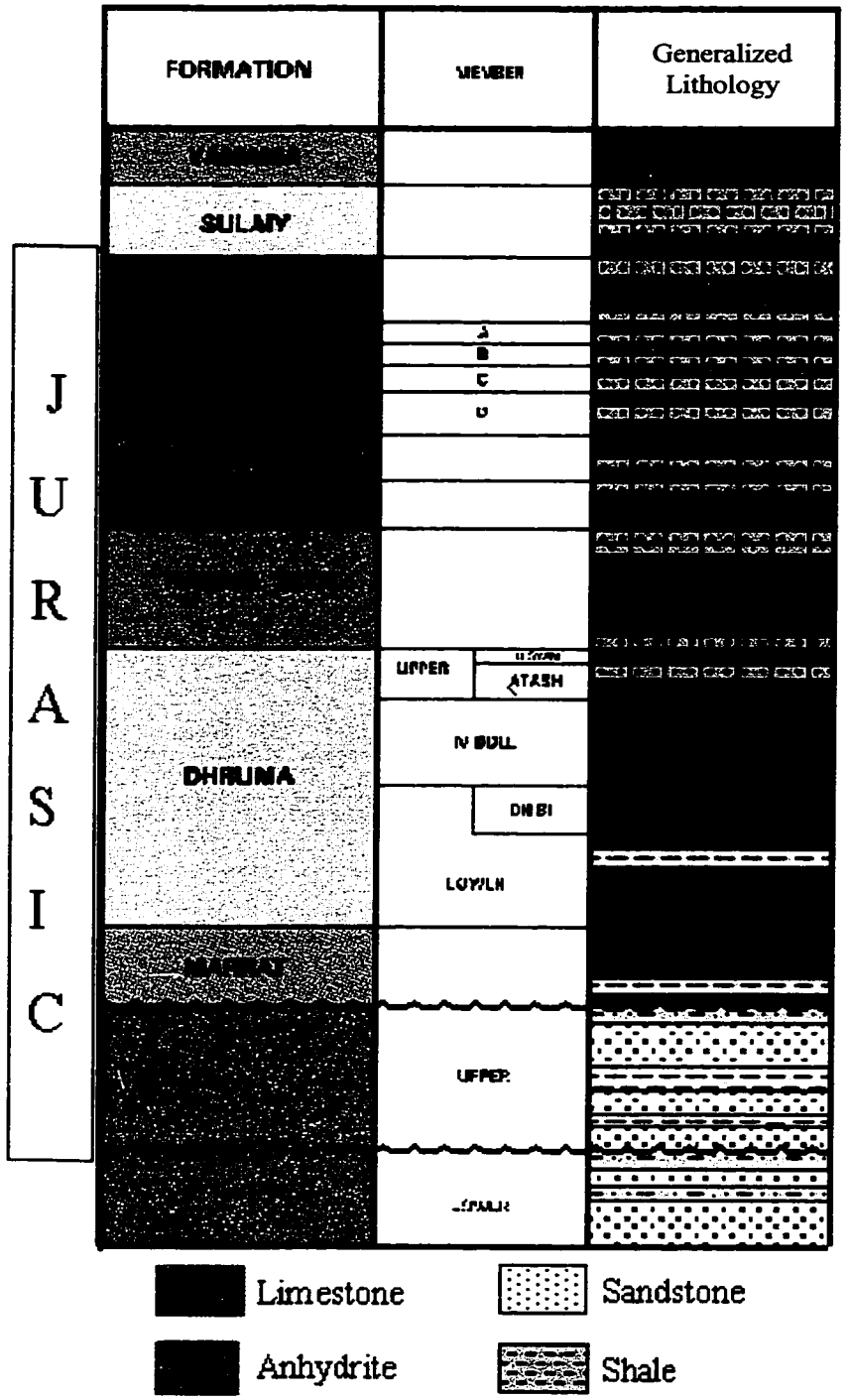

Figure 2.2: Generalized Saudi Arabian stratigraphic of the Jurassic (From Saudi Aramco)

2.2.2 Hanifa Formation

Alsharhan (1986) describes the Hanifa Formation as "characterized by shallow water limestone that is composed of alternating aphanitic and oolitic calcarenitic limestone." During the late Callovian and Oxfordian time, two important and large intrashelf anoxic basins existed: the Arabian and the Gotnia (Figure 2.3). In these basin organic rich mudstone has accumulated (Saudi Aramco, 1991; Alsharhan and Kendall, 1986). Ayres (1982) suspects that these organic rich deposit are the main source rocks for most of the oil reservoir in the Jurassic section in Saudi Arabia (Ayers et al, 1982).

During the Late Jurassic, the Berri Field area was located on a ramp margin, which was dipping gently from the Rimthan carbonate platform in the north to the Arabian Basin in the south. Shallow water, lagoonal and peritidal facies of the Hanifa occur on the Rimthan Platform north of the field. Above the fair weather wave base, high-energy sediments were deposited such as skeletal and peloidal grainstones and associated small biohermal buildups. In the southern part of the Berri Field, sedimentation below fair weather wave base replaced high-energy carbonates. Low to medium energy sediments were deposited such as packstones and wackstones. These low energy deposits change southward into anoxic and organic rich basinal mudstones (McGuire, 1993).

In 1988, Saudi Aramco initiated a study to construct new geological models for the Hanifa and Hadriya Reservoirs. These models eventually were used for reservoir simulation using Sequence Stratigraphy principles along with data from conventional cores, and openhole logs were used in formulating the new models (McGuire, 1993; Saudi Aramco, 1991).

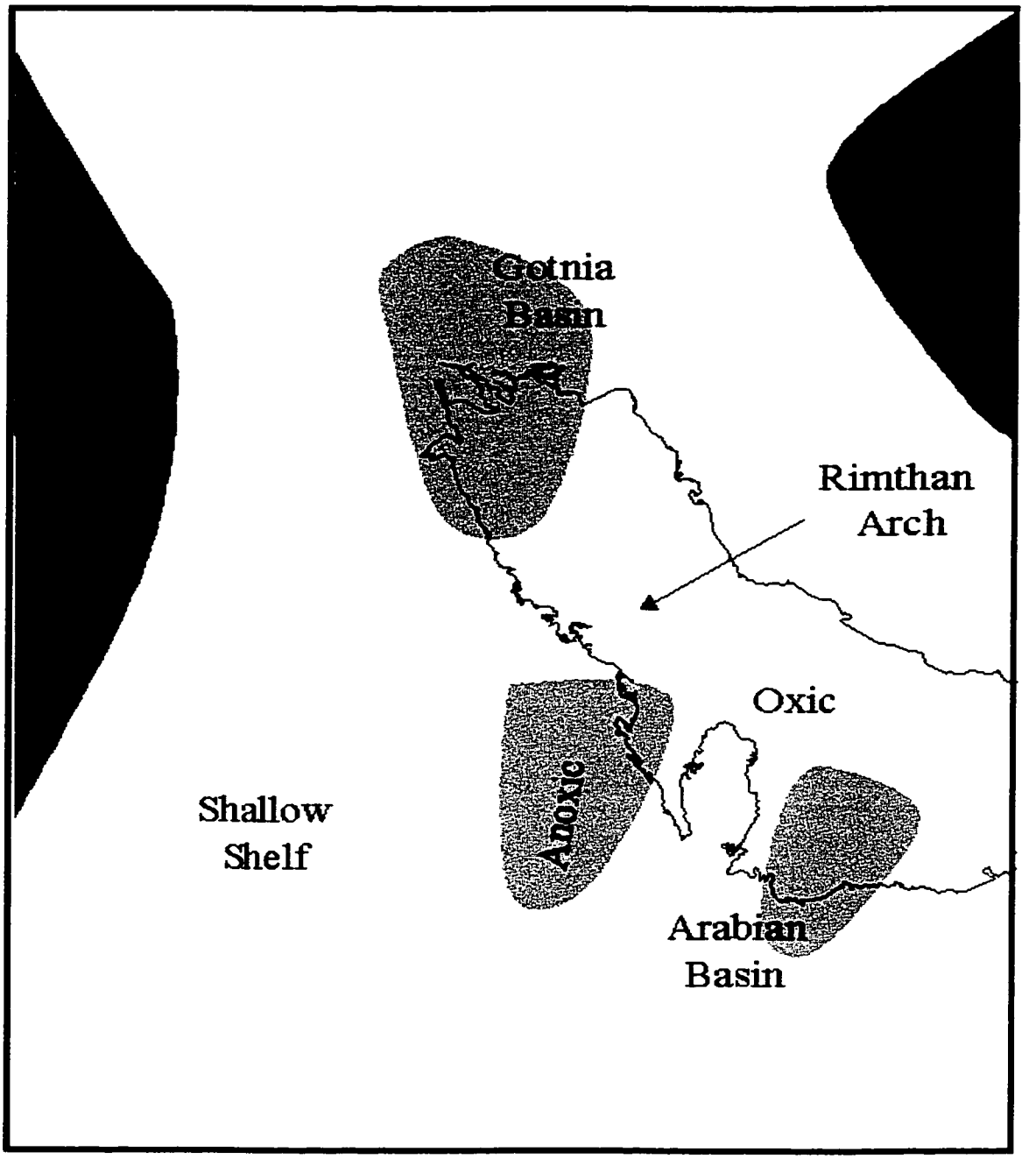

Figure 2.3: Paleogeography of the Gulf area in Late Jurassic (From Saudi Aramco, 1991)

The Saudi Aramco study described Hanifa Formation with the Berri Field area as a large-scale coarsening- and shallowing-upward carbonate platform sequence of about 500 feet thick. In general, Hanifa consists of two major units: a lower non-reservoir unit of organic-rich laminated lime mudstones and low porosity skeletal wackestones, and an upper reservoir unit of grain rich carbonates including skeletal packstones, grainstones and boundstones (Figure 2.4).

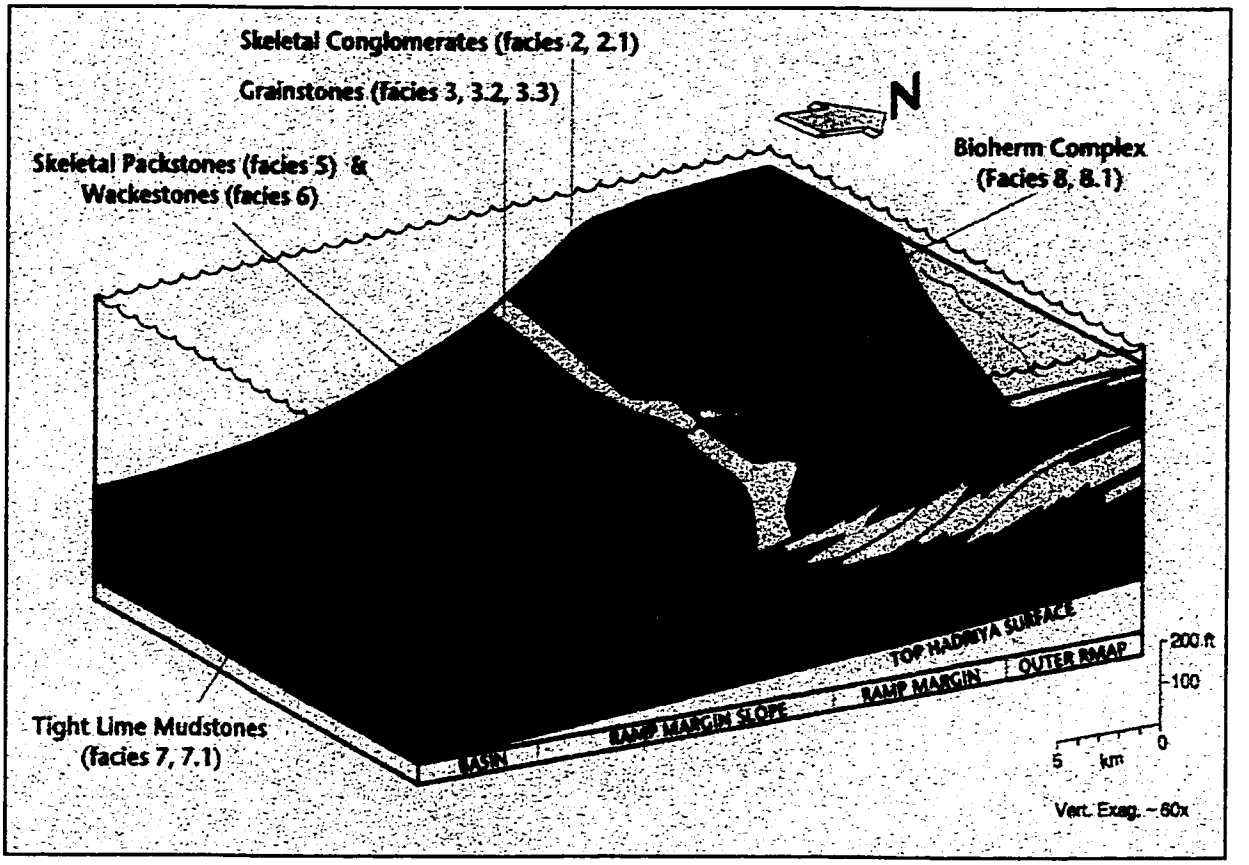

Figure 2.4: Depositional facies model for Hanifa Reservoir in Berri Field (From Saudi Aramco, 1991)

Due to the minor effect of diagenesis, the Saudi Aramco study has defined the Hanifa Reservoir facies based on depositional features. From a total of eleven facies, the study has recognized nine reservoir and two non-reservoir facies (Figure 2.4). The best reservoir facies consist of skeletal conglomerates and grainstones (Facies 2 and 2.1). The skeletal/intraclasts conglomerate facies has exceptional reservoir quality, with very high permeability and porosity. The bioherm-associated facies (Facies 8 and 8.1) exhibit discontinuous, lenticular geometries and are characterized by intermediate reservoir quality.

Three facies have intermediate reservoir quality, which are massive skeletal/peloidal grainstone, cross-bedded skeletal/peloidal grainstone and burrowed skeletal peloidal grainstone (Facies 3, 3.2 and 3.3). Skeletal packstones and skeletal wackestones have in general low reservoir quality (Facies 5 and 6). The mudstones, which have very low porosity and almost no permeability, are classified as non-reservoir facies (Facies 7 and 7.1). Figure 2.5 to figure 2.10 display thin section photos for each main facies in Hanifa Reservoir.

The porosity in the Hanifa Reservoir is primarily intergranular with lesser moldic and intragranular porosity. Moldic porosity is the only secondary porosity that is significant, but has very low impact on the total reservoir compared to the intergranular porosity (Saudi Aramco, 1991).

Figure 2.5: Thin section from facies 2 displays very coarse to medium-grained skeletal intraclast and peloid grainstone. Sample porosity is 24% and permeability is 675 md. Scale bar is 0.2 mm. (From Saudi Aramco, 1991)

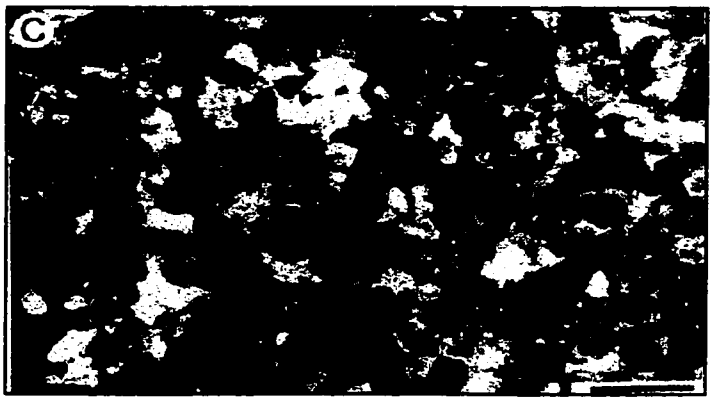

Figure 2.6: Thin section from facies 3 displays burrowed fine-grained peloid skeletal grainstone. Sample porosity is 16% and plug permeability is 6.7 md. Scale bar is 0.2 mm. (From Saudi Aramco, 1991)

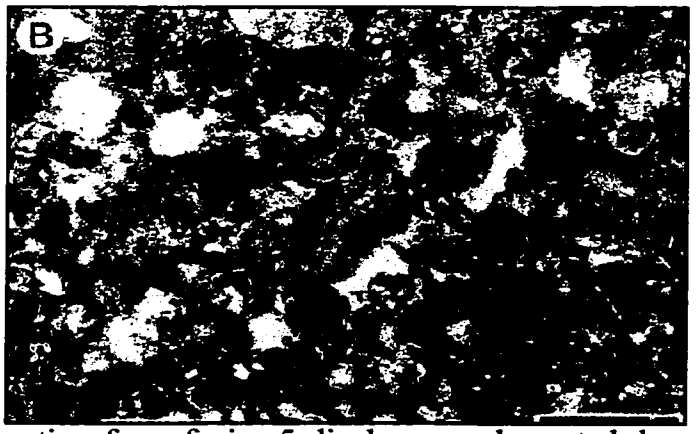

Figure 2.7: Thin section from facies 5 displays poorly sorted, burrowed peloid skeletal packstone. Sample porosity is 11% and permeability is 0.3 md. Scale bar is 0.1 mm. (From Saudi Aramco, 1991)

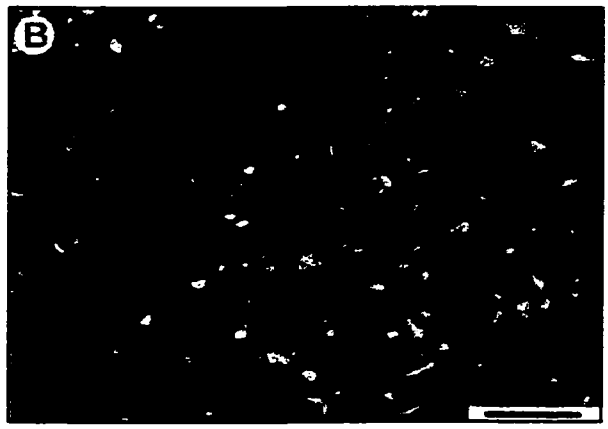

Figure 2.8: Thin section from facies 6 displays very fine-grained skeletal wackestones, consisting of abundant sponge spicules. Sample porosity is 2.4% and permeability is 0. Scale bar is 0.5 mm. (From Saudi Aramco, 1991)

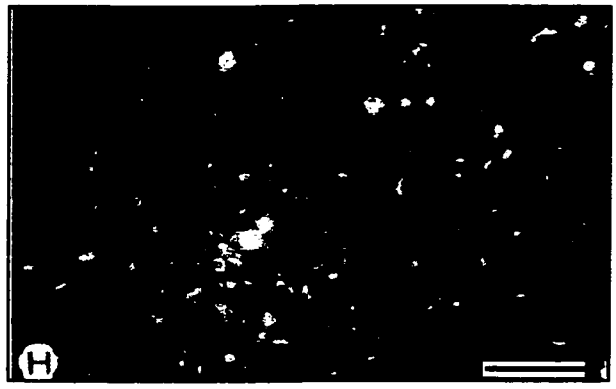

Figure 2.9: Thin section for facies 7 displays muddy to very fine-grained wackestone/mudstone. Sample porosity and permeability are both 0. Scale bar is 0.5 mm. (From Saudi Aramco, 1991)

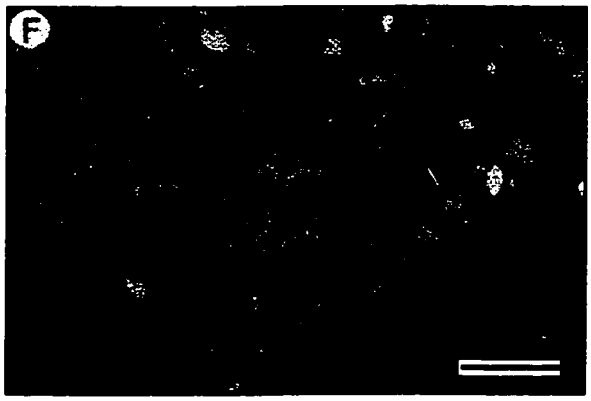

Figure 2.10: Thin section from facies 8 shows the microstructure of large Stromatoporoid specimen. Sample porosity is 15.5% and permeability is about 44 md. Scale bar is 2.5 mm. (After Saudi Aramco, 1991)

2.2.3 Berri Field

Berri is located about 100 km north of Dhahran in the Eastern Province of Saudi Arabia. Most of the field's surface area is located offshore in the Arabian Gulf with a small onshore locality (Figure 2.11). The areal size of Berri field is about 32 kilometers by 40 kilometers. The field ranks as the 22nd largest in the world and is in a mature state of development (Kompanick, 1993).

It was discovered in 1964 based on seismic surveys of the area (Alsharhan and Kendall, 1986). Six oil zones have been discovered which are Arab A, B, C and D reservoirs, Hanifa Reservoir and the Fadhli Reservoir. In 1968 oil had been discovered in the Hadriya reservoir, raising the number of reservoirs in Berri to seven. The Hanifa and the Hadriya Reservoirs are the main producing reservoirs in this field. Average oil gravity for both reservoirs is about 38° API. The field has been on production since 1967 and a peripheral water flood has been in effect since 1973 (Kompanick, 1993; Beydoun, 1988).

Tuwaiq Mountain and Hanifa Formations are believed to be the source rocks for most of the oil in the Jurassic section in Saudi Arabia (Ayres et al., 1982). Moreover, these rocks are within the oil generation window. The dominant migration path for this oil is laterally from the basinal areas to the high areas (Stoneley, 1990). Based on this picture, Hanifa Formation could be the main source for its oil. Oil has migrated from the organic rich basinal mudstones to the high structure and good porosity grainstones in Berri Field. Oil was prevented from migrating upward by Jubaila mudstone that represents the reservoir caprock (Ayres et al, 1982).

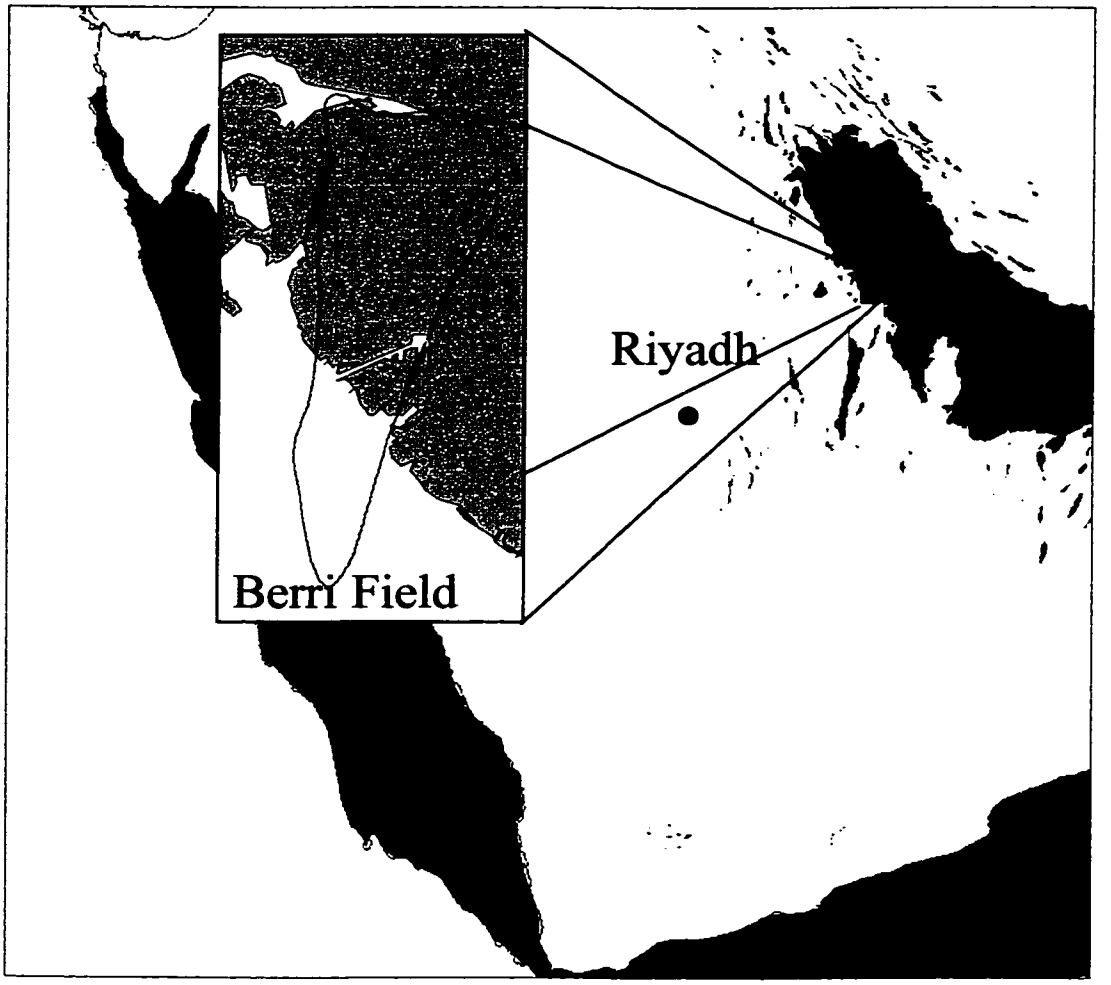

Figure 2.11: Location map of Berri Field in Saudi Arabia.

2.2.4 History of Hanifa Reservoir Modeling

The earlier models for Hanifa Reservoir were built on the basis of cake stratigraphy. Such models used methods to interpolate porosity between the wells independently of facies or any geological data. This approach failed to capture the true geology of the Hanifa Reservoir and could not explain the anomalies of water breakthrough in different wells (McGuire, 1993).

The 1991 Saudi Aramco study developed a new facies and layering scheme that is based on the sequence stratigraphy principle. This study defined 11 facies and 45 geological zones throughout Hanifa Reservoir in Berri Field. It represented a major breakthrough in the understanding of the geology of Hanifa Reservoir. In addition, it was the first study done in Saudi Aramco based on sequence stratigraphy. This study showed clearly that there is a direct relation between facies and porosity and that geology controls the lateral and vertical porosity distributions (Kompanick, 1993).

Porosity modeling has been executed in two stages. In the initial stage, a facies model was built to control the facies distribution between wells. Then, this model was utilized to control the eventual porosity model. This was performed by building separate porosity models for each reservoir facies based on the porosity distribution within that facies. Then, the facies model was used to isolate porosity values from the generated porosity models and generate a composite model. This was the only way to generate a porosity model based on geology at that time (Kompanick, 1993).

In 1999 Saudi Aramco geologists revised the layering scheme based on newly drilled wells and came up with 52 geological zones. The facies definitions and number of facies remained the same. Also a pilot 3-D seismic area has been shot over the Berri

Field. Based on the new data sets, Saudi Aramco contracted created an updated reservoir simulation model that integrates all available data using geostatistical methods.

Saudi Aramco geological modelers grouped the eleven facies into six facies. This grouping was based on core porosity and permeability relationships as shown in table 2.1. They also compared two different layering schemes: one with 52 layers and the other with 13 layers. The 13-layer scheme was developed to see if they could preserve the reservoir heterogeneity with fewer layers. The facies and porosity modeling results from the two layering schemes came in very similarly. This methodology supports the idea that flow modeling could be done with less facies and geological zones. Consequently, this assumption could positively impact the speed of modeling and reduce the possibilities human errors.

Grouped Facies	Depositional Facies
A	2, 2.1
B	3
C	3.2
D	3.3, 5, 6
E	7,7.1
F	8,8.1

Table 2.1: Grouped facies and depositional facies

The facies models were built by Sequential Indicator Simulation (SIS) using one directional semivariogram with a strong anisotropy that has 40,000 meters in the south direction and 10,000 meters in the west, and an azimuth direction of N70W. This was needed to make it similar to the conceptual geological model. This model was used to create a porosity model by using facies based on Sequential Gaussian Simulation (FBsGs) (Saudi Aramco, 2000).

2.3 Geostatistics Review

2.3.1 Background

Geostatistics is a branch of statistics that deals with random variables distributed in space and/or time with some degree of continuity. Geostatistics has emerged with the work of Daniel Krige in the South African mining industry in the early 1950s. It was used as a tool to estimate the recoverable reserves for mining deposits (Goovaerts, 1997). Beginning in mid 60s and mid 70s it became much more closely affiliated with the work of Georges Matheron. During this time, the use of geostatistics was focused toward the mining industry. In 1978, Journel and Huijbregts published "Mining Geostatistics," which focuses on the use of geostatistics in the mining industry (Journel and Huijbregts, 1978).

In the late 1980s, geostatistics was essentially viewed as a mean to describe spatial patterns, and interpolate the value of the attribute of interest to unsampled locations. In 1989, Isaaks and Srivastava published "Applied Geostatistics," which focuses on exploratory data analysis and uncertainty assessment. In 1992 Deutsch and Journel published "Geostatistical Software Library" (GSLIB). That was a guidebook for geostatistical algorithms, which has been written in FORTRAN by the authors and

students from Stanford University. The GSLIB covers different geostatistical techniques from semi-variogram calculation to Kriging and Stochastic Simulation (Goovaerts, 1997). RC-Squared geostatistical modeling algorithms are built based on GSLIB principles (RC-Squared, 2000). In 1997 Goovaerts published "Geostatistics for Natural Resources Evaluation". This book covers topics such as exploratory data analysis and assessments of uncertainty, along with different geostatistical algorithms (Goovaerts, 1997).

In the past geostatistical research and development have been done in a few research schools in France and in the United States. However, in recent years the petroleum industry has been active both in the research and development of Geostatistics (Damsieth and Omre, 1997).

2.3.2 Semi-Variogram

A semi-variogram is a mathematical tool to quantify the spatial correlation and continuity of a variable. It is a plot of the average squared difference in value between data points against their separation distance. It is computed as half the average squared difference between the components of every data pair.

$$\gamma(h) = \frac{1}{2N(h)} \sum_{i=1}^{N(h)} [z(x) - z(x+h)]^2,$$

where $N(h)$ is the number of pairs of data locations a vector h (lag distance) apart and z is the measurement at locations x and $x+h$. The output is represented by an experimental semivariogram as shown in Figure 2.12.

The lag spacing defines the incremental distance at which the semi-variogram is calculated as shown in figure 2.13. The first lag distance must be at least equal to the sample spacing. The number of lags used usually varies from 10 to 15 and it should be

restricted to the dimensions of the data coverage. On average the maximum lag distance is about half the diagonal of the data extent (Coombes, 1997).

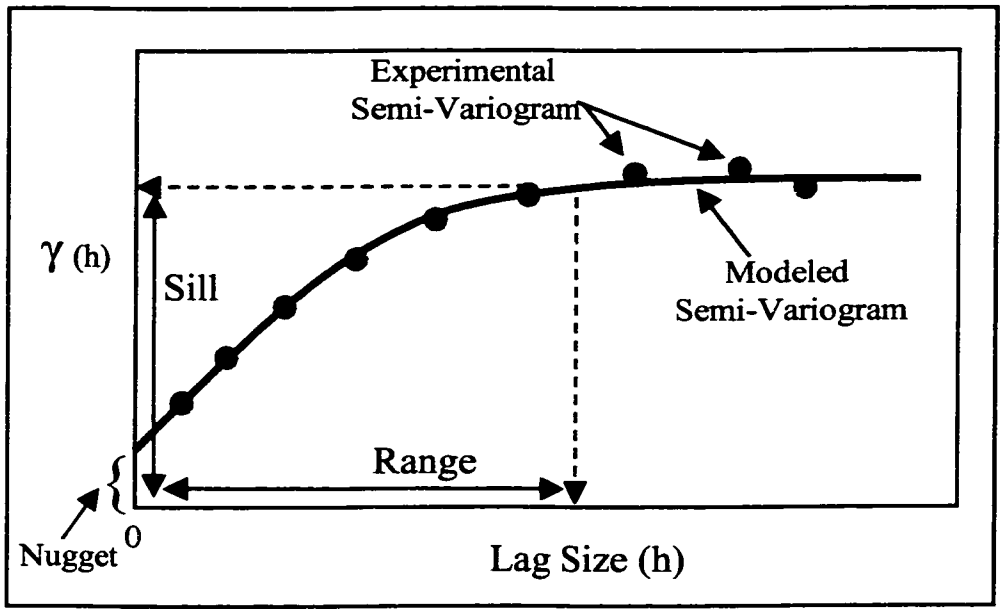

Figure 2.12: Main characteristics of a semi-variogram (From Coombes, 1997)

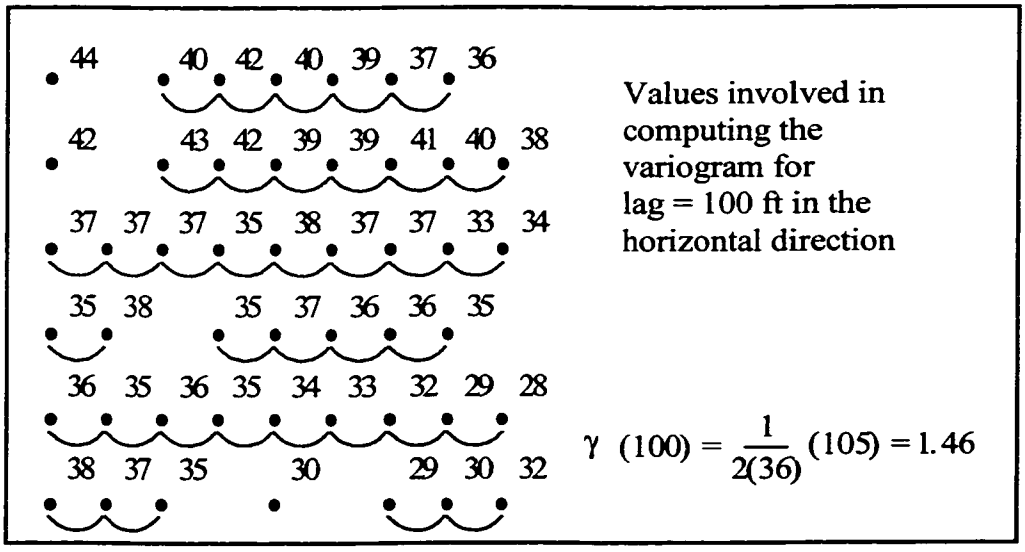

Figure 2.13: An example showing semi-variogram calculations for a lag of 100 ft in the horizontal direction. (Modified after Coombes, 1997)

The experimental semi-variogram must be fitted with an appropriate model semi-variogram. Several mathematical models are available and well described in the literature and can be used for fitting proposes. Examples of such models are: spherical, exponential, gaussian, power and periodic (figure 2.14). The rule when selecting a model is that it should fit most points near the origin. In addition, the same model should be used when calculating directional semi-variograms (Isaaks and Srivastava, 1989 and Journel and Huijbregts, 1978).

Spatial correlation is dependent on the separation distance and on the azimuth of separation. If the values of the semi-variogram parameters (e.g. range, sill) are identical in all directions then it is called isotropic; otherwise, it is called anisotropic. There are two types of anisotropy: geometric and zonal as shown in figures 2.15 and 2.16. The geometric anisotropy is indicated by semi-variograms having different ranges in different directions, while the sill value is the same. Different ranges and sill values in different directions reflect the effect of zonal anisotropy. Most geological phenomena tend to reflect anisotropic behavior (Isaaks and Srivastava, 1989).

The behavior of the semi-variogram near the origin reveals important information about the variable continuity. There are four main types of behavior: continuous, linear, nugget and random (figure 2.17). Continuous types displays parabolic behavior near the origin and represent a variable with a high degree of continuity. Linear types display oblique tangent at the origin and represent a variable with an average degree of continuity. Nugget type shows discontinuity at the origin. If the last type displays continuous randomness, it might reflect undetectable spatial correlation (Al-Salem, 1996).

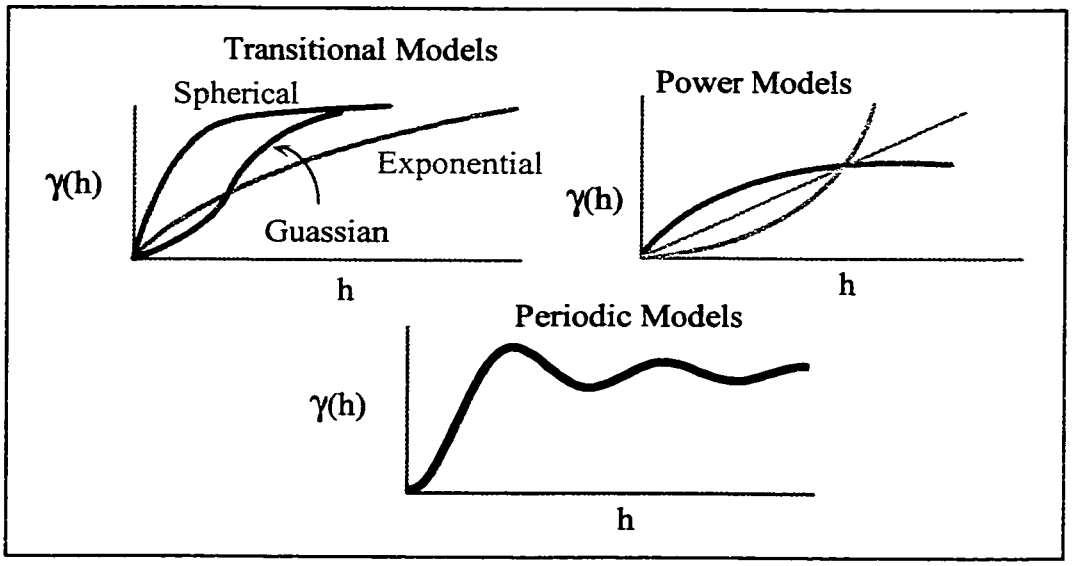

Figure 2.14: Different semi-variogram models that can be used to fit an experimental semi-variogram. (From Isaaks and Srivastava, 1989 and Journel and Huijbregts, 1978)

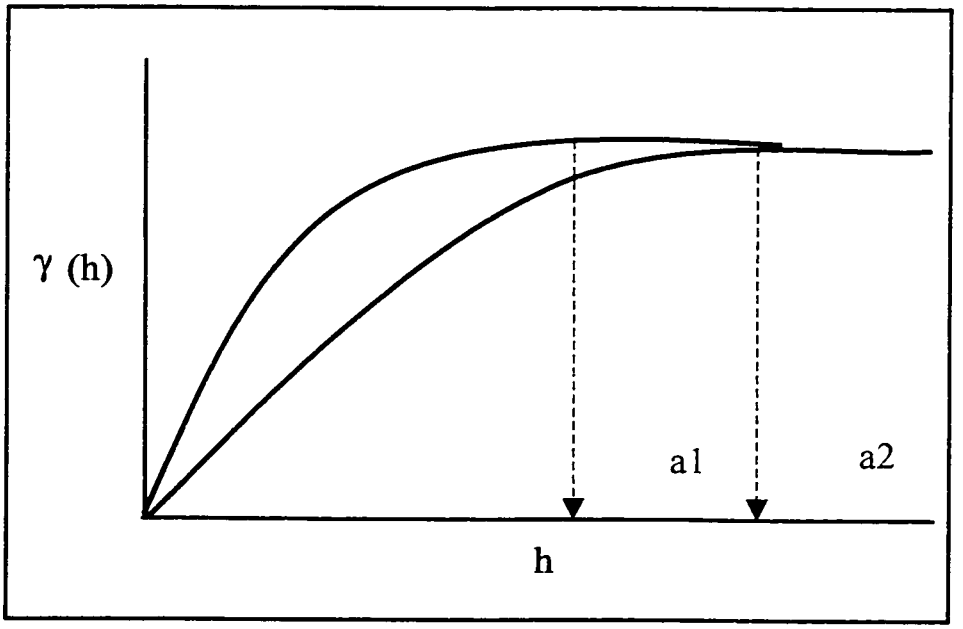

Figure 2.15: Geometric anisotropy. (After Isaaks and Srivastava, 1989 and Journel and Huijbregts, 1978)

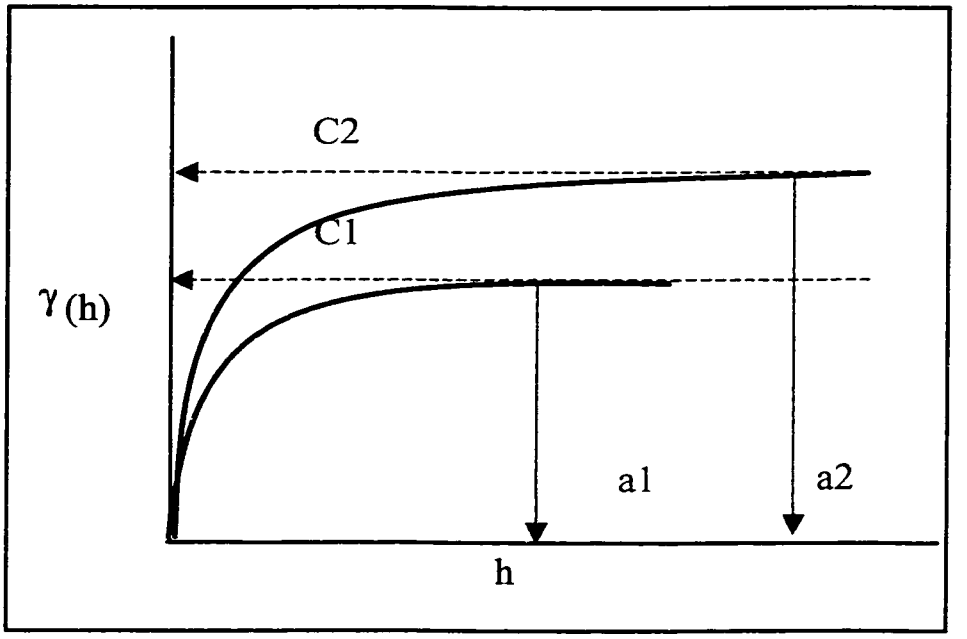

Figure 2.16: Zonal anisotropy. (After Isaaks and Srivastava, 1989 and Journel and Huijbregts, 1978)

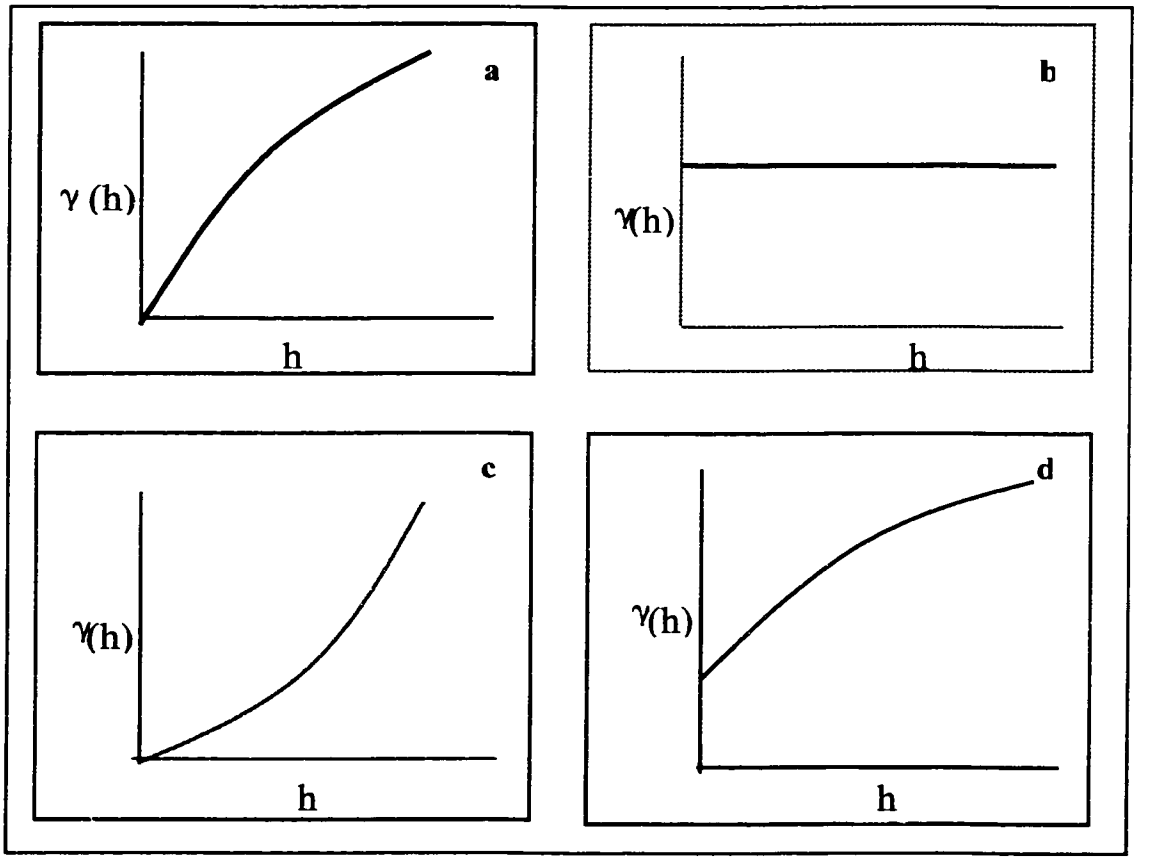

Figure 2.17: The four main types of semi-variogram behavior at the origin: a- linear, b- random, c- continuous and d- nugget. (After Al-Salem, 1978)

2.3.3 Kriging

Kriging is a generic name adopted by geostatisticians for a family of generalized least square regression algorithms in recognition of the pioneering work of Daniel Krige. Kriging is also known as BLUE (Best Linear Unbiased Estimator). It uses a linear combination of surrounding sample values and assigns weight to each one in order to calculate the best predictions. Kriging, also, allows the derivation of weights that result in optimal and unbiased estimates. All Kriging estimators are of the basic linear regression estimator $z^*(x)$ defined as

$$z^*(x) - m = \sum_{\alpha=1}^{n(x)} \lambda_\alpha(x)[z(x_\alpha) - m(x_\alpha)]$$

Where

z(x) is a vector model at locations x
m is the mean of z(x)
z*(x) is the linear regression estimator
$\lambda_\alpha(x)$ is the weight assigned. The weight accounts for the proximity of the data to the location being estimated and the clustering of data.

The above equation represents the simplest form of Kriging. By modifying the above-mentioned formula, other kriging algorithms can be derived such as Simple Kriging and Ordinary Kriging. Other important types of Kriging are Indicator Kriging, Block Kriging, Kriging with external drift and CoKriging. Kriging with external drift and CoKriging are used to integrate two different types of data (Goovaerts, 1997).

Simple Kriging considers the mean "*m*" to be known and constant throughout the study area. The simple kriging estimator is unbiased and the error mean is equal to zero. Simple Kriging equation is expressed as follow:

$$Z^*_{SK}(x) = \sum_{\alpha=1}^{n(x)} \lambda^{SK}_{\alpha}(x) * z(x_{\alpha}) + \left[1 - \sum_{\alpha=1}^{n(x)} \lambda^{SK}_{\alpha}(x)\right] m$$

Ordinary Kriging (OK) considers the mean "*m*" to be localized, which accounts for local data fluctuations. OK accounts for local variations in the mean by limiting the mean to a local neighborhood around the location being estimated. As in SK the error mean is equal to zero. The OK equation is expressed as follow:

$$Z^*_{OK}(x) = \sum_{\alpha=1}^{n(x)} \lambda^{OK}_{\alpha}(x) * z(x_{\alpha}) \quad \text{with} \quad \sum_{\alpha=1}^{n(x)} \lambda^{OK}_{\alpha}(x) = 1$$

Block kriging is a linear estimate of a value over an area, which has several data points. Block estimates are smoother than the point estimates. In addition, the smoothing increases with the increase in block size. The block kriging smooths out the short-range variation of concentration and erase discontinuities near data locations (Goovaerts, 1997).

Indicator Kriging estimates the probability that the variable value is below or above a critical threshold at a certain location. It is a method that allows using different models of spatial continuity for different values of the categorical data. Indicator kriging provides a probability distribution at each grid node that quantifies the local uncertainty in the model. These distributions provide a good idea on how much difference can be expected among different realizations of a stochastic model of facies predictions (Isaaks and Srivastava, 1989).

Kriging with an external drift simply extracts the trend from the soft data and uses it to guide the estimation of the hard data. Usually hard data refers to data values at well

locations, and soft data refers to any other data that is more extensively sampled than the well data. For example in a reservoir, porosity logs at the wells are considered to be hard data, and seismic data are soft data. The estimations reflect a linear rescaling of the units of the trend. The basic relationship between hard and soft data should make physical sense and should be correlated (Chambers, 1994).

Kriging with external drift and CoKriging have different mathematical equations, but both have the same objective, that is to integrate soft and hard data. They are popular techniques for data integration. Two conditions must be meet before doing any data integration. The relation between hard data and soft data must be linear. Also the secondary data must be known at all hard data locations and at all locations being estimated (Fournier, 1995).

2.3.4 Simulation

Stochastic simulation is the process of building alternative, equiprobable, high-resolution models. Each of these models is called a realization. Simulation is conditional if the resulting realizations utilize the hard data values at their locations. Either categorical or continuous variables may be conditionally simulated.

The sequential simulation procedure in simulating data points is as follows: it first assigns data values to closest grid node. After that it establishes a random path through all of the grid nodes. Then it visits each grid node in the model and find nearby data and previously simulated grid nodes and krige a value from all available data. This value will be used to construct conditional distribution function (cdf). Then a simulated value will be drawn randomly from the cdf and assign it to the grid node. This process will be

repeated until all grid nodes have been simulated. All the simulated values should honor the data semi-variograms and histograms (GSLIB, 1999)

Simulation is unlike estimation, because in estimation only a unique image could be constructed. But in simulation, multiple realizations can be generated with the same probability of existence. The sequential simulation algorithm requires the determination of the conditional cumulative density function (ccdf) at each location being estimated using the kriging estimate and its variance. There are two major stochastic simulation algorithms that are gaussian and indicator simulation. Gaussian simulation is used to simulate continuous values such as porosity, while indicator simulation is used mainly for categorical data such as facies. All sequential simulation algorithms honor the data points at their locations. (Chambers, 1994)

Simulation is used in uncertainty assessments and it honors extreme values. However, estimation is locally accurate, smooth and good for visualizing trends. It is not used in uncertainty assessments and it does not honor extreme values, mainly because the smoothing effect is a characteristic of all estimation algorithms including kriging. The simulation techniques are used to reproduce local variability within control points (Wolf, 1994).

CHAPTER 3

DATA ANALYSIS

3.1 Model Description

Statistical data analysis is a preliminary step in reservoir modeling. It serves several objectives, such as checking the data quality and looking for trends. Before proceeding with statistical analysis and modeling, model geometry must be defined. The model geometry must be based on the stratigraphic framework of the reservoir, so it will have better representations of the reservoir.

Aramco geologists have made detailed stratigraphic correlations between sequences of Hanifa Reservoir based on the 1991 study. They have defined 52 reservoir zones in Hanifa Reservoir in Berri Field. In a recent modeling project, RC-Squared built two models for Hanifa Reservoir using two layering scheme. The first model was based on 52 zones and the other on 13 zones. The modeling results were very similar. In this study we are going to use 12 zones. These zones are defined based on core data, gamma

ray and porosity logs, and they are corelatable surfaces across the field. These are the significant sequence boundaries according to Aramco geologists. They are adequate for this study, because they capture the reservoir geometry. Figure 3.1 compares the two different layering schemes. Figure 3.2 shows a structure map for the top of the Hanifa Reservoir at the study area. Figure 3.3 shows a 3-D view for all structures that were used in this study.

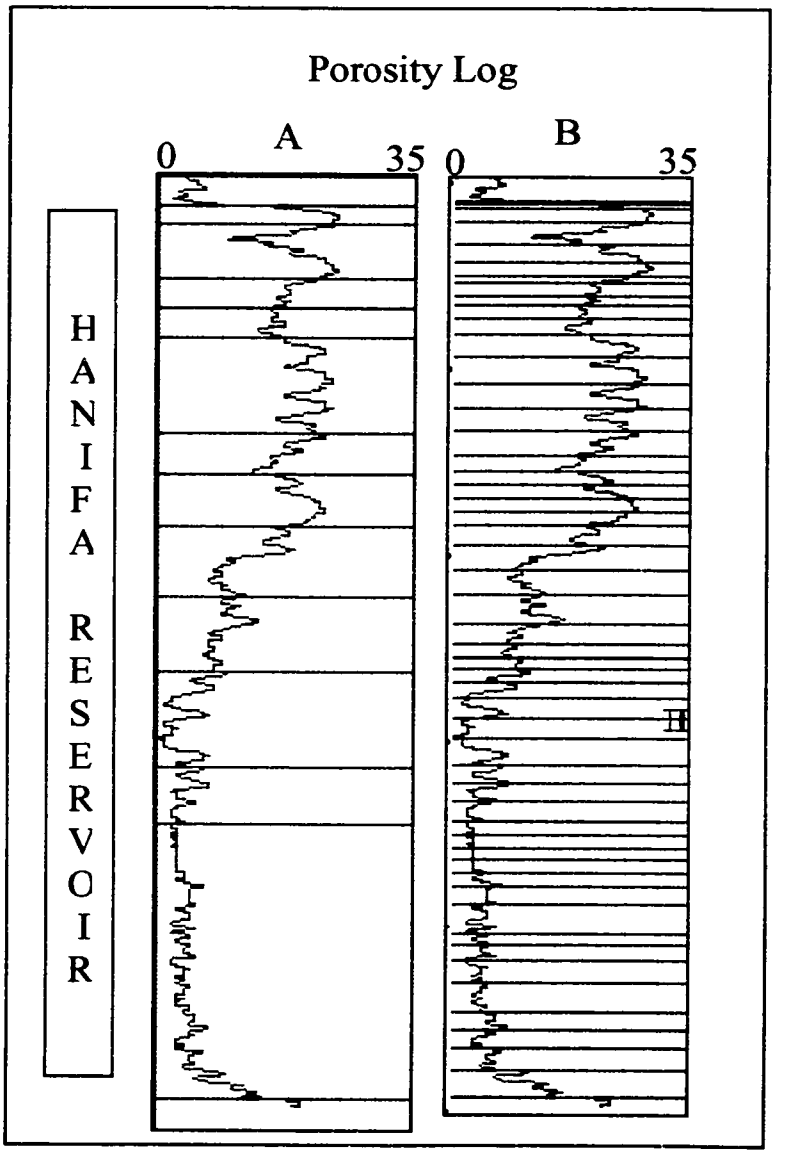

Figure 3.1: An example comparing the 12 (A) and 52 (B) layering schemes on a porosity log for the same well across the Hanifa Reservoir

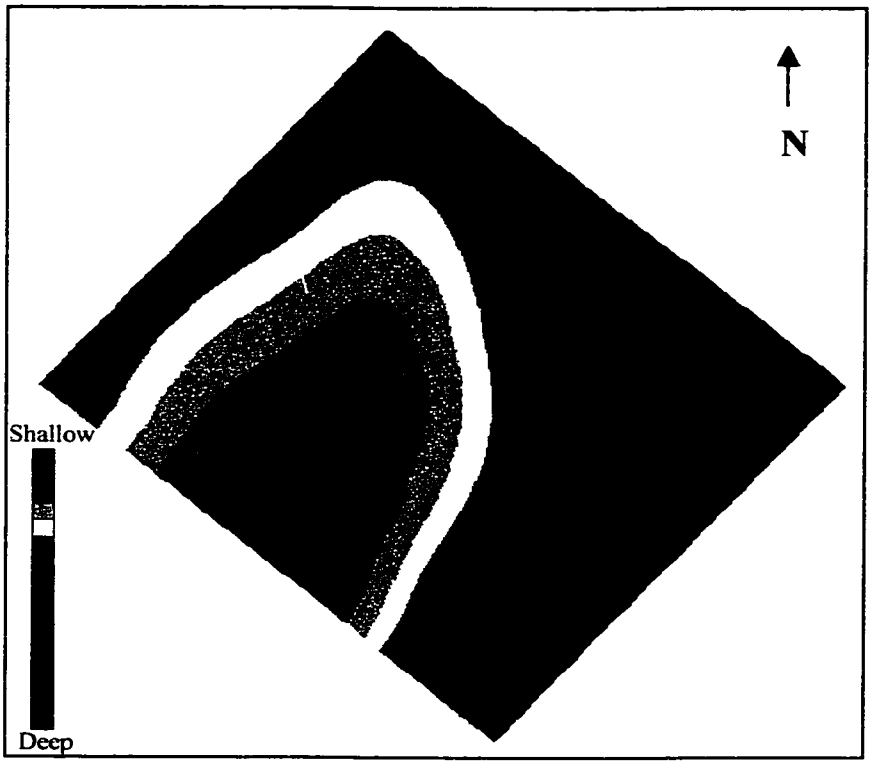

Figure 3.2: Structure map of the top of Hanifa Reservoir at the study area.

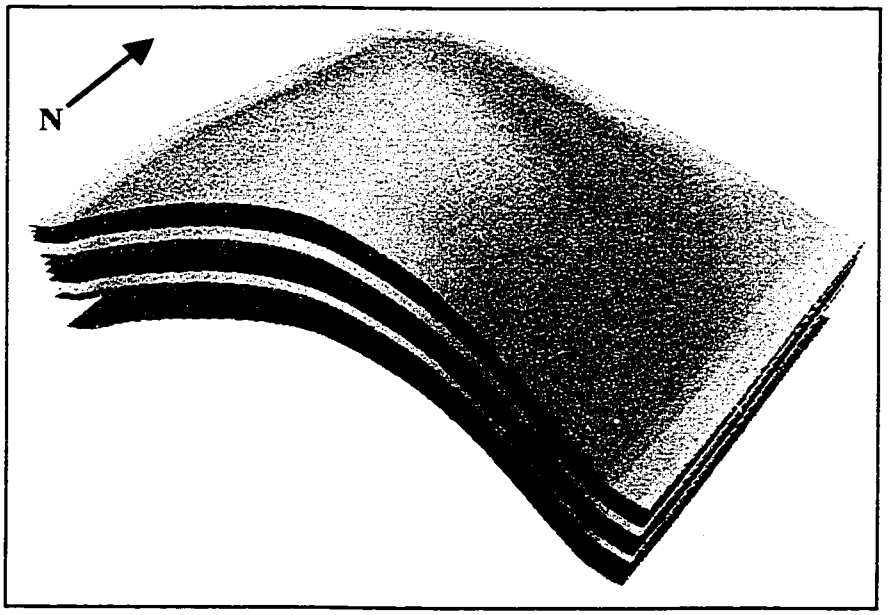

Figure 3.3: 3-D view of different structure map that are used in this study.

To capture the reservoir heterogeneity and optimize the number of cells, cell thicknesses vary from one reservoir zone to another. In the upper part of the reservoir, where we have good quality rocks, cell size is small. Whereas in the lower part, where there are mostly non-reservoir rocks, the cell size is larger. Table 3.1 represents the thickness variations in each zone and the number of assigned cells to each zone. Total number of vertical cells is 122. Thickness of cells varies from 0.2 feet in the good reservoir rocks to 10 feet in the non-reservoir rocks.

Zone Number	Thickness (feet)			Number of Cells
	Maximum	Minimum	Average	
1	16.5	8	11.4	6
2	28	3	16	6
3	29.5	1.5	12	5
4	33.5	1	10.5	5
5	57.5	5	29	9
6	26	4.5	16	6
7	47.5	14.5	33	10
8	51	10.5	33.5	9
9	57	16.5	40.5	10
10	74	42	55.5	15
11	49.5	30	34	10
12	310	124	189	30

Table 3.1: Reservoir zones thickness and cell assignments

The size of the study area is 11,750 meters by 13,500 meters. The standard cell areal dimensions used by Aramco are 250 x 250 meters. This study will follow Aramco standards. Based on that, the model areal dimensions will be 47 cells in width by 55 cells in length as shown in figure 3.4. The total number of cells in the model is 315,370 cells.

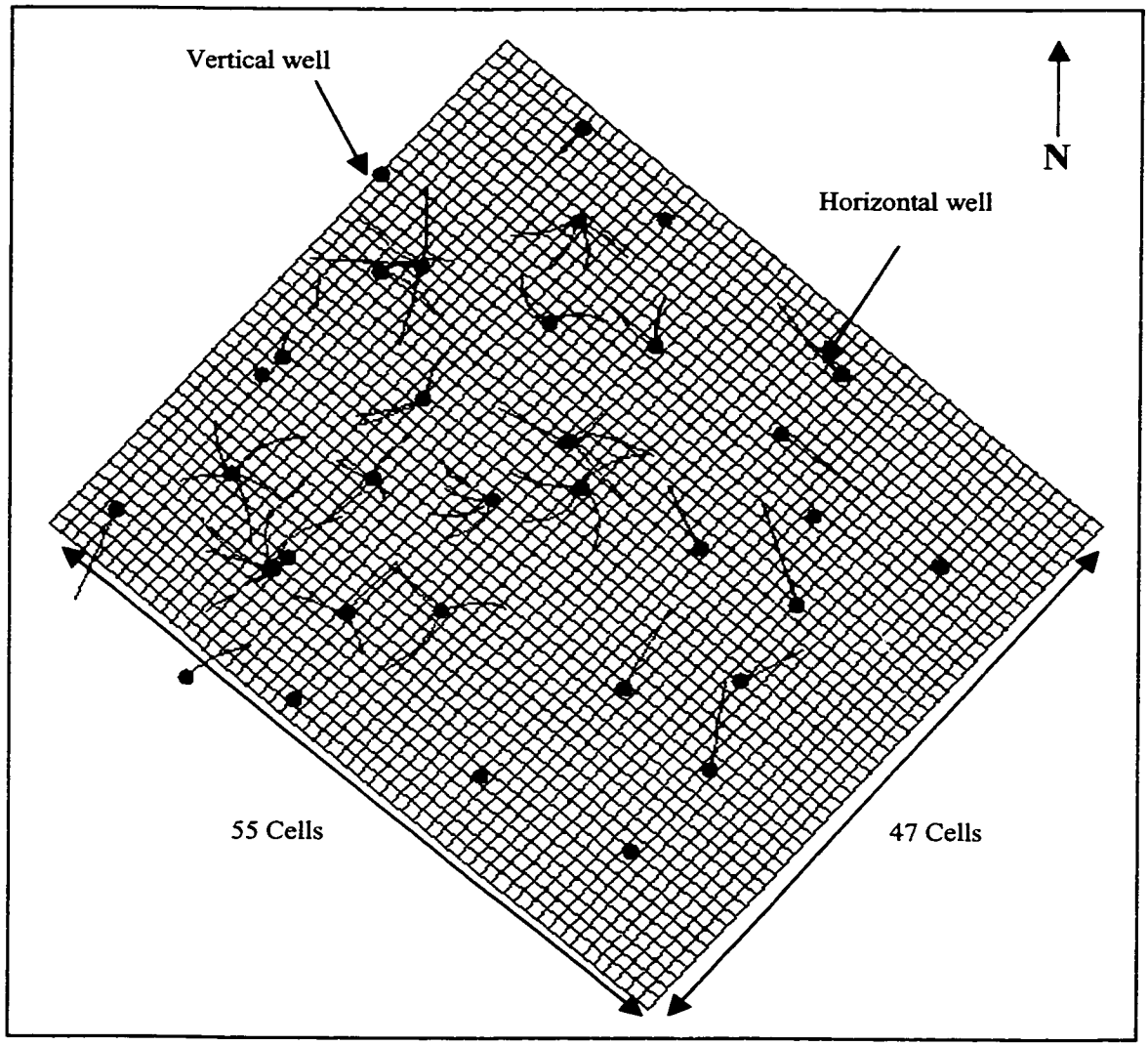

Figure 3.4: Areal grid of the study area, red dots are wells that are used for validation (each cell size is 250 x 250 meters)

3.2 Univariate Analysis

Univariate statistical analysis is an essential step before geostatistical modeling. This analysis is important because it shows the data distribution and detects erratic values. Distribution type is determined by generating histograms for the variables under study. Histograms are an excellent way to present the most important data; they show maximum, minimum and type of distribution. Also, univariate analysis provides important statistical parameters in a simple form, such as mean, standard deviation, etc. Maximum and minimum values of the data might indicate the existence or absence of erratic values.

From this step and onward, ten wells have been excluded from the database and kept for a later validation stage (figure 3.4). Univariate statistical analysis has been conducted for facies and porosity logs. This analysis is based on well logs that have a ½ foot resolution. These analyses were conducted for all reservoir zones as a group (Figure 3.5 and 3.6) and for every individual reservoir zone as well (Figure 3.7 to Figure 3.8). Table 3.2 shows the main porosity statistical parameters per reservoir zone.

Figure 3.4 shows that the mudstone facies have the highest percentage among other facies in the Hanifa Reservoir. Moreover, figure 3.5 shows that there are two porosity distruibation in the reservoir. By comparing the porosity distribution with the facies distribution in each zone, a clear relationship between log porosity and depositional facies will apear. For example zone 1 where a good reservoir facies exists, porosity distribution tends to have normal distribution with high mean. Where as, in zone 12 where mudstone facies dominate, the porosity distribution tends to be skewed with low mean porosity.

The upper zones, generally, are dominated by grain-rich rocks such as facies 2 and facies 3. This explains the high porosity values in these zones. Whereas the lower zones, especially zone 12, are dominated by mudstone facies. This explain the very low porosity in these zones and confirms that porosity distribution is directly related to facies distribution.

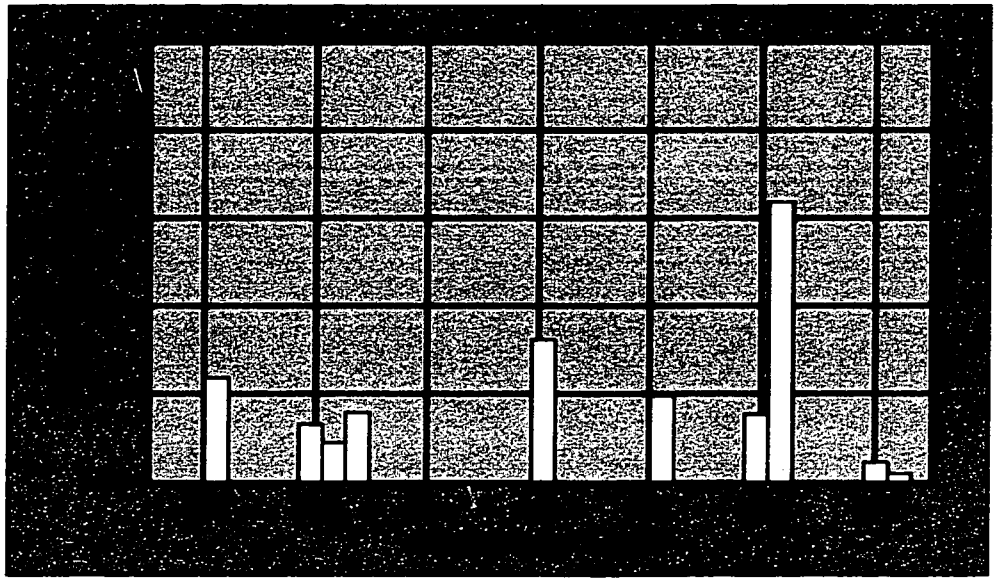

Figure 3.5: Facies distribution within the Hanifa Reservoir in Berri Field

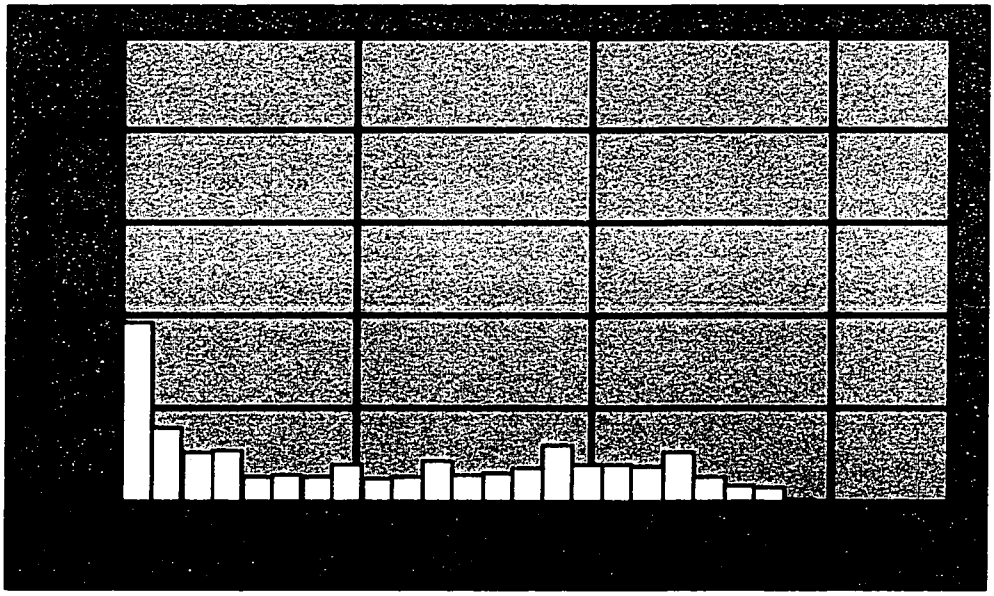

Figure 3.6: Porosity distribution within the Hanifa Reservoir in Berri Field

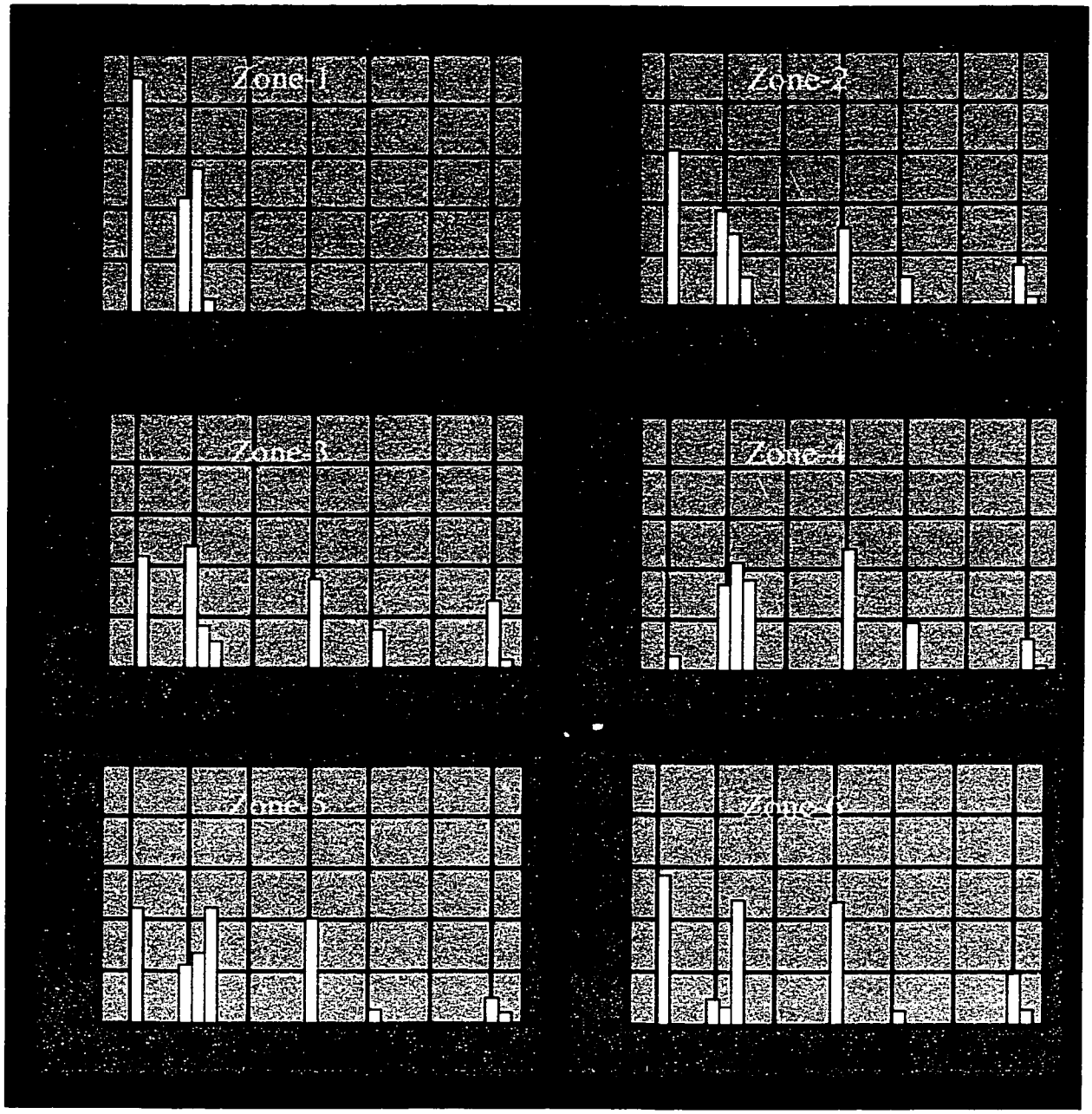

Figure 3.7: Facies distribution in reservoir zones 1 to 6.

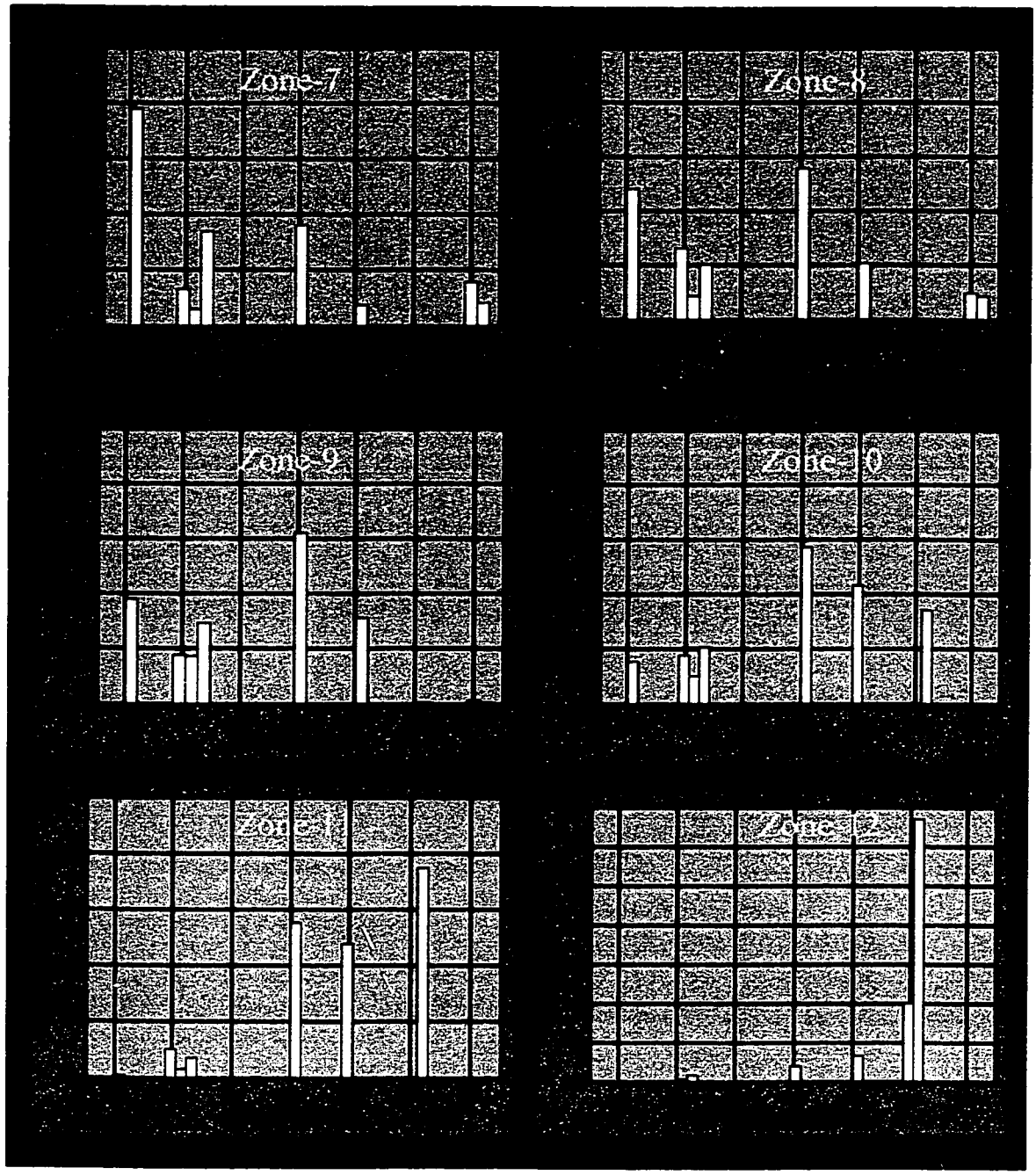

Figure 3.8: Facies distribution for reservoir zones 7 to 12.

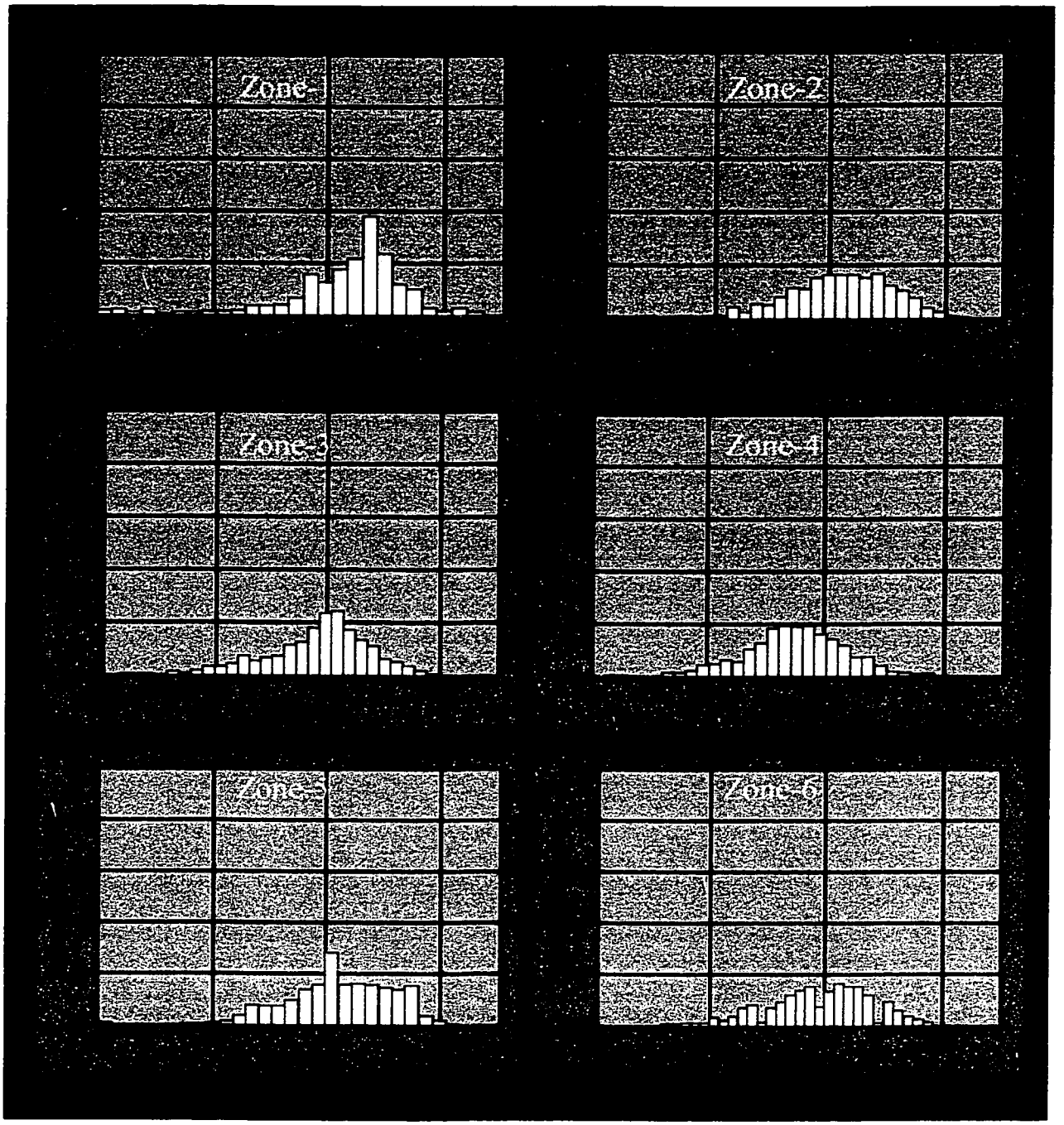

Figure 3.9: Porosity distribution in reservoir zones 1 to 6.

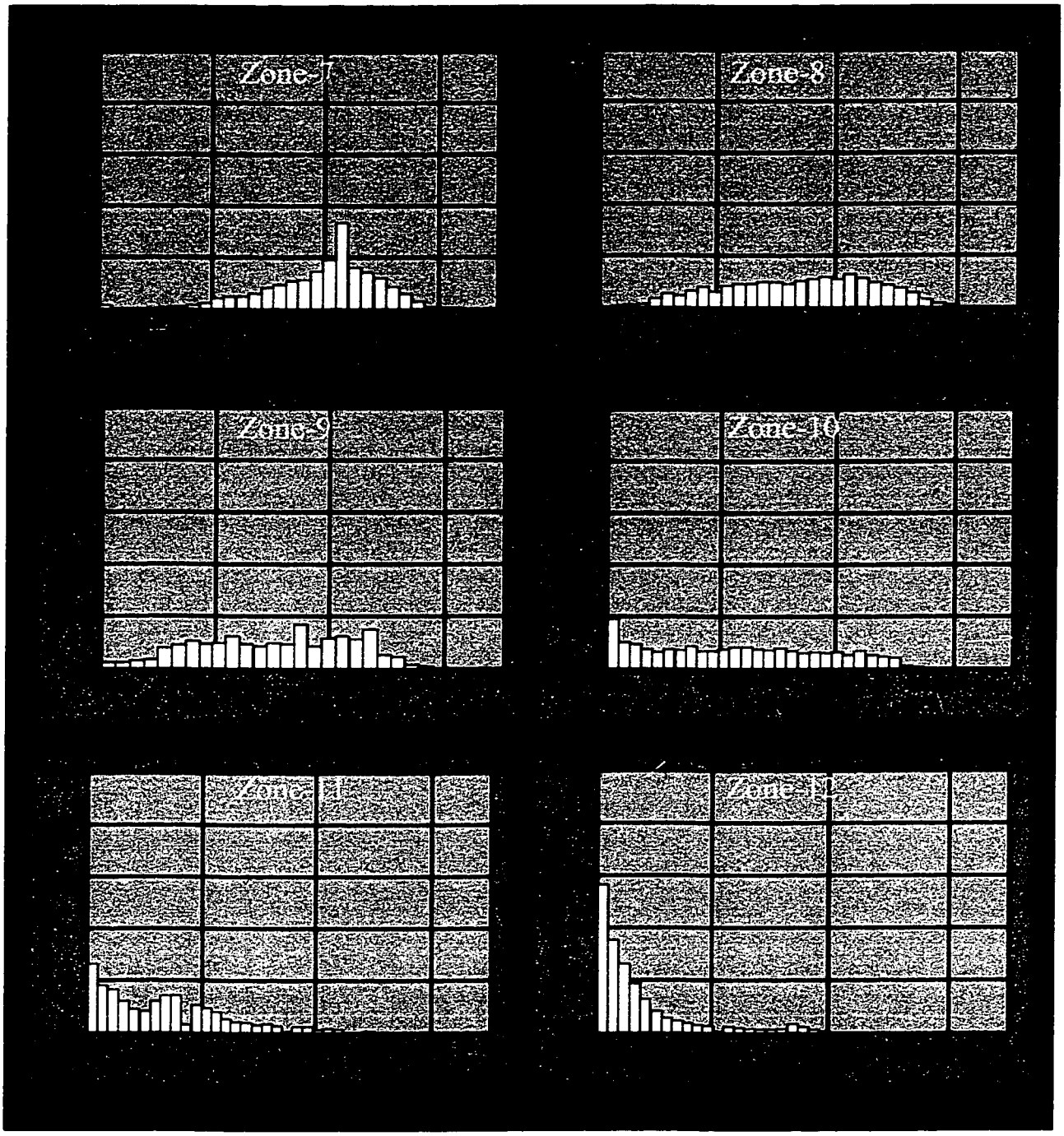

Figure 3.10: Porosity distribution in reservoir zones 7 to 12.

Zone Number	average	median	minimum	maximum	standard deviation	skewness coefficient
1	0.21	0.22	0.00	0.37	0.059	-1.385
2	0.20	0.21	0.01	0.31	0.054	-1.004
3	0.19	0.20	0.01	0.32	0.048	-0.765
4	0.18	0.18	0.01	0.30	0.044	-0.293
5	0.21	0.21	0.00	0.34	0.048	-0.731
6	0.19	0.20	0.06	0.30	0.046	-0.400
7	0.19	0.21	0.05	0.30	0.046	-0.400
8	0.20	0.20	0.00	0.32	0.050	-0.180
9	0.15	0.15	0.00	0.35	0.067	-0.147
10	0.11	0.10	0.00	0.29	0.077	0.229
11	0.07	0.06	0.00	0.26	0.056	0.839
12	0.04	0.02	0.00	0.26	0.047	1.940

Table 3.2: Main porosity statistical parameters for reservoir zones in Hanifa Reservoir

3.3 Bivariate Analysis

Normally, bivariate analysis is a useful tool to understand the linear relationships between two variables. The correlation between two variables could be one of three types: positive, negative and no correlation. Positive correlation occurs if the values of variable X are increasing with the increase in values of variable Y. A negative correlation occurs when values of variable X increase at the expense of values of variable Y and vice versa. No correlation reflects that there is no relation between the values of variable X and value of variable Y.

A correlation has to be established between the primary variable and the secondary variable before any data integration can take place. The correlation coefficient is generally used to quantitatively summarize the linear relation between two variables. The correlation coefficient ranges from +1 to –1. The spread and shape of the scatter plot cloud of two variables indicate the type of correlation that they have. It is considered a very useful tool in quantifying erroneous data.

The porosity and impedance cross-plot for 22 wells that have impedance logs, shows a double trend and some noise, figure 3.11. After investigating this phenomenon, this observation was due to five wells that have been processed differently than the rest of wells, figure 3.12. These wells do not have density logs, so a constant density value was assigned to them. This assigned density was used to compute the impedance log at the wells, which has resulted in an unreliable impedance log. By removing these wells for the cross plot, a very strong relationship between porosity and impedance has appeared as shown in figure 3.13. The correlation between porosity and impedance has increased from

-0.74 to –0.97. Based on this, the seismic impedance is considered as a good estimator of porosity in Hanifa Reservoir.

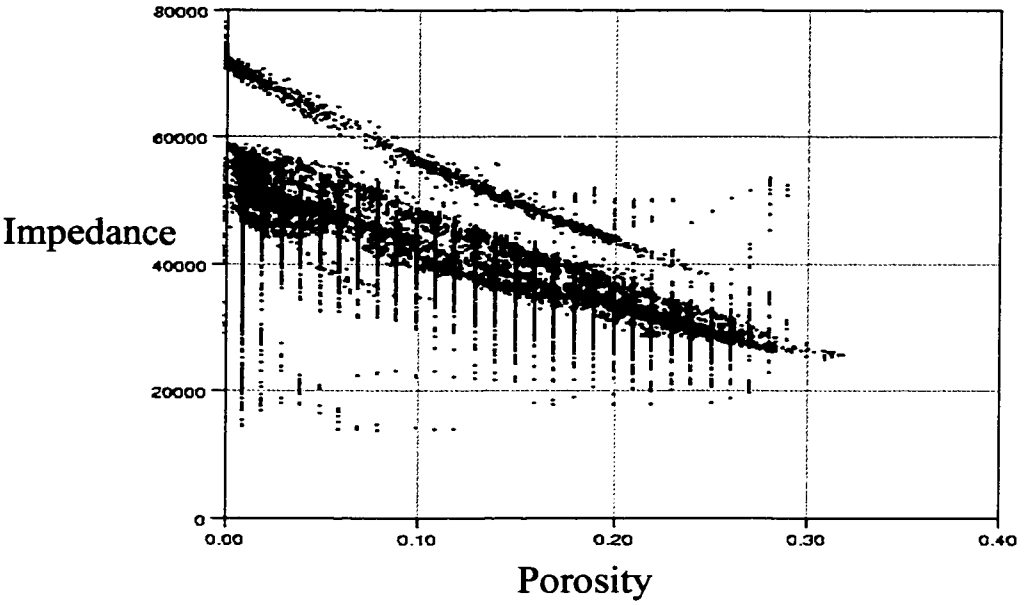

Figure 3.11: Porosity and impedance cross-plot for all wells

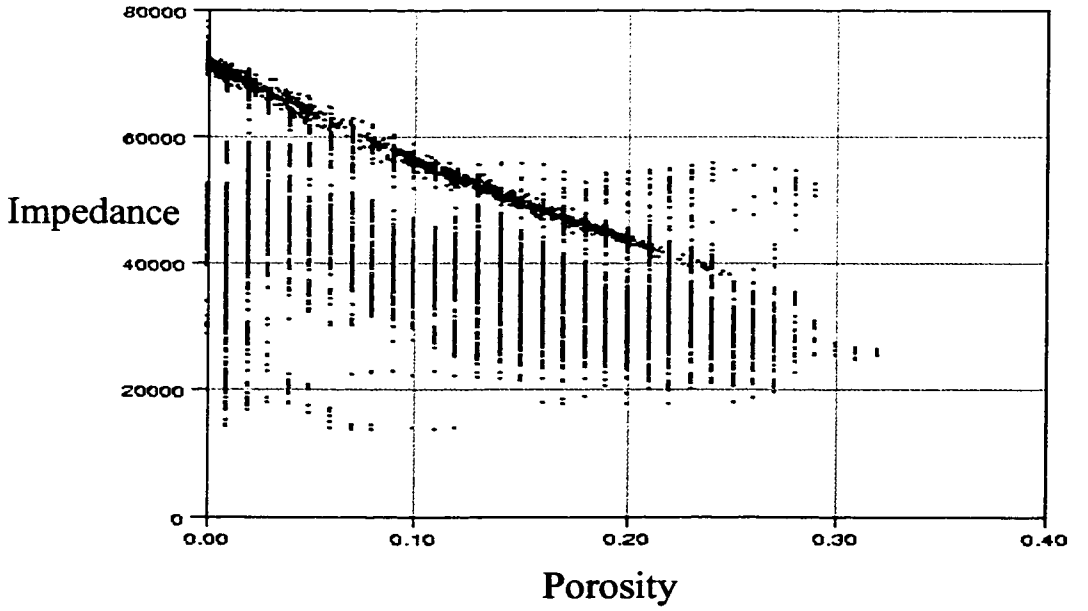

Figure 3.12: Porosity and impedance cross-plot for the 5 wells that have problems in impedance.

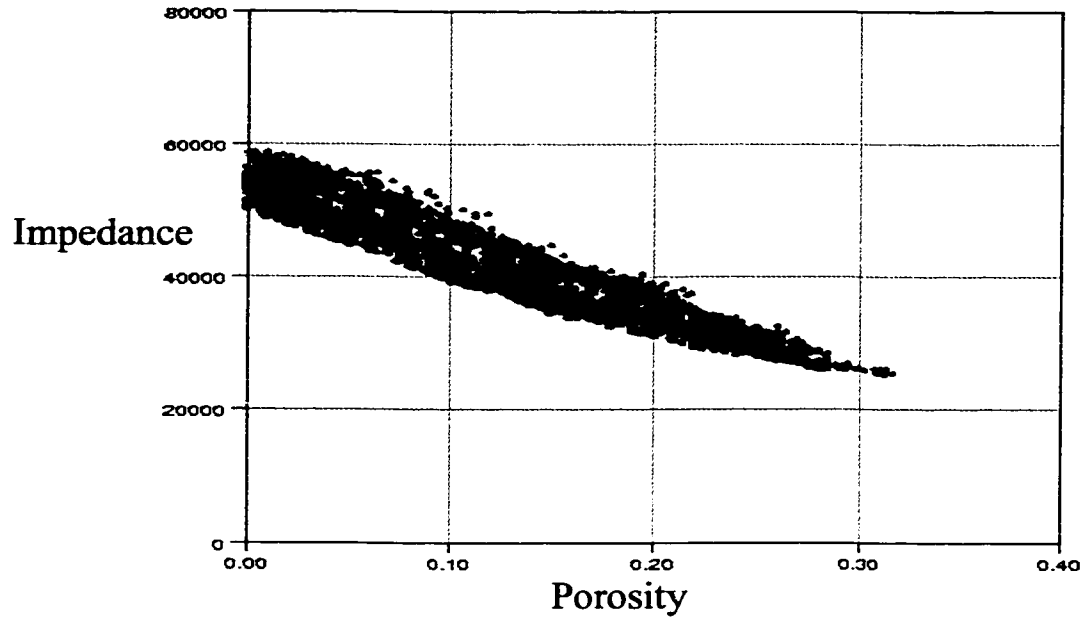

Figure 3.13: Porosity and impedance cross-plot for wells that have correct impedance.

No useful impedance-facies relationship has been found, as shown in figure 3.14. This means that impedance is not a good indicator for facies variations in Hanifa Reservoir in Berri Field and, it should not be used as secondary data in facies modeling.

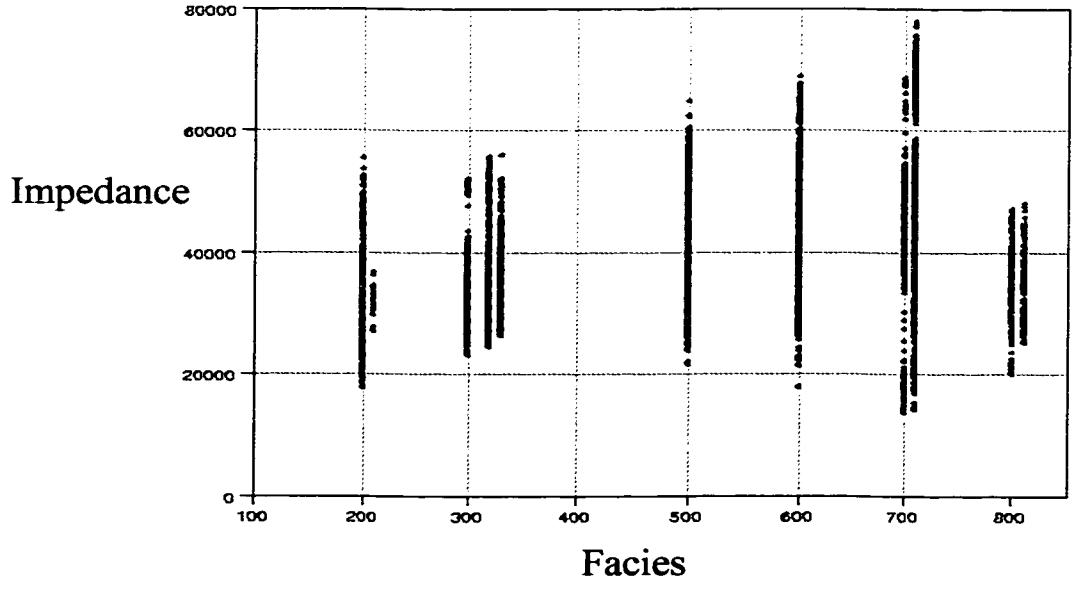

Figure 3.14: Facies and impedance cross-plot

3.4 Spatial Analysis

Geostatistical techniques are computationally intensive, however they produce more reliable results. Most geostatistical methods are based on need semi-variograms parameters to generate 2-D or 3-D models. The quality of the simulation results depends on the time taken to choose an appropriate semi-variogram model. Needless to say, poor semi-variogram models may produce estimates that are worse than other simple interpolation methods such as least square. Also, the semi-variogram models should not create information that contradict the geological understanding of the area based on core and log studies. In other words, geological controls should be observed in semi-variogram facies models.

In this study, semi-variograms are calculated for facies and porosity. A qualitative interpretation of the facies semi-variogram is conducted to check the accuracy of these models.

3.4.1 Facies Semi-Variogram

Grouping Procedure

The first geostatistical model to be built is the facies model. As observed in the univariate analysis in section 3.2, there is a strong relationship between facies and porosity distribution. If the spatial facies distribution in 3-D could be predicted, then this would help in predicating the 3-D porosity spatial distribution. In other words, the objective for building a 3-D geostatistical facies model is to use it as a guide for porosity modeling.

Eleven depositional facies are defined in the Hanifa Reservoir. In order to simplify and speed up the modeling process, a decision to group facies with similar

characteristics was implemented. To apply this, geological depositional settings, as well as reservoir quality and distribution of each facies within the reservoir have been reviewed. Porosity distribution histograms for each facies (figure 3.15) and core porosity and permeability cross plots (figure 3.16) have been generated for each facies to observe differences and similarities within each facies.

Facies, which have similar porosity distribution and core porosity and permeability cross-plots, were grouped together such as facies 3, 3.2 and 3.3. On the Other hand, facies that have distinct porosity distribution and core porosity and permeability cross-plots were kept separate such as facies 5 and facies 6. Based on this work, these eleven depositional facies have been grouped into six facies groups as shown in table 3.3.

Depositional Facies	2, 2.1	3, 3.2, 3.3	5	6	7, 7.1	8, 8.1
Grouped Facies	2	3	5	6	7	8

Table 3.3: Depositional facies grouping used in this study for Hanifa Reservoir.

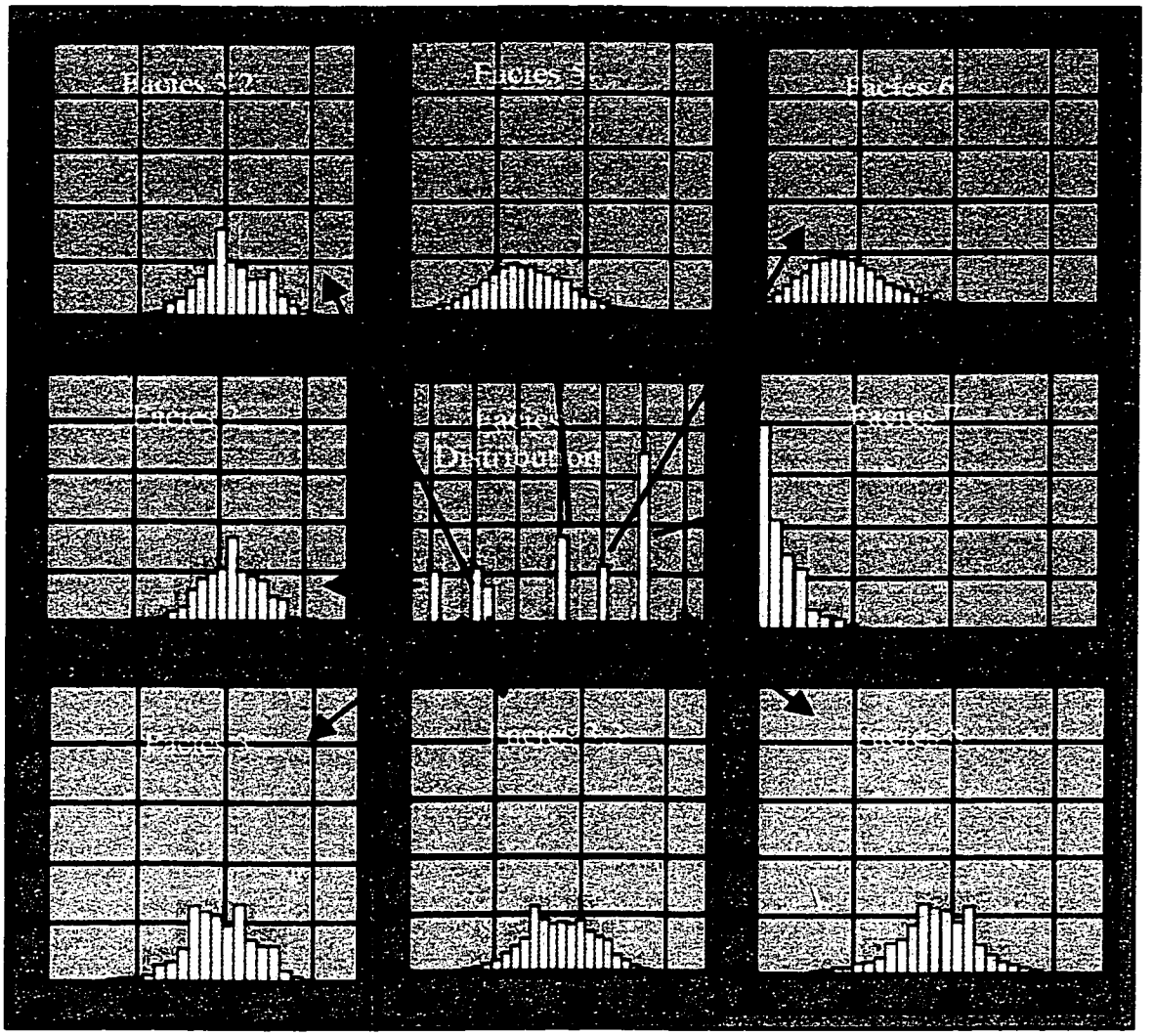

Figure 3.15: Porosity distribution histograms for each facies in the Hanifa Reservoir.

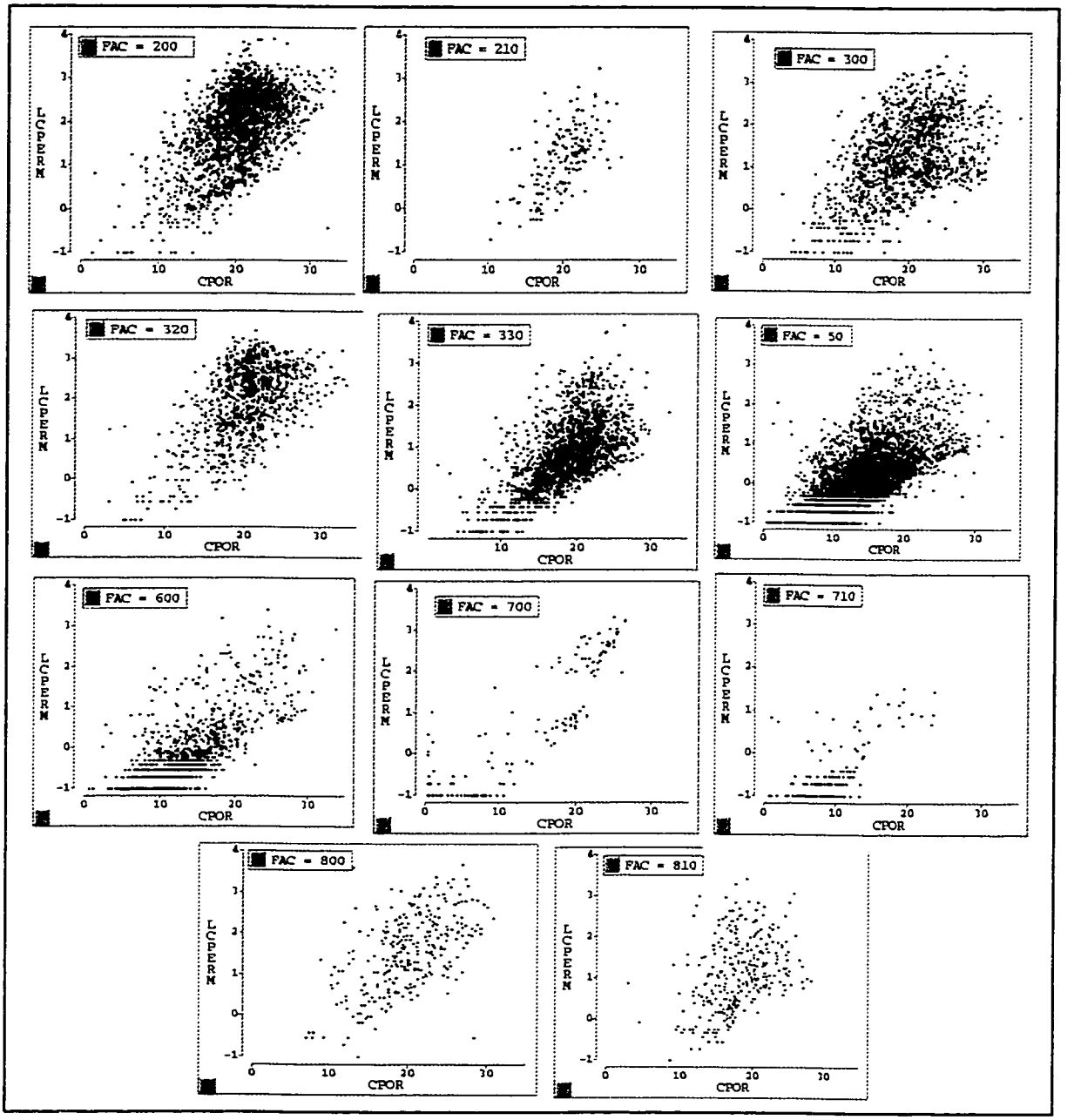

Figure 3.16: Core porosity and core permeability cross plots for depositional facies in Hanifa Reservoir.

Semi-variogram Computation and Modeling

The next step was to calculate the lag sizes that are appropriate for this study. Four possible lag sizes have been selected which are 1000, 1500, 2000 and 3000 meters, figure 3.17. Lag size 1500 meters was selected because it gave us good distribution of pairs per lag increment. Lag size of the vertical semi-variogram will be ½ foot, which is the same as the facies log resolution.

Semi-variograms were calculated in omni-direction and in multi directions for each grouped facies for the whole reservoir. The results from this step were poor as in figure 3.18. This is because some facies group exists only on the upper part of the reservoir while another exists at the lower part. Based on these results, semi-variograms were calculated in the reservoir zone in which these facies are dominant. The results were very good, which meant that these facies groups tend to be constrained by reservoir zonation and have certain spatial and vertical correlation as expected from the depositional model and the facies univariate analysis. Next was to calculate vertical semi-variograms for each facies groups. Tables 3.4 and 3.5 show the main vertical and directional semi-variogram parameters. Figure 3.18 shows examples for semi-variograms calculated for facies group 2. More semi-variogram examples are shown in the appendices.

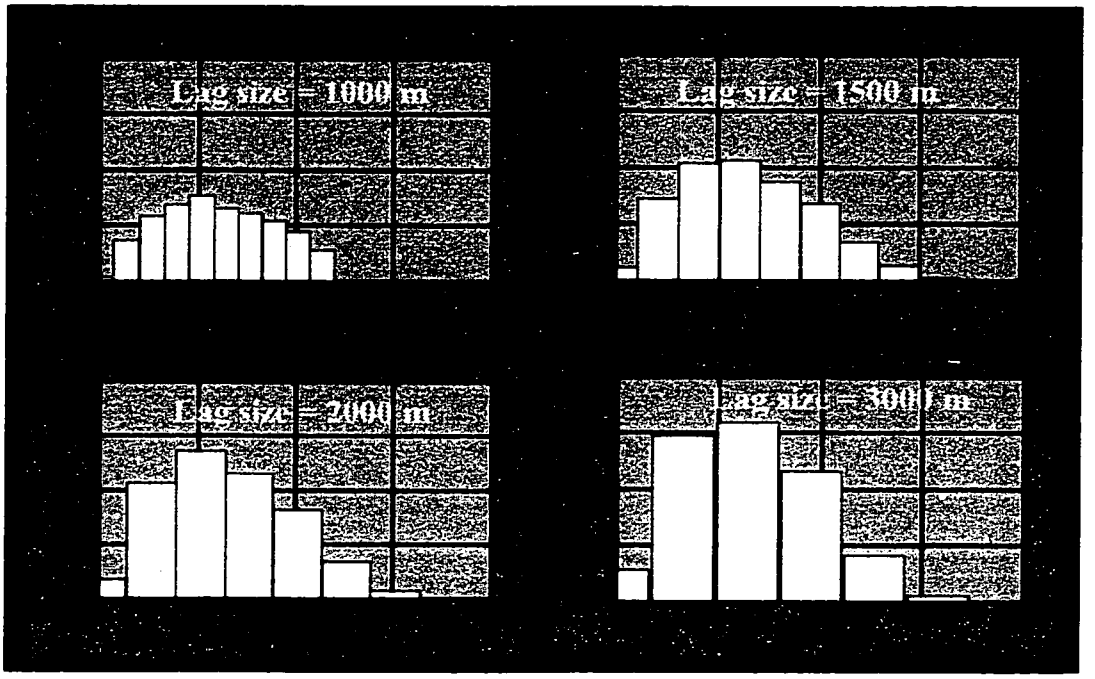

Figure 3.17: Four different lag sizes selected and tested for this study.

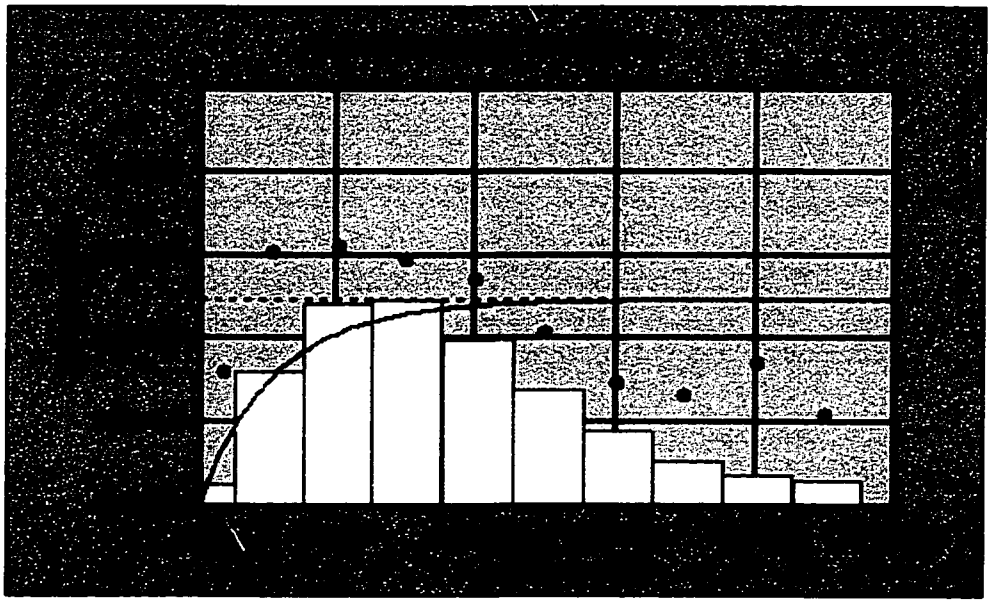

Figure 3.18: An example for a poor semi-variogram that was calculated for facies 2 by data from the full reservoir

Facies Group	Range (Meter) X	Range (Meter) Y	Sill	Model	Nugget	Azimuth	Anisotropy Ratio
2	5294	4280	0.20	Exponential	0	-33	1.5:1
3	4277	3154	0.25	Exponential	0	-30	1.4:1
5	3410	2916	0.17	Exponential	0	-14	1.1:1
6	3400	2920	0.07	Exponential	0	-19	1.2:1
7	3815	3571	0.14	Exponential	0	-9	1.1:1
8	4971	3452	0.07	Exponential	0	-33	1.4:1

Table 3.4: Main directional semi-variogram for grouped facies

Facies Groups	Range	Sill	Model	Nugget
2	6.5	0.10	Spherical	0
3	4.7	0.14	Exponential	0
5	4.8	0.08	Exponential	0
6	4.9	0.06	Exponential	0
7	8.4	0.04	Exponential	0
8	9.7	0.04	Exponential	0

Table 3.5: Main vertical semi-variogram for grouped facies

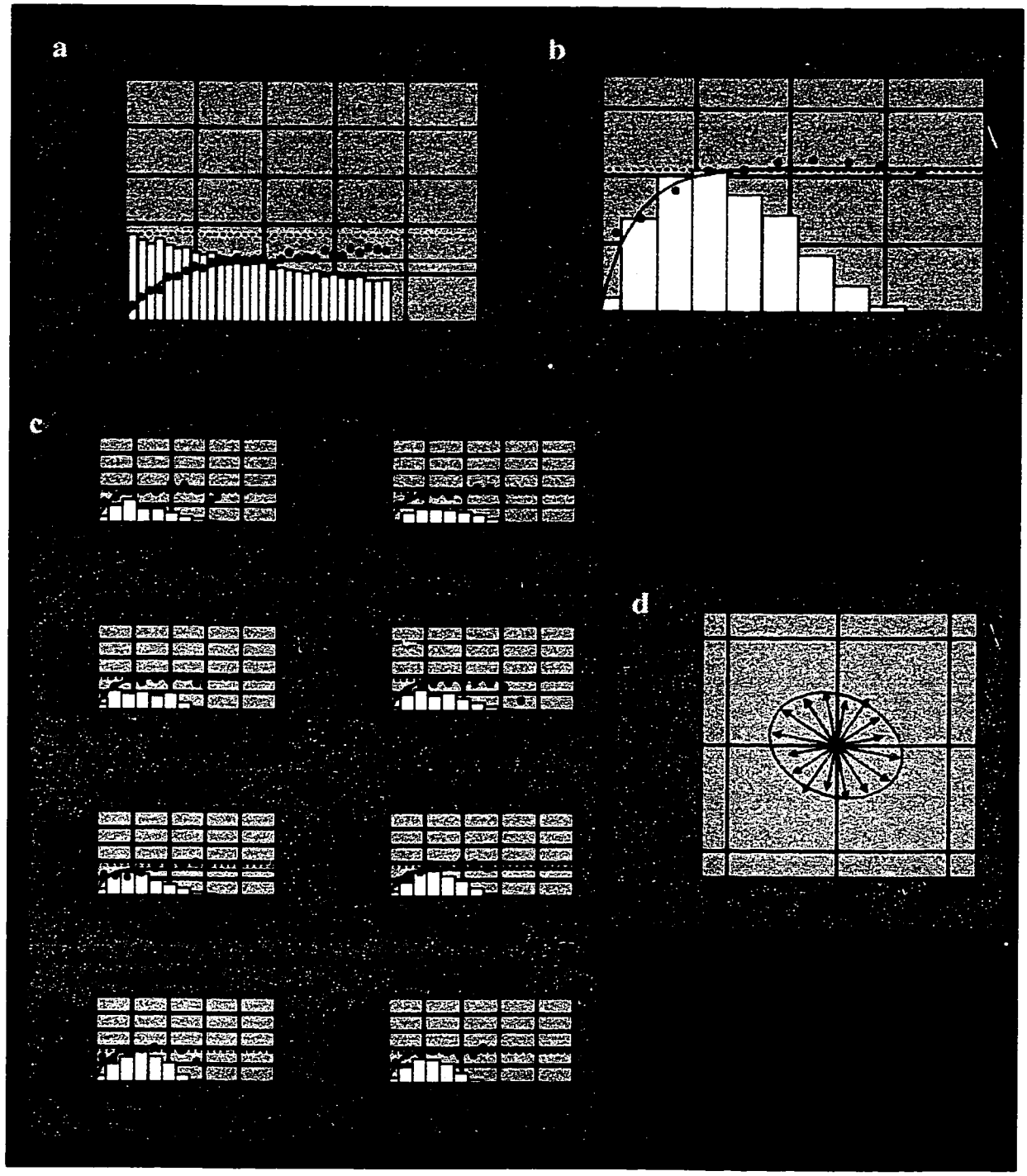

Figure 3.18: Example for semi-variograms calculated for facies group 2, a-vertical, b-omnidirectional, c and d directional semi-variogram.

Facies Semi-Variogram Interpretation

Along with this thesis work a study was conducted to understand the geological controls that affect semi-variograms behavior. This study covered the full Hanifa Reservoir in Berri Field and utilized the information of 200 wells (Al-Khalifa and Makkawi, 2001).

Although this thesis work is based on a sector area in the Berri Field and utilized the information from 97 wells only, the results of the semi-variogram calculation and modeling came very close to what have been presented in the above-mentioned study. One of the most important interpretations introduced in that work is the role of paleo-structure. It is clearly shown that the time of deposition is the dominant factor affecting facies distribution. Also, facies are laterally distributed from north to south, independently of the current structure. Most of the models display linear shape at the origin, which means that they have average continuity. The low sill values in the vertical direction, especially facies group 7, indicate the absence of layering within a facies group. Full details about this issue is shown is (Al-Khalifa and Makkawi, 2001).

3.4.2 Porosity Semi-Variogram

In this step we are going to utilize what has been found when calculating the facies semi-variogram. The selected horizontal lag size is 1500 meters because it gives the optimum number of pairs and helps to capture the spatial distribution of porosity. The lag size for the vertical semi-variogram is ½ foot, which is the same as the porosity log resolution. The calculations were conducted for every reservoir zone

to capture the porosity distributions. The main parameters of the vertical semi-variograms are shown in table 3.6, and for the directional ones in table 3.7.

Zone Number	Range (meters)	Sill	Model
1	7.2	0.002	Spherical
2	7.3	0.002	Spherical
3	5.5	0.001	Spherical
4	5.9	0.001	Spherical
5	7.2	0.001	Spherical
6	6	0.001	Spherical
7	6.6	0.001	Spherical
8	8.1	0.001	Spherical
9	7.6	0.001	Spherical
10	7.8	0.001	Spherical
11	7.2	0.001	Spherical
12	8.6	0.0007	Spherical

Table 3.6: Main parameters for porosity vertical semi-variogram.

Zone	Range (meters)		Sill	Model	Nugget	Azimuth	Anisotropy
Number	X	Y					Ratio
1	3468	2440	0.002	Exponential	0	-24	1.4:1
2	2543	2440	0.003	Exponential	0	-21	1:1
3	3410	2440	0.003	Exponential	0	-36	1:1
4	2254	2916	0.002	Exponential	0	-36	0.8:1
5	3005	3154	0.001	Exponential	0	-36	1.1:1
6	3236	2976	0.001	Exponential	0	-38	1.1:1
7	3410	3333	0.002	Exponential	0	-38	1:1
8	3410	2976	0.003	Exponential	0	-43	1.1:1
9	2254	3452	0.001	Exponential	0	-43	0.7:1
10	3283	3035	0.001	Exponential	0	-43	1.3:1
11	3699	2678	0.002	Exponential	0	-23	1.4:1
12	3641	3809	0.001	Exponential	0	-23	1:1

Table 3.6: Main parameters for porosity directional semi-variogram.

CHAPTER 4

GEOSTATISTICAL MODELING AND VALIDATION

4.1 Workflow

The modeling workflow will vary slightly from one modeling method to another depending on the type of data being modeled. The general modeling workflow for this study is shown in figure 4.1.

4.1.1 Simple Geostatistical Models

For simple geostatistical models where one type of data is used, such as porosity or facies from wells only, the modeling sessions will start by selecting wells in the study area excluding ten randomly selected wells, which have been selected in the previous chapter. Next, the 12 zones markers will be selected to define the vertical dimension of

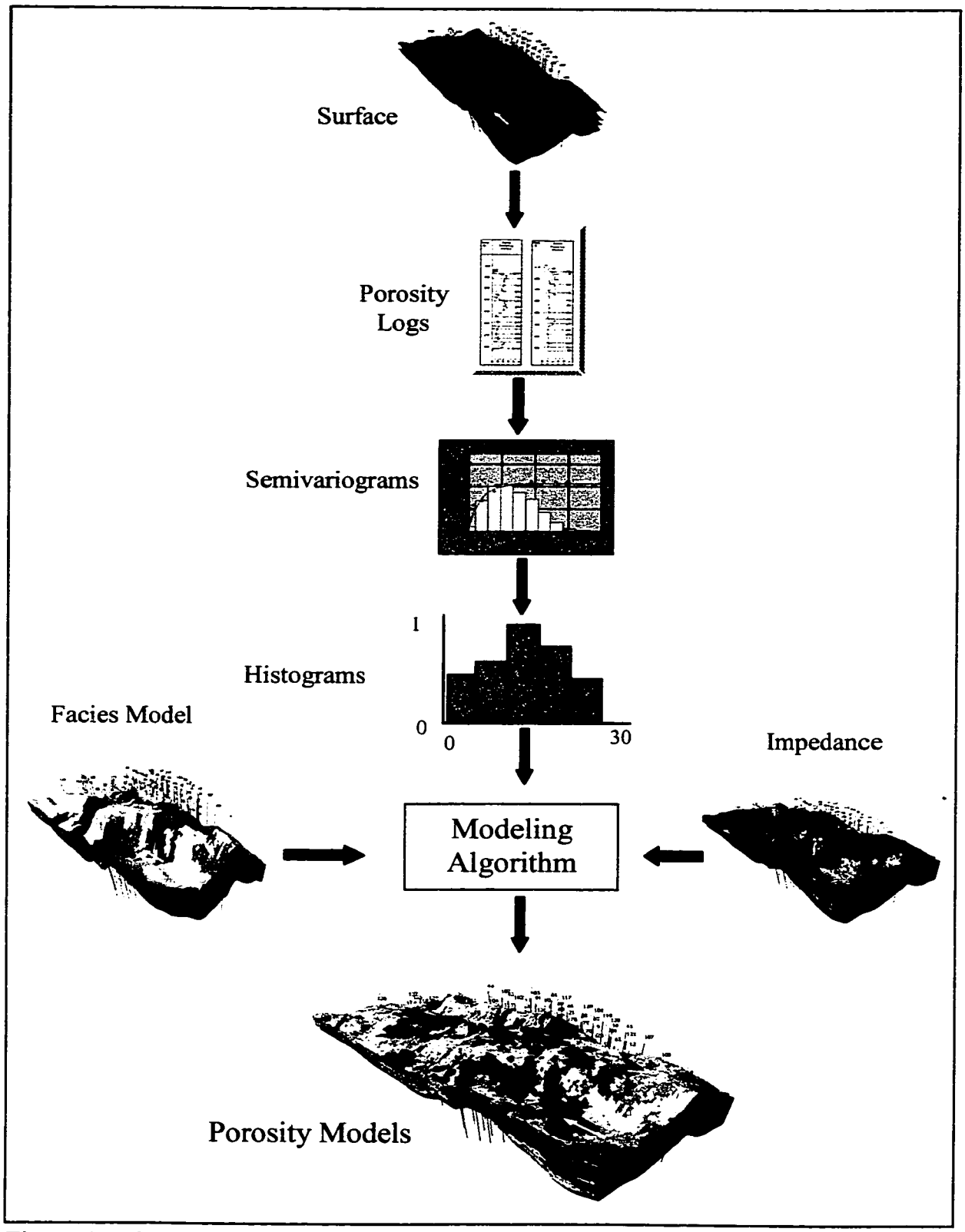

Figure 4.1: Generalized modeling workflow for this study.

each zone. This is followed by selecting the type of data to be modeled, whether continuous or discrete. That will be followed by defining the model geometry as described in section 3.1. Next, all structure maps of the different reservoir zones will be loaded. An appropriate modeling technique with the proper semi-variograms and histograms will be selected to simulate porosity values at each cell within the defined model geometry. This will complete the modeling work and the generated model will be validated for quality and accuracy.

4.1.2 Integrated Geostatistical Models

For the other models where different data types are integrated, the change will be in the modeling step. In this step, soft data will be selected (seismic, facies or both). A correlation coefficient between hard and soft data or histograms for soft data will be input to define the relation between the hard and soft data. Then the simulation will be performed and the generated models validated. Computation time for this type of model will take longer than for simple models because different data types must be accounted for. For each porosity modeling method, ten realizations will be generated. These realizations are sufficient for the scope of this study.

4.1.3 Model Validation

The validation will be done qualitatively and quantitatively. In the qualitative approach the input data histograms will be compared to the model histograms in order to check whether the software and algorithms reproduce the input data statistics. Several

model slices and cross sections will be generated to visualize the model results. The depth and location of the model slices and cross sections will be the same for all models. This will help in comparing the porosity distribution from the different models.

The quantitative approach will be to estimate the porosity trace at each location for the ten wells that have been excluded from the model. Figure 4.2 shows the locations of these wells. A correlation coefficient will calculated between the actual porosity trace and the simulated trace for each realization. There are ten realizations for each of the four modeling methods and ten wells to be utilized in this step.

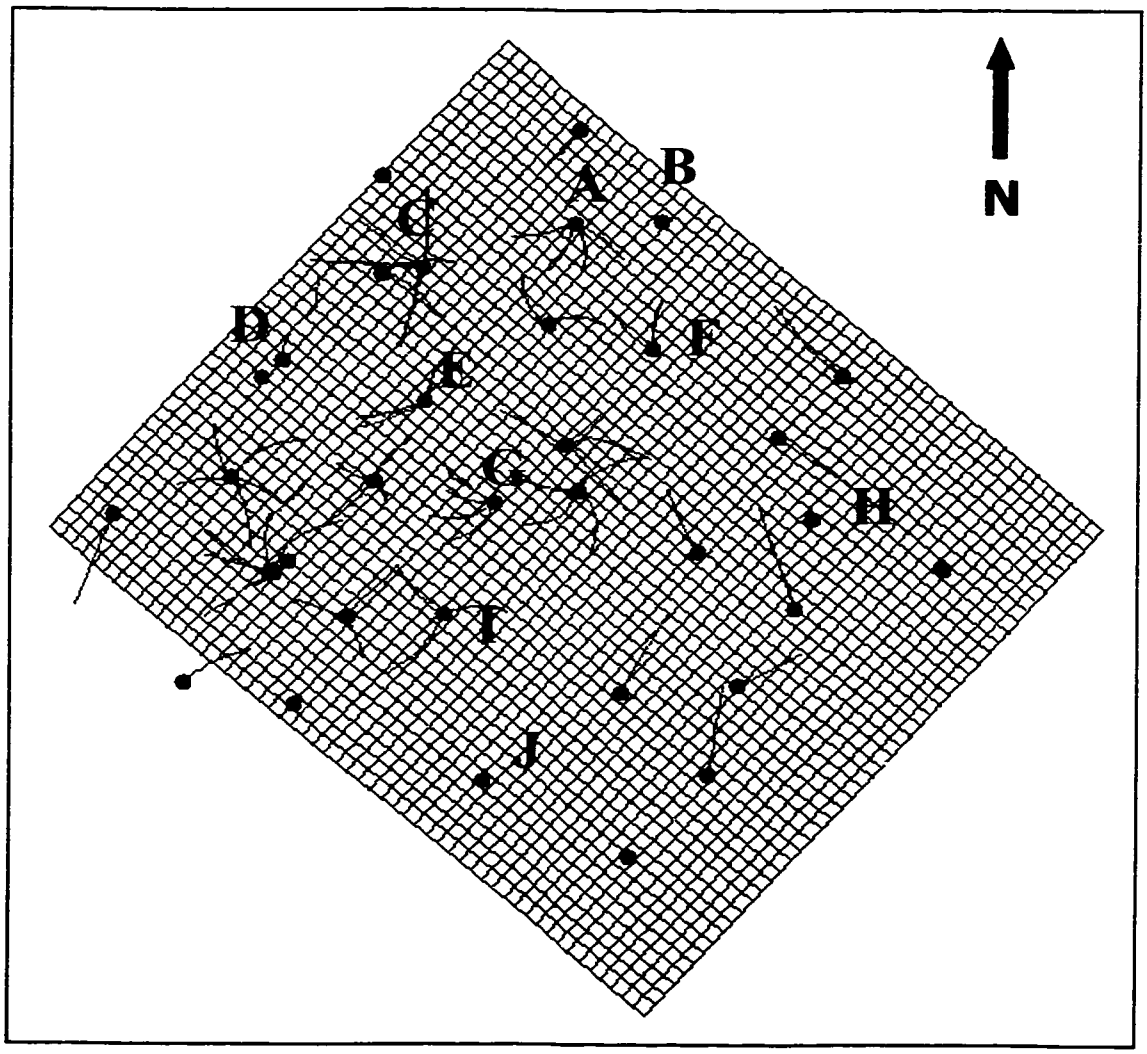

Figure 4.2: Location of the ten wells to be used in the validation step

4.2 Facies Modeling

The first geostatistical model to be generated was the facies model. It was used as a guide for porosity simulation. Facies model have been successfully used to improve 3-D porosity distribution (Al-Qassab et al.; 2000). The method used to generate the facies model is the Sequential Indicator Simulation (SIS). It is one of the sequential simulation algorithms, mostly used for categorical data such as facies. The algorithm converts the property being modeled to binary values of 1 or 0. Then a local cumulative density function (cdf) is determined using indicator kriging. A uniformly distributed random number in (0,1) samples generates the cdf. Then the sample value is back-transformed. Each newly simulated node value becomes part of the values for subsequently simulated nodes. The process is continued until all nodes are simulated. (Daly, 1994)

This facies model was generated by using logs from 87 wells, which were interpreted based on core description and porosity logs. Facies have been defined into six main groups as shown in section 3.4.1. Vertical and directional facies semi-variograms along with the facies histogram have been utilized, table 3.3.

To check the quality of the generated facies model, several model slices have been generated and displayed in figure 4.3. Also, two cross sections across the model have been created as shown in figure 4.4 and 4.5.

The model slices start with layer 2, which is at the upper part of the reservoir, and end with layer 106, which is at the lower most part. Most of the facies groups are showing high continuity in the NW-SE direction. The model slices show that facies groups 2 and 3 are the most dominant in the upper layers and their occurrence, generally, decreases until they terminate in the lower zones.

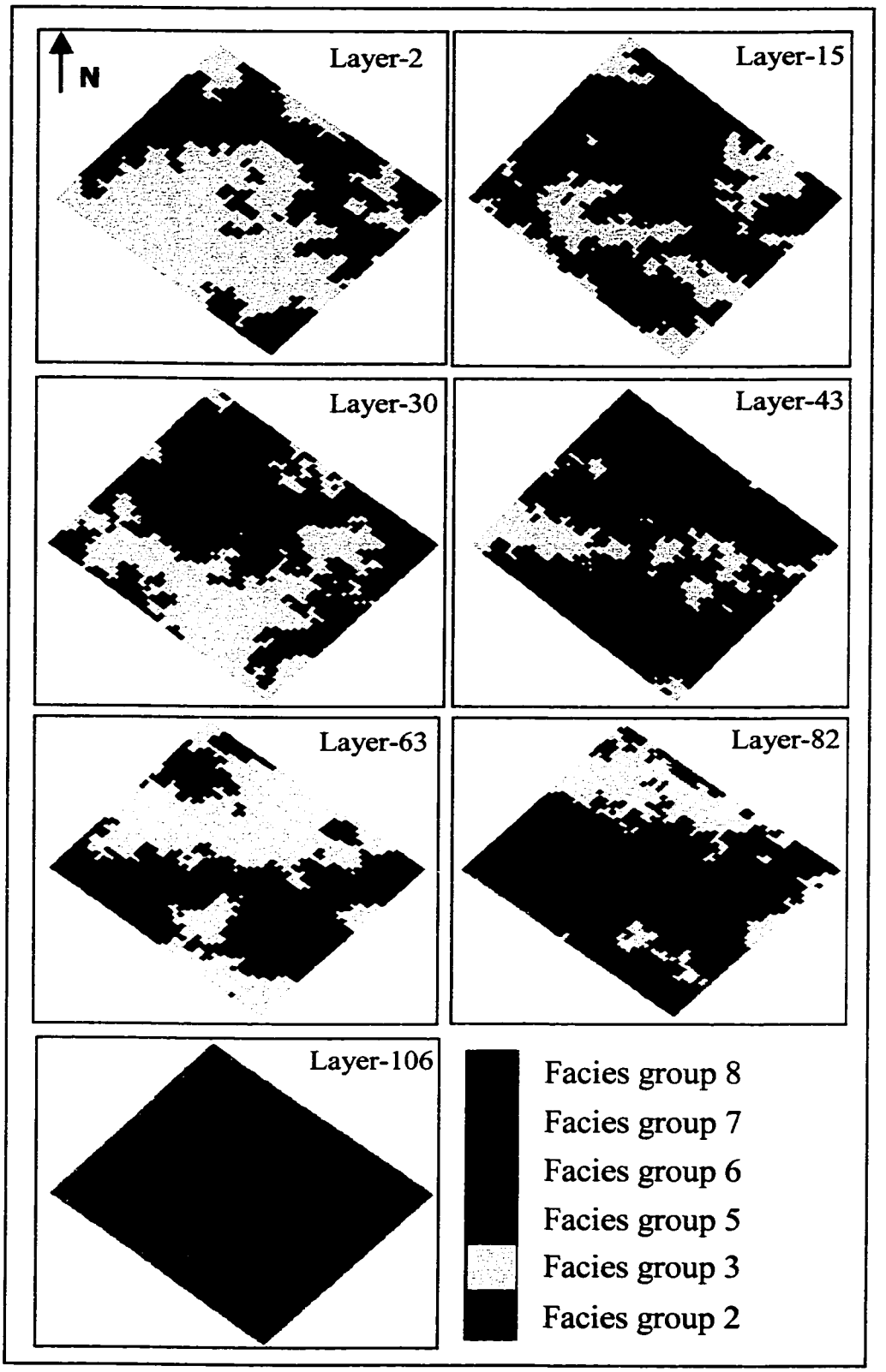

Figure 4.3: Different slices through the facies model

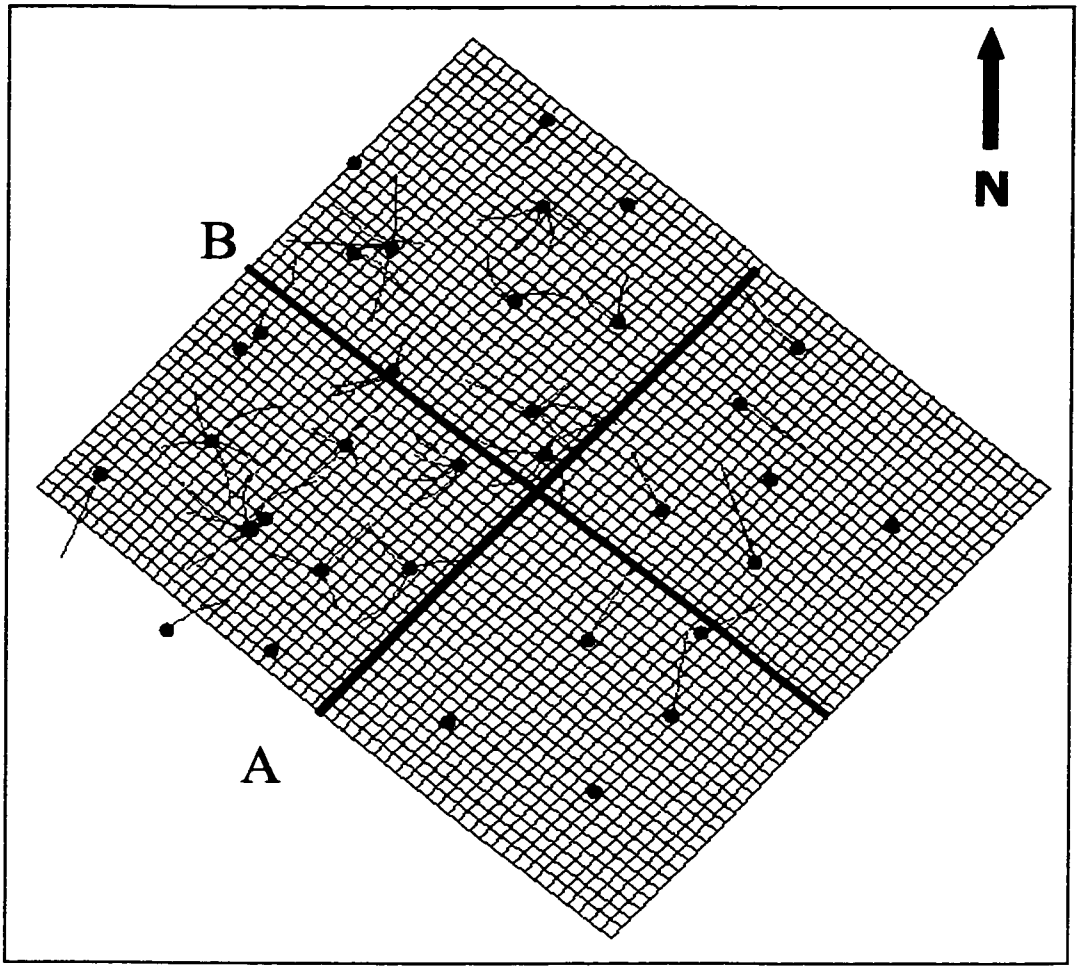

Figure 4.4: Location of cross sections A and B across the study area

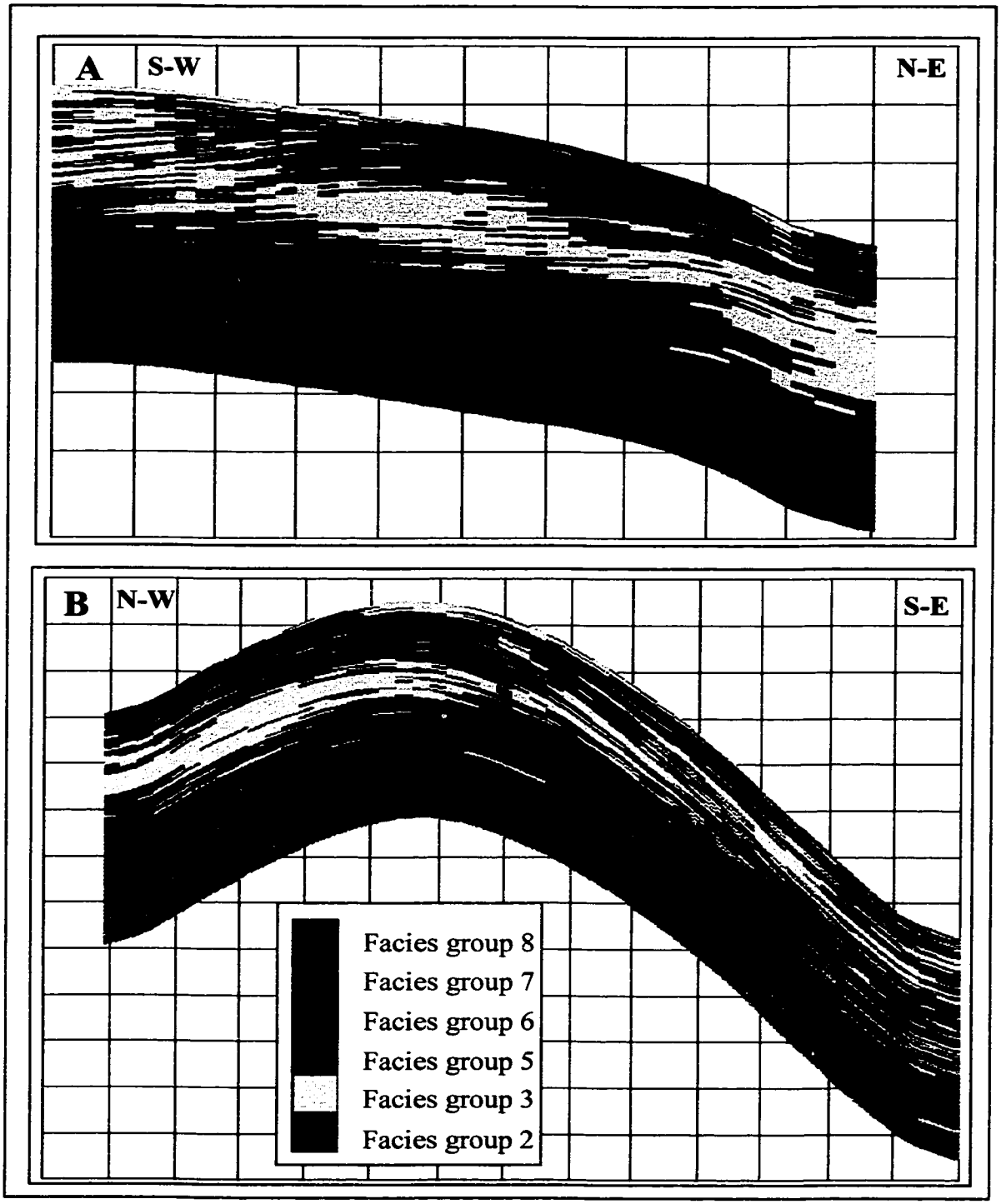

Figure 4.5: Cross section A and B across facies model

Facies group 7 only occurred at the lower part of the reservoir. Facies group 8 is generally restricted to the middle reservoir zones.

Cross sections A and B, figure 4.5, display the vertical and lateral facies distribution. The lower part of the cross section is dominated by mudstone -facies group 7- in all parts of the study area. The middle part is a mixture of packstone and wackestones -facies group 5 and 6- with mostly packstones overlying wackstones. The grainstone-rich facies, facies group 2 and 3, dominates the upper part of the reservoir. This represents a coarsing upward sequence according to the 1991 Saudi Aramco study.

Cross section A displays the lateral facies changes in the Hanifa Reservoir. The grainstone rich facies at the N-E area changes laterally to packstones, then to wackestones and to mudstones at the S-W area. Our geological understanding of the reservoir confirms these observations, which increases the confidence in this facies model and its ability to represent the reservoir (Saudi Aramco, 1991).

4.3 Porosity Modeling

In this study four porosity model methods will be generated by using different geostatistical modeling techniques. The first model will be generated by using porosity logs from wells only. Seismic impedance will be used as soft data in the second porosity model. The third model will be generated based on the facies model presented in section 4.2. By utilizing seismic impedance and facies models along with porosity from well logs, a fourth porosity model will be generated.

4.3.1 Well Data Models

The first porosity model will be generated from well porosity logs by using Sequential Gaussian Simulation (sGs) algorithms. Principles of Sequential Gaussian Simulation method have been reviewed in section 2.3.4. The porosity semi-variograms and histograms, which have been computed in section 3.2 and 3.4.2, were used in generating this model. Ten realizations have been created by this modeling method and they were used in the validation part.

The first part of the qualitative validation is to check the reliability of this model by comparing histograms of the simulated values with input data histograms. This comparison is done for every reservoir zone as shown in figures 4.6 and 4.7. They have the same distribution type, which indicates that the sGs has preserved, generally, the statistical characteristics of the input data. Several slices were created through the first realization of this method, figure 4.8, as well as two cross sections, figure 4.9. The model slices and the cross sections show that porosity, generally, decreases from top to bottom, which is related to compaction and to the type of depositional facies. The grainstones rich

facies, which are facies group 2,3 and 8, have high porosity and the mudstone facies, which is facies group 7, have low porosity.

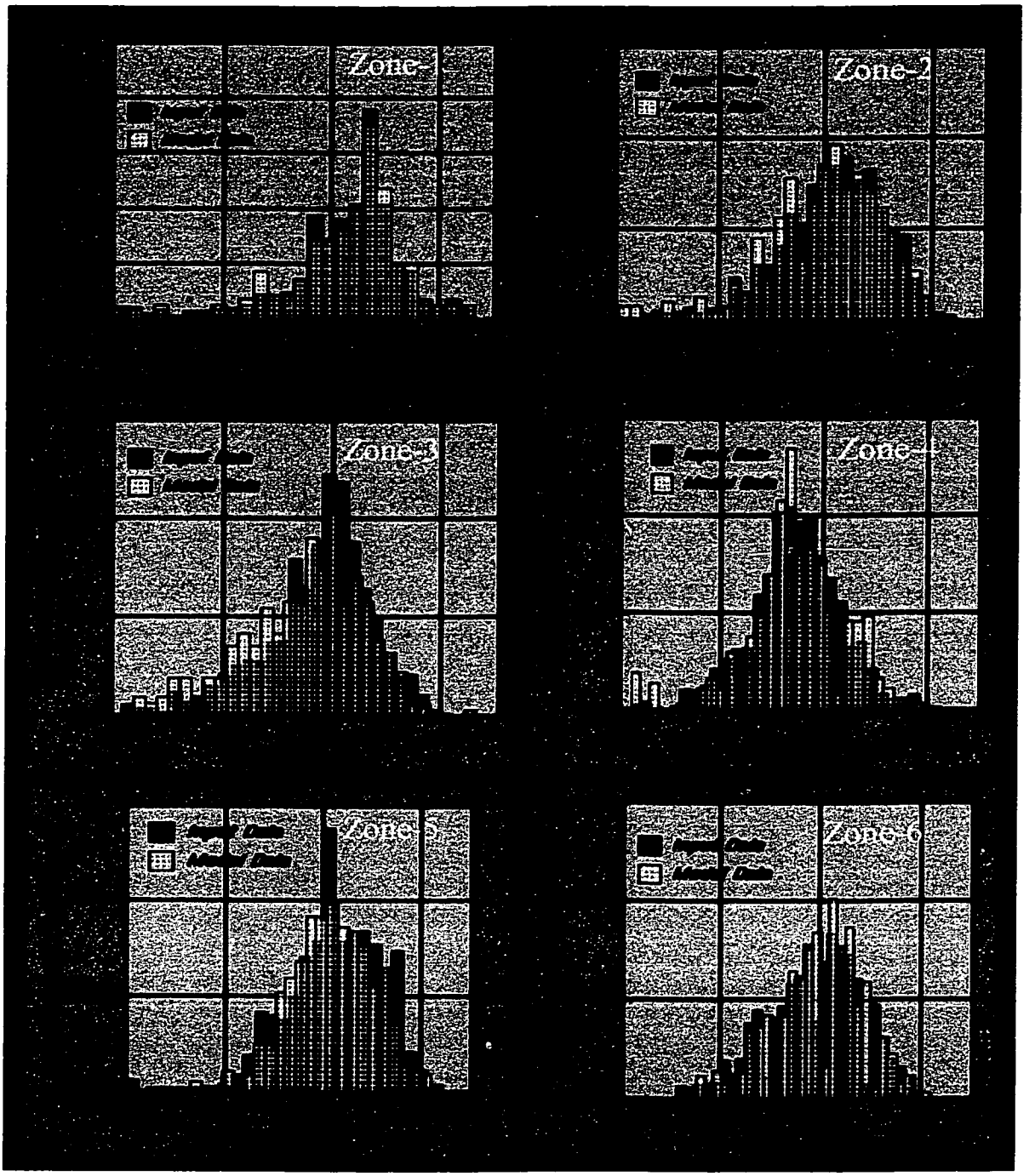

Figure 4.6: Comparison of histograms for observed and simulated values obtained from Sequential Gaussian Simulation and input data histograms for reservoir zones 1 to 6.

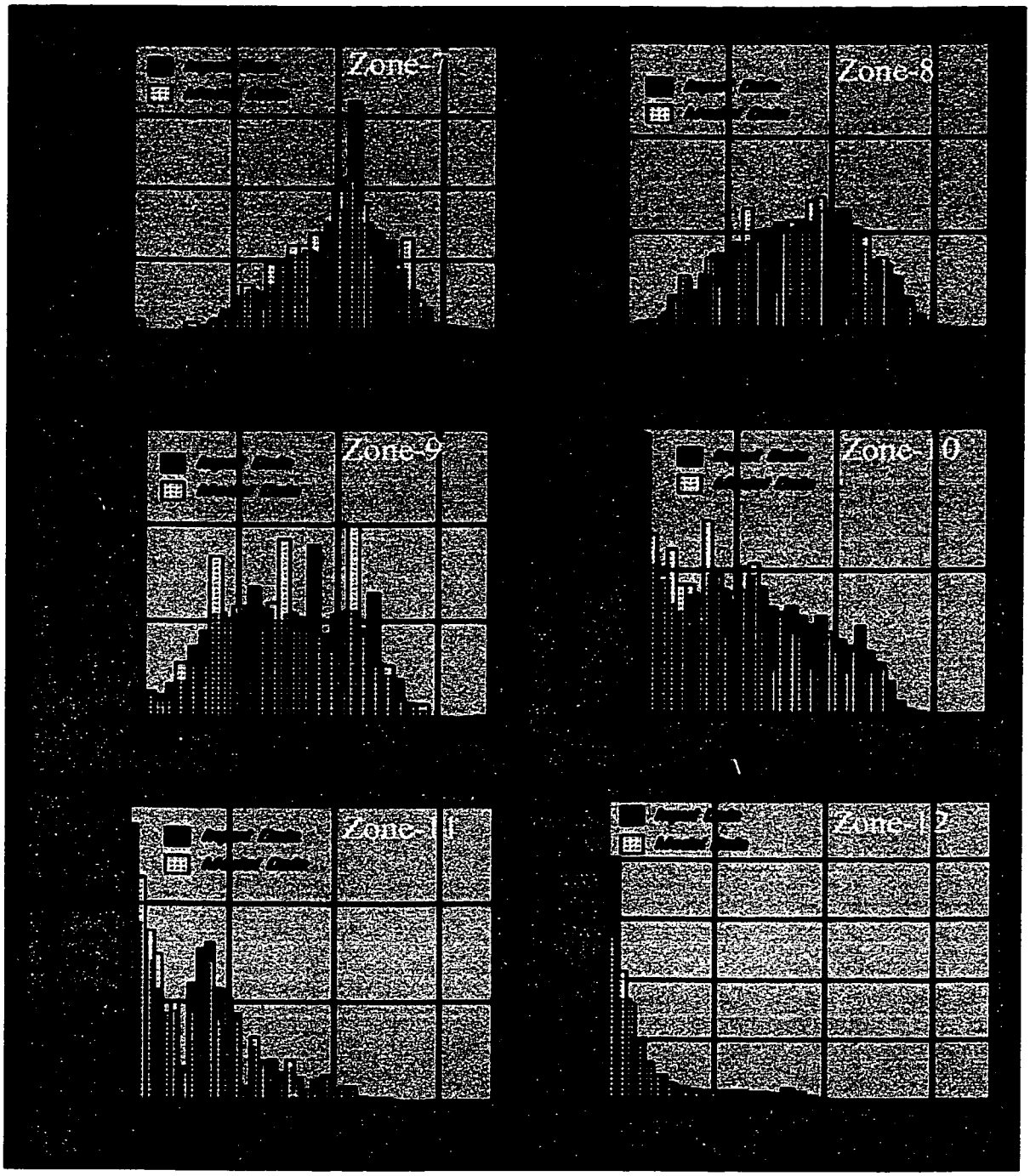

Figure 4.7: Comparison of histograms for observed and simulated values obtained from Sequential Gaussian Simulation and input data histograms for reservoir zones 7 to 12.

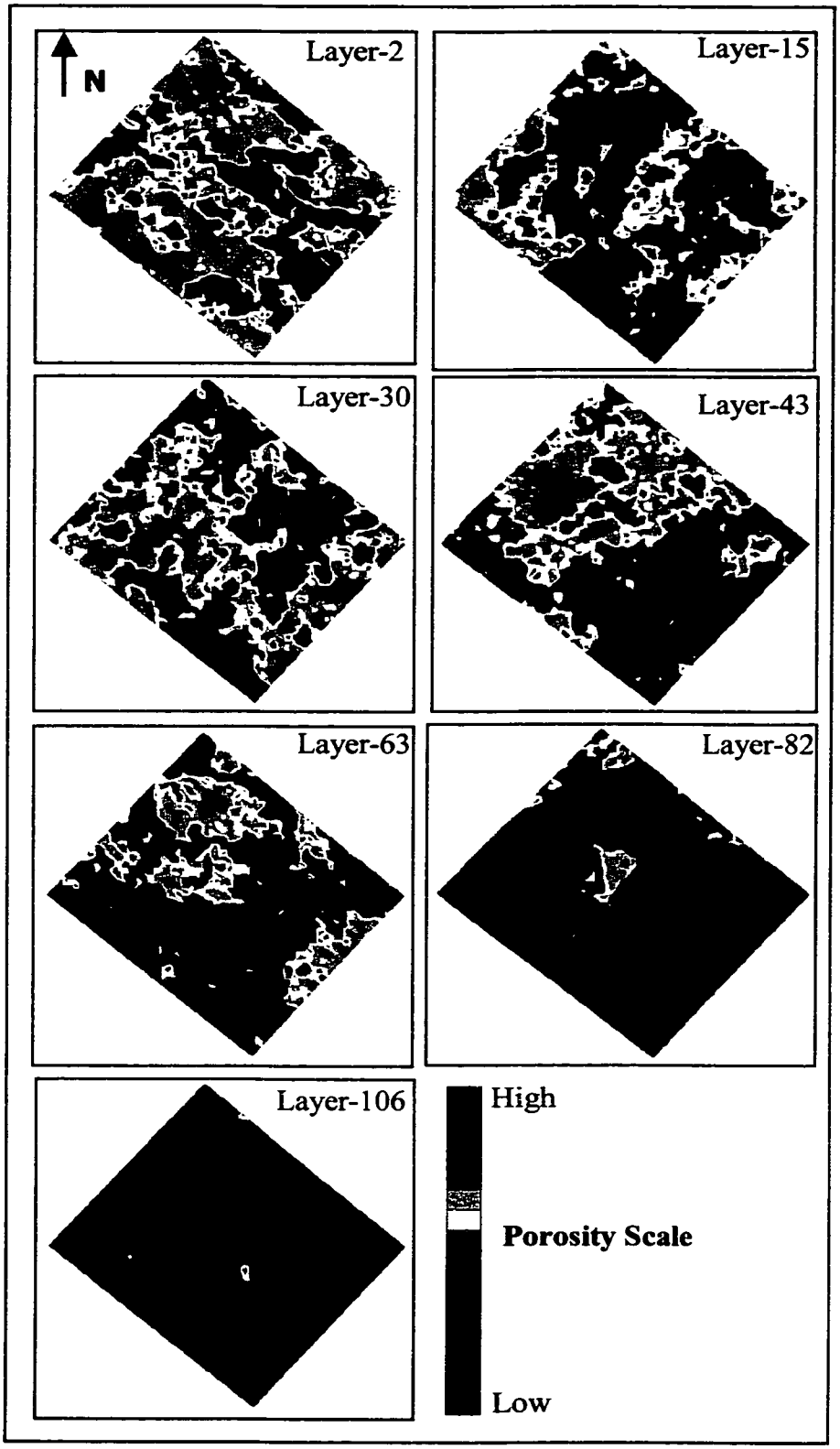

Figure 4.8: Different slices showing the wells only porosity model

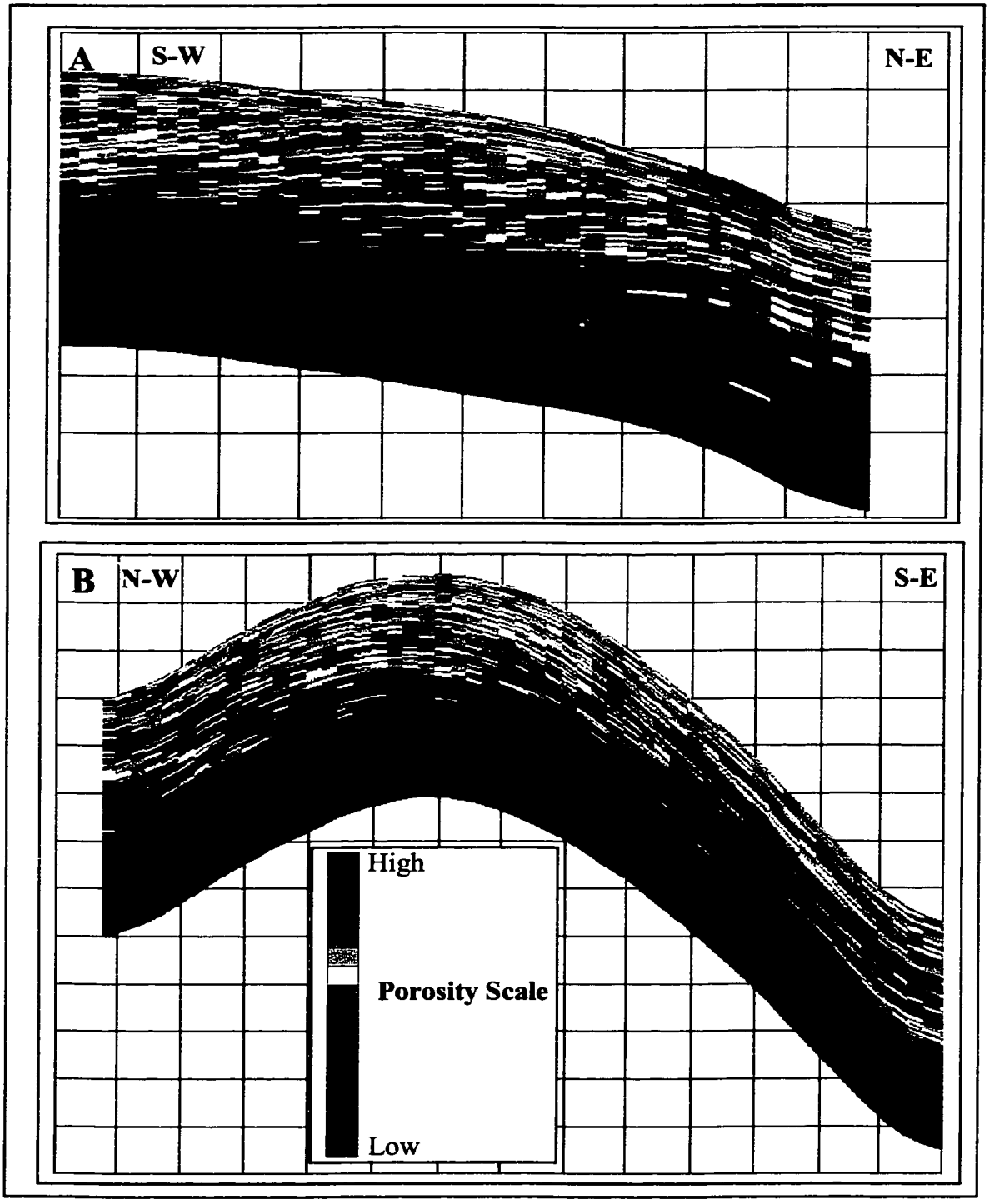

Figure 4.9: Cross section A and B across the porosity model wells only

In the quantitative validation step we will check model ability to predicate the porosity traces for the ten wells. Porosity traces for each well have been computed from each realization and compared to the true porosity trace. A correlation coefficient was calculated between the true and the simulated porosity trace to measure the accuracy as shown in Table 4.1. Figure 4.10 displays the distribution of the calculated correlation coefficient.

The best estimate has a correlation coefficient of 85% and the lowest 18%. Wells C, E and I, have the highest average accuracy in estimating the porosity. While wells B, H and J have the lowest average accuracy. Wells with high accuracy tend to be located in high-density areas, while wells with low accuracy tend to be in sparse well areas. This shows that the accuracy of models that are built based on wells only depends on the sample density of the data modeled.

Well	R1	R2	R3	R4	R5	R6	R7	R8	R9	R10	Average	Max	Min
A	67%	60%	62%	58%	64%	64%	62%	60%	70%	60%	63%	70%	58%
B	45%	46%	40%	52%	51%	54%	45%	27%	52%	47%	46%	54%	27%
C	81%	82%	85%	84%	81%	85%	81%	80%	81%	80%	82%	85%	80%
D	71%	71%	67%	71%	74%	68%	68%	66%	75%	65%	70%	75%	65%
E	72%	80%	72%	77%	76%	80%	81%	75%	81%	74%	77%	81%	72%
F	63%	71%	71%	64%	68%	70%	71%	62%	72%	62%	67%	72%	62%
G	71%	54%	68%	63%	58%	50%	68%	59%	66%	64%	62%	71%	50%
H	18%	36%	25%	33%	38%	33%	31%	32%	18%	19%	28%	38%	18%
I	76%	78%	77%	80%	82%	80%	84%	77%	80%	82%	80%	84%	76%
J	56%	53%	57%	56%	59%	62%	62%	65%	52%	59%	58%	65%	52%

Table 4.1: Correlation coefficients between the true porosities and the simulated porosities obtained from Sequential Gaussian Simulation for the ten wells.

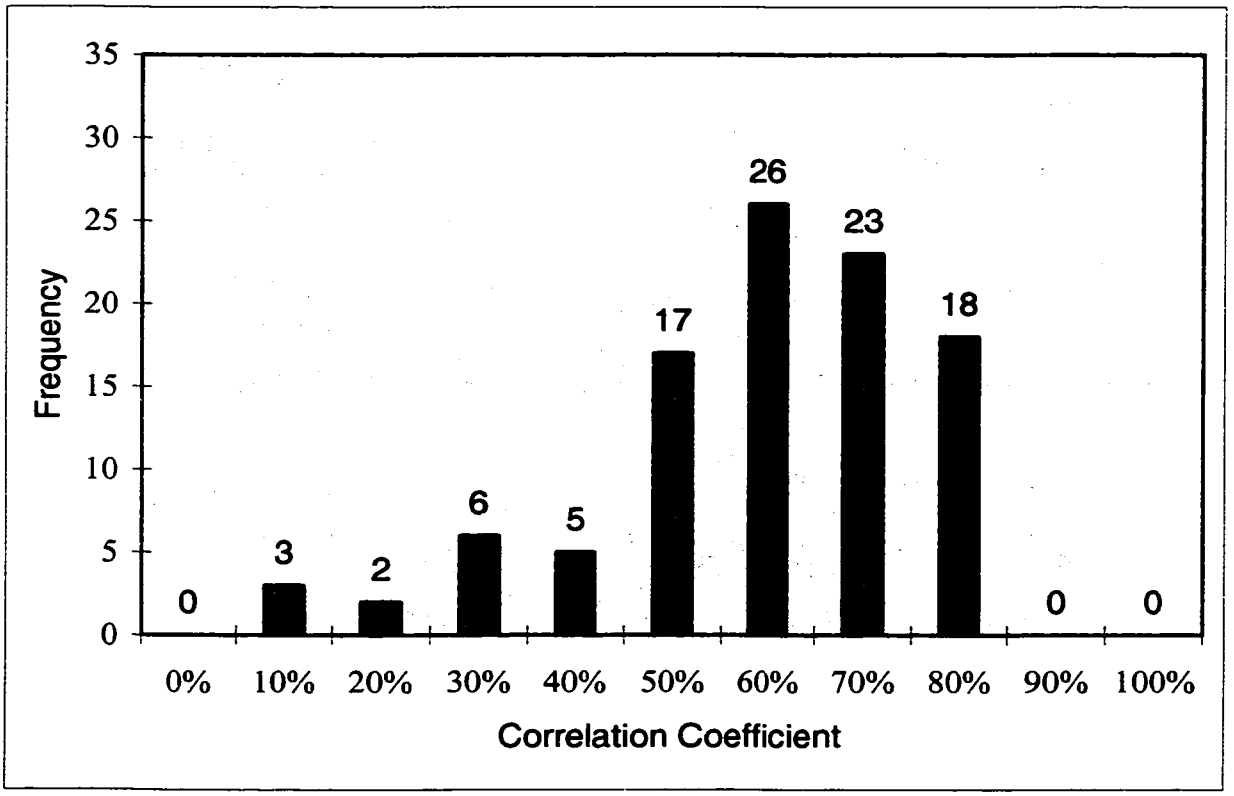

Figure 4.10: Distribution of the correlation coefficients between true and simulated porosity values obtained from Sequential Gaussian Simulation

4.3.2 Wells and Seismic Data Models

These models have been generated by using Sequential Gaussian Simulation with Collocated Cokriging (sGs_Cok). This is a powerful and fast method for integrating soft data, such as seismic, with hard data. It has been widely used for conditioning 3-D porosity models based on seismic impedance (Al-Qassab et al., 2000; Vejbaek, 1996 and Xu et al., 1992). The main advantage that seismic has over well data is that it has higher sampling density than well data.

To be able to use this method, a correlation coefficient has to be established between porosity and impedance. In section 3.2, the correlation coefficient between porosity and impedance has been calculated to be –0.96. This shows that there is a strong inverse relation between the porosity and impedance. Areas that have low impedance will have high porosity and vice versa. Based on this, the seismic impedance is expected to improve porosity prediction.

The other requirement that is needed for the applicability of this method is an impedance model that has the same model dimension as the model to be generated. Saudi Aramco has supplied the 3-D impedance model, which has been already scaled to match our model geometry. Figure 4.11 shows slices through the impedance model. Figure 4.12 shows two cross sections across the impedance model. Some parts at the N-W area of the study were not covered by the seismic survey and hence they have no impedance values. Saudi Aramco could not run the seismic survey in that particular area because it was too shallow for the ship that was operating the seismic survey.

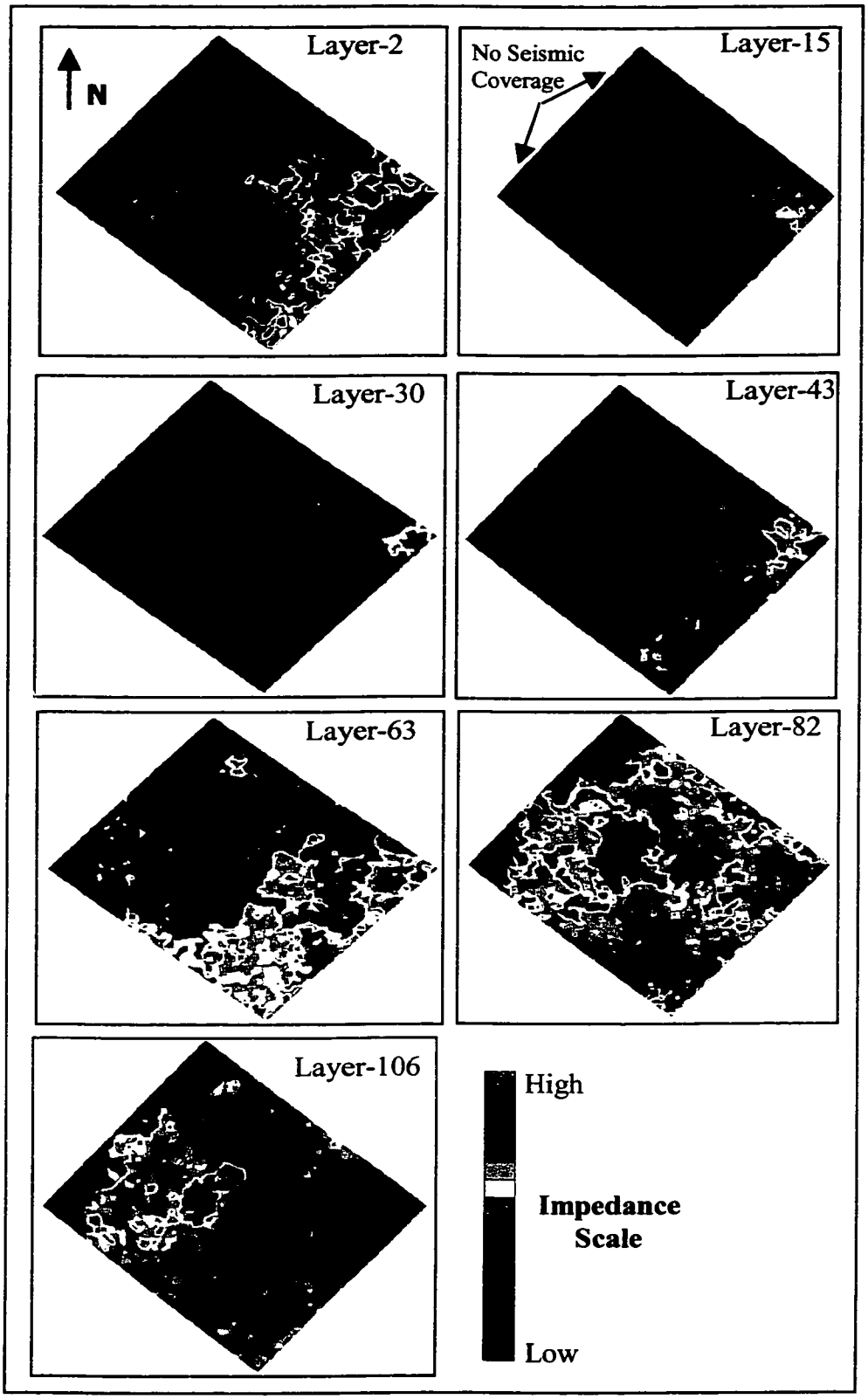

Figure 4.11: Different slices through the impedance model

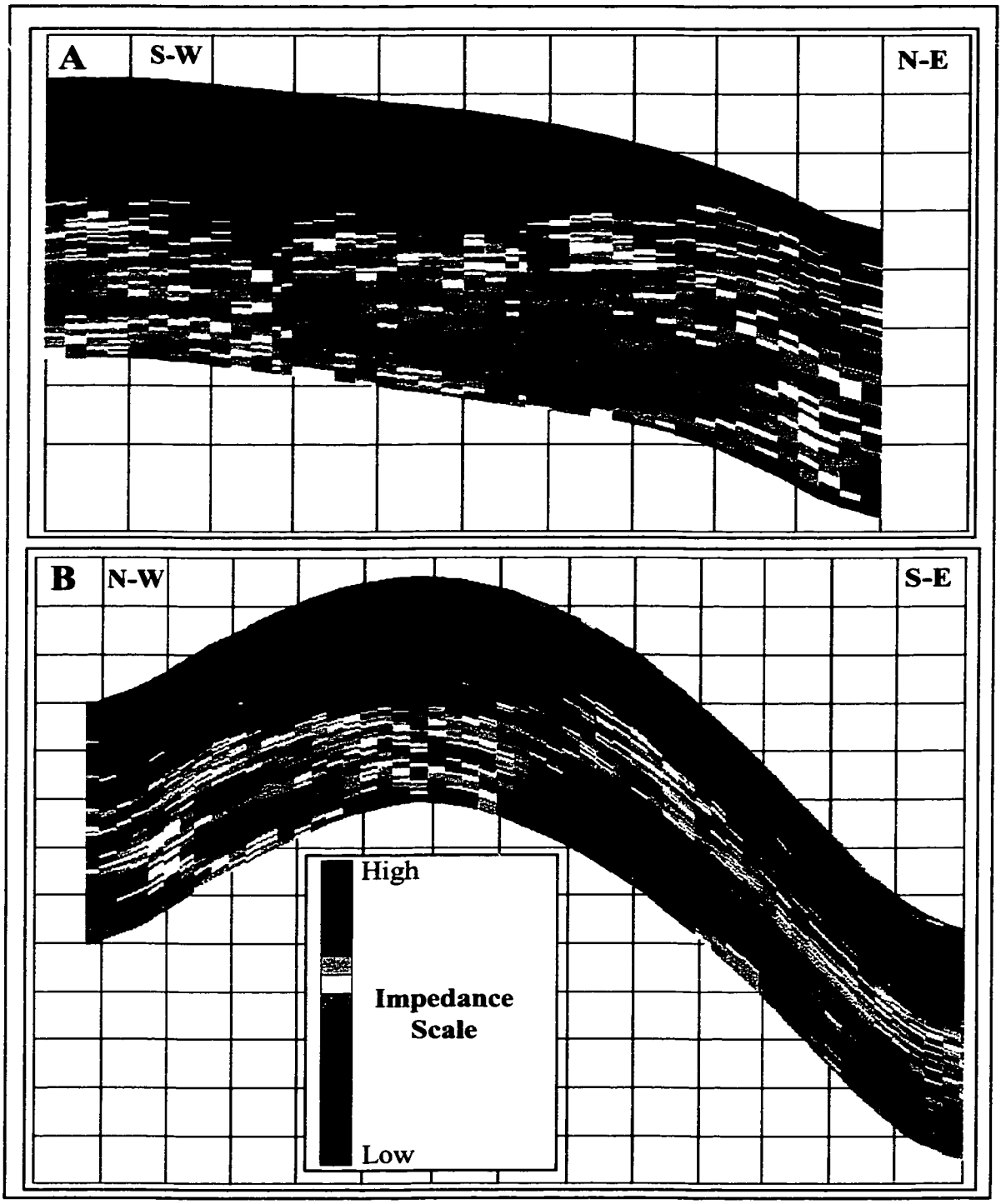

Figure 4.12: Cross section A and B across the impedance model

The same porosity semi-variograms and histograms that have been used to generate the sGs porosity model were used in this model. The porosity-impedance correlation coefficient was used to guide the sGs_Cok algorithm to simulate porosity based on seismic impedance. Ten realizations have been generated for this porosity model and they will be used in the validation part.

As with the previous model, reliability of this model will be checked by comparing input data histograms with histograms of the simulated values from the model. Figure 4.13 and 4.14 show these histograms for the input data and for the simulated values from the model. Generally, the sGs_Cok algorithm preserved the statistical and spatial characteristics of the input data.

Figure 4.15 show different slices through the model, and figure 4.16 shows two cross sections across the model. The model slices and cross sections clearly show the effect of the impedance on the porosity-simulated model. The lateral and vertical porosity trends are highly affected by the impedance model. This is expected, due to the high correlation coefficient that was used. The overall porosity trend is similar to the wells data only model and, hence, the signature of the general variation in the facies is preserved.

The next step is to check the model's ability to predict the porosity traces for the ten wells. As with the previous model, porosity traces for each have been computed from each realization and compared to the true porosity trace and a correlation coefficient was calculated as shown in table 4.2. Figure 4.17 displays the distribution of the calculated correlation coefficients.

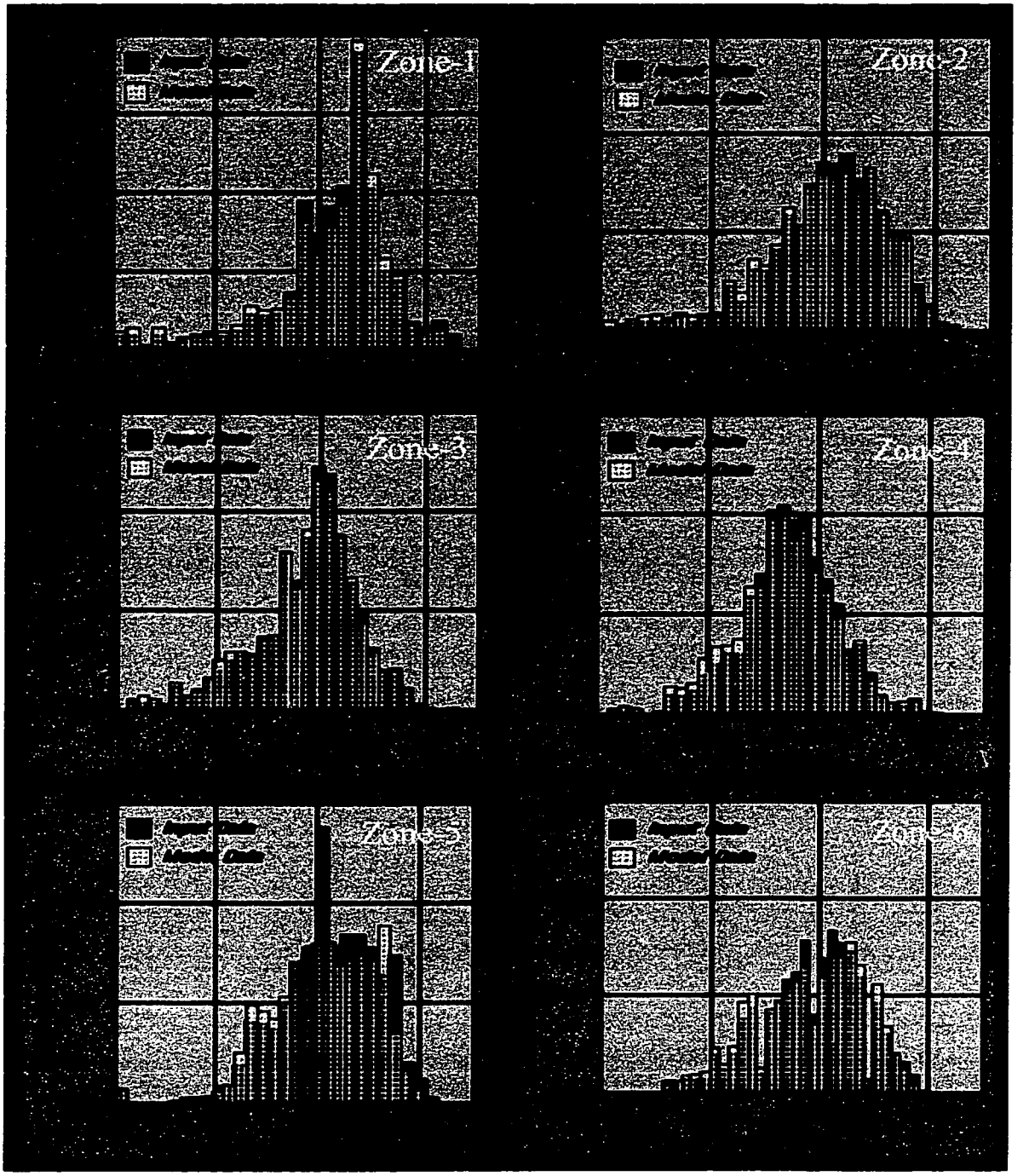

Figure 4.13: Comparison of histograms of observed and simulated porosity values obtained from Sequential Gaussian Simulation with Collocated Cokriging for reservoir zones 1 to 6.

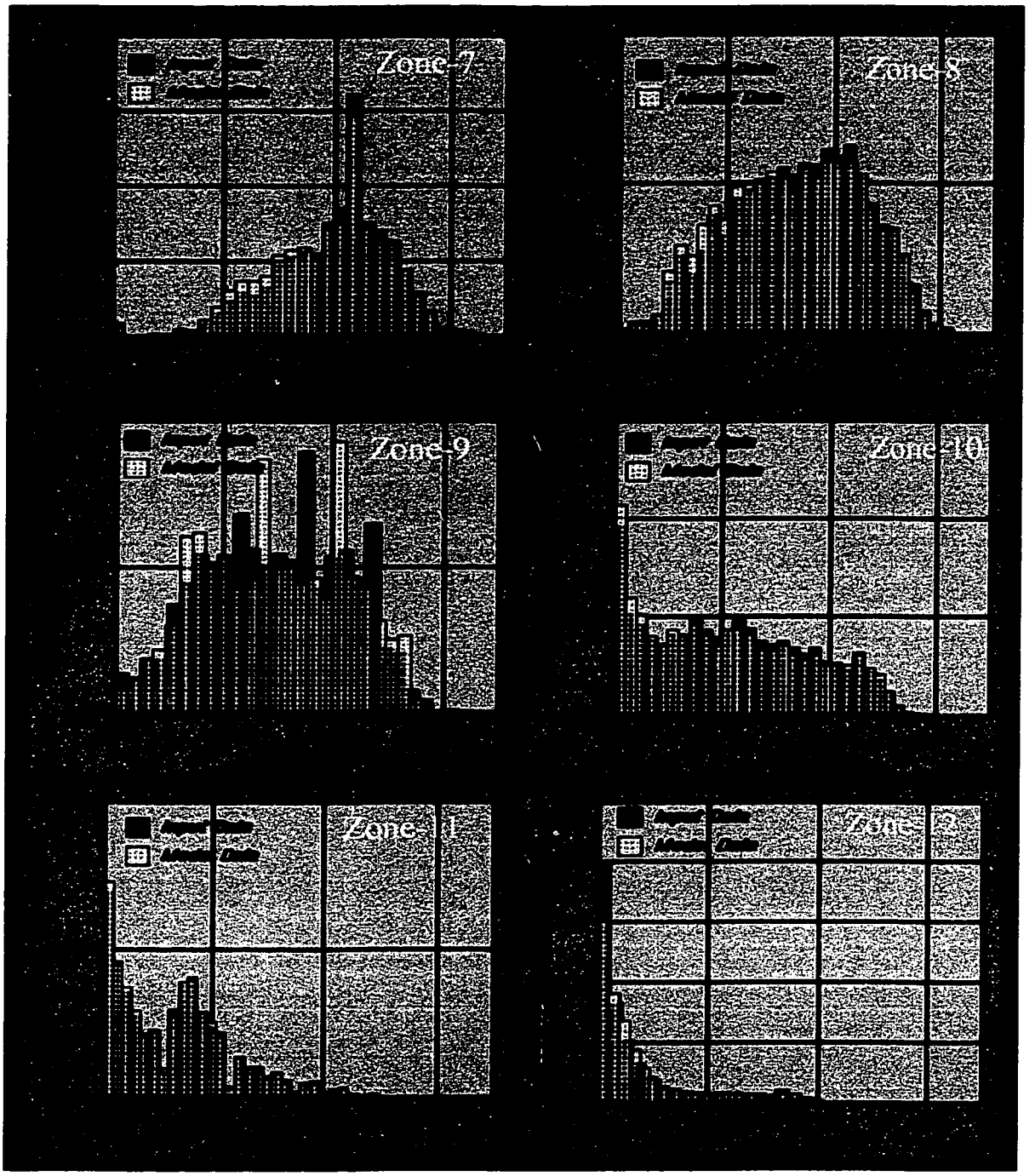

Figure 4.14: Comparison of histograms of observed and simulated porosity values obtained from Sequential Gaussian Simulation with Collocated Cokriging for reservoir zones 7 to 12.

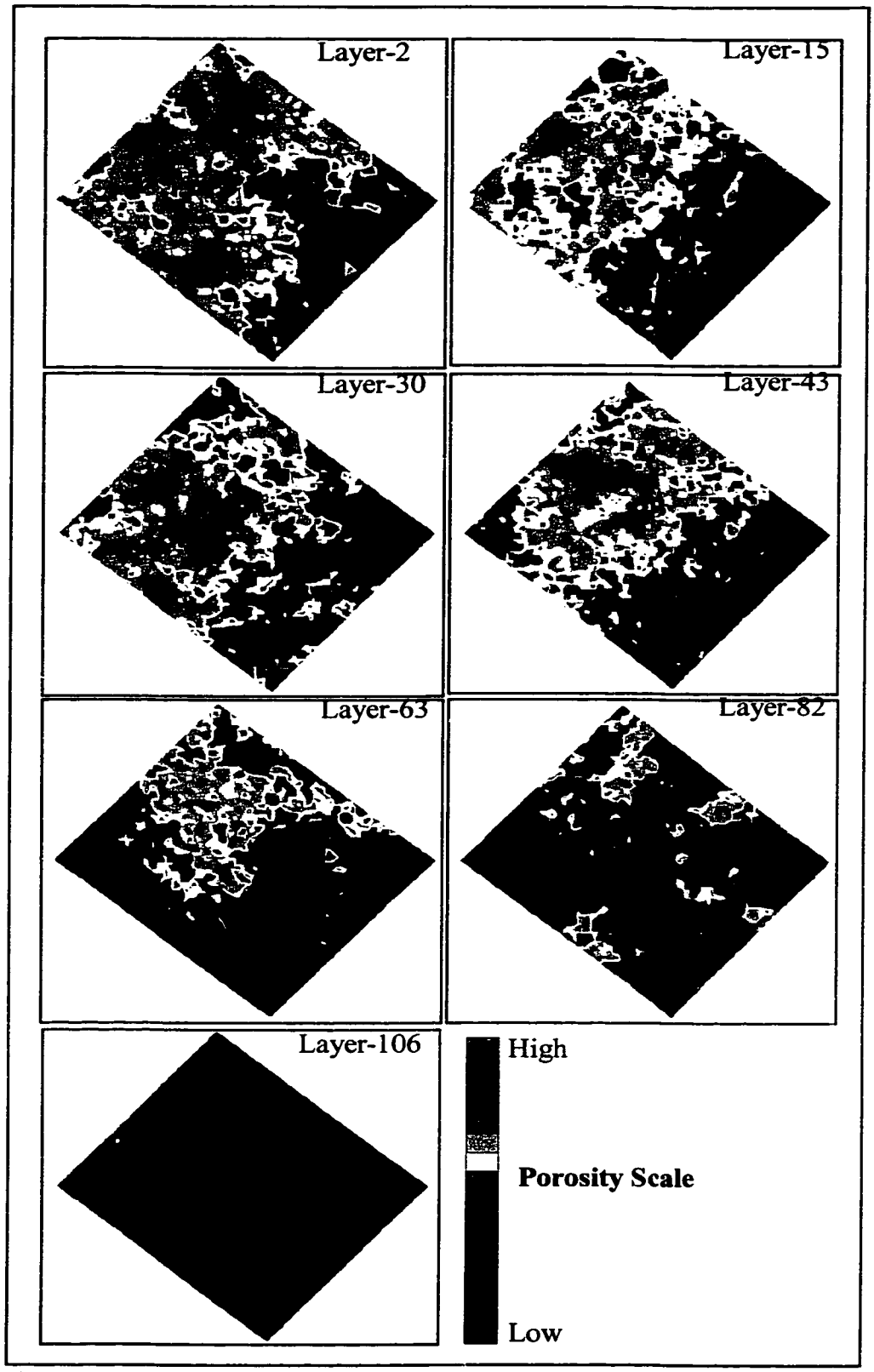

Figure 4.15: Different slices through the seismic controlled porosity model

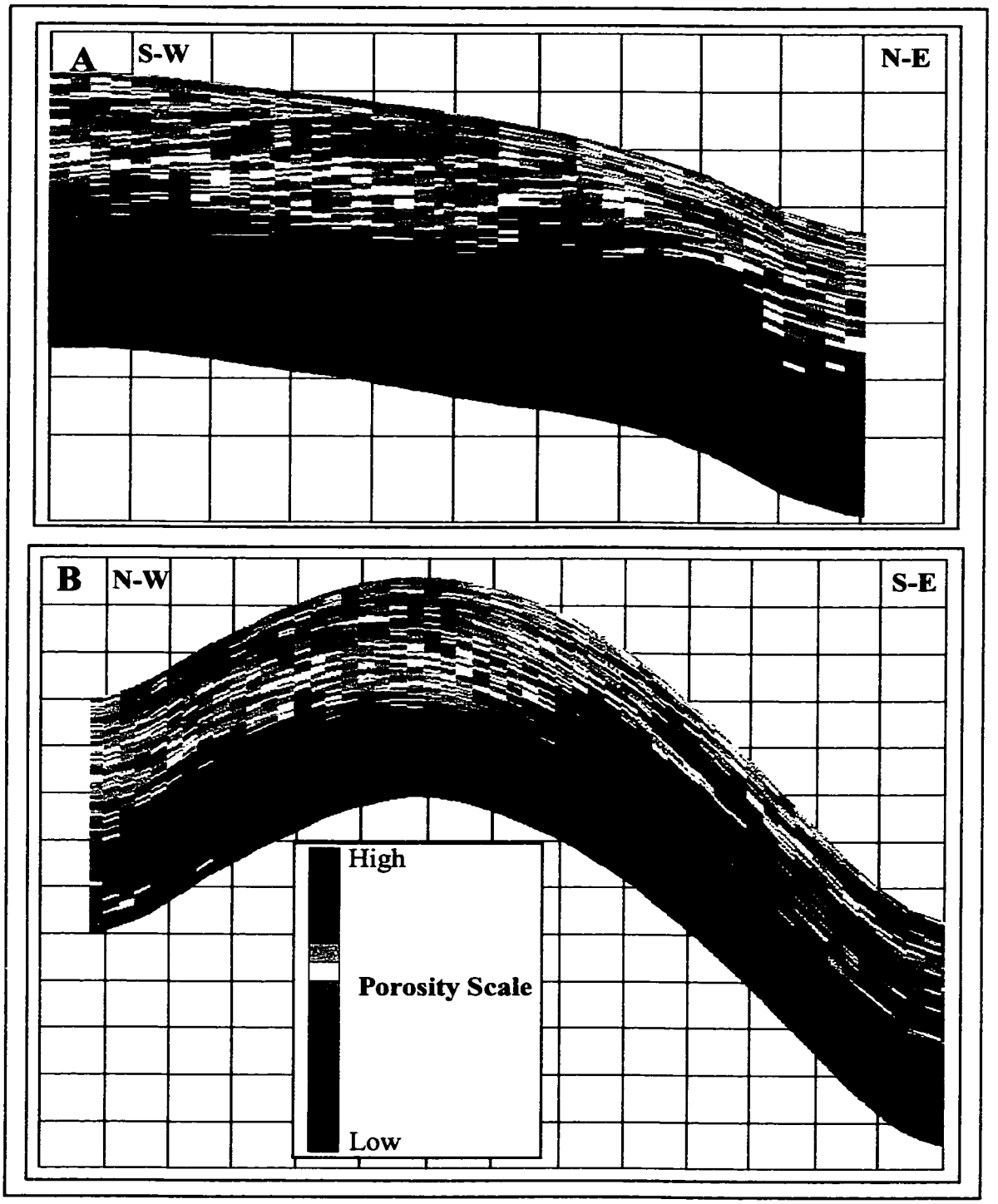

Figure 4.16: Cross A and B across the seismic controlled porosity model

WELL	R1	R2	R3	R4	R5	R6	R7	R8	R9	R10	Average	Max	Min
A	67%	65%	65%	61%	66%	66%	64%	61%	65%	60%	64%	67%	65%
B	52%	47%	54%	52%	53%	56%	52%	41%	55%	49%	51%	56%	41%
C	81%	83%	85%	84%	84%	86%	81%	83%	82%	82%	83%	86%	81%
D	72%	55%	72%	73%	72%	70%	71%	72%	74%	80%	71%	80%	55%
E	76%	80%	78%	82%	82%	78%	82%	81%	82%	79%	80%	82%	76%
F	56%	60%	58%	60%	62%	62%	62%	61%	62%	53%	59%	62%	53%
G	60%	52%	64%	51%	55%	54%	63%	63%	57%	63%	58%	64%	51%
H	38%	40%	40%	39%	48%	36%	53%	45%	56%	40%	43%	56%	36%
I	70%	76%	75%	72%	75%	77%	75%	72%	74%	75%	74%	77%	70%
J	82%	78%	78%	77%	79%	79%	80%	82%	81%	79%	80%	82%	77%

Table 4.2: Correlation coefficients between the true porosities and the simulated porosities obtained from Sequential Gaussian Simulation with Collocated Cokriging for the ten wells

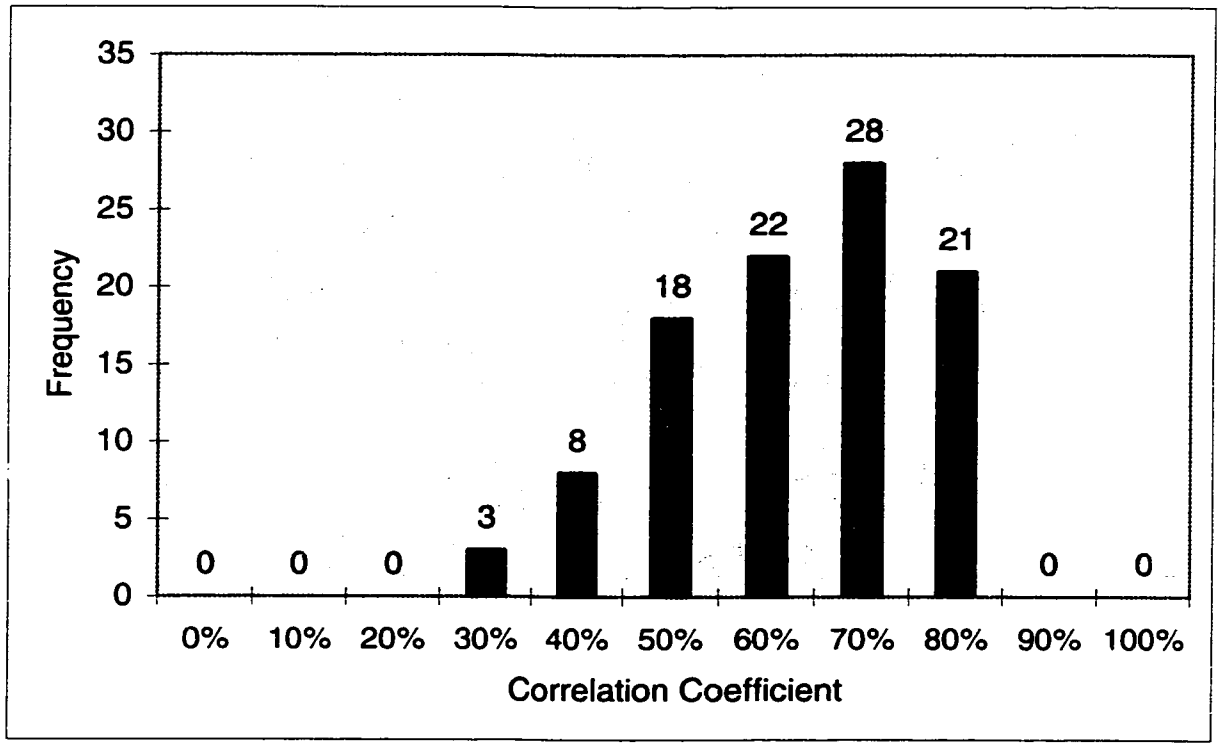

Figure 4.17 Distribution of the correlation coefficients between true and simulated porosity values obtained from Sequential Gaussian Simulation with Collocated Cokriging for ten wells

The best estimate has a correlation coefficient of 86% and the lowest has 36%. Wells that had a high correlation coefficient in the previous model still have a high correlation coefficient in this model. The improvement in the correlation coefficient has occurred in wells that are located in a low well density area, such as well H and J. The average correlation coefficient for Well J has increased from 58% to 80%, which is a significant improvement. Well H shows similar improvement, the average correlation coefficient for that well has increased from 28% to 43%.

The use of the seismic impedance has increased the accuracy of the model. This improvement is significant in wells that are located in sparse wells areas such as wells J and H. This is due to two factors: the seismic spatial sampling rate is much higher than that of the wells, and there is an excellent correlation between seismic impedance and log-derived porosity. This illustrates that seismic information has an important role in improving the accuracy of porosity-simulated models.

4.3.3 Wells and Facies Data Models

Facies models can be used to generate a continuous property model such as porosity or permeability in which the spatial statistics are facies dependent. The main idea behind this method is to honor the statistical porosity distribution in each facies and at the same time honor the overall porosity distribution as well. The algorithm used is called Sequential Gaussian Simulation Facies Based (sGs_FB). It uses porosity data from well logs and a facies model to perform the simulation. At each location it determines the facies present from the facies model and uses the porosity semivariogram along with histograms to simulate a value at that location.

In this method we are going to use the facies model that has been generated in section 4.2. The same porosity semi-variograms that have been used in the previous models were used in this one. Porosity histograms for each facies and for each reservoir zone were used in this model. Ten realizations were generated and used in the validation step.

The reliability of this model will be checked by comparing input data histograms with histograms of the simulated values. Figures 4.18 and 4.19 show histograms of the input data and for the simulated values, respectively. The sGs_FB algorithm preserved the statistical characteristics of the input data.

Figure 4.20 shows different slices through the model, and figure 4.21 shows two cross sections across the model. In the model slices and cross sections, the facies model signature is clear. High porosity areas correspond to grainstone-rich facies - group 2,3 and 8- and the low porosity areas correspond to mudstone facies, group 7.

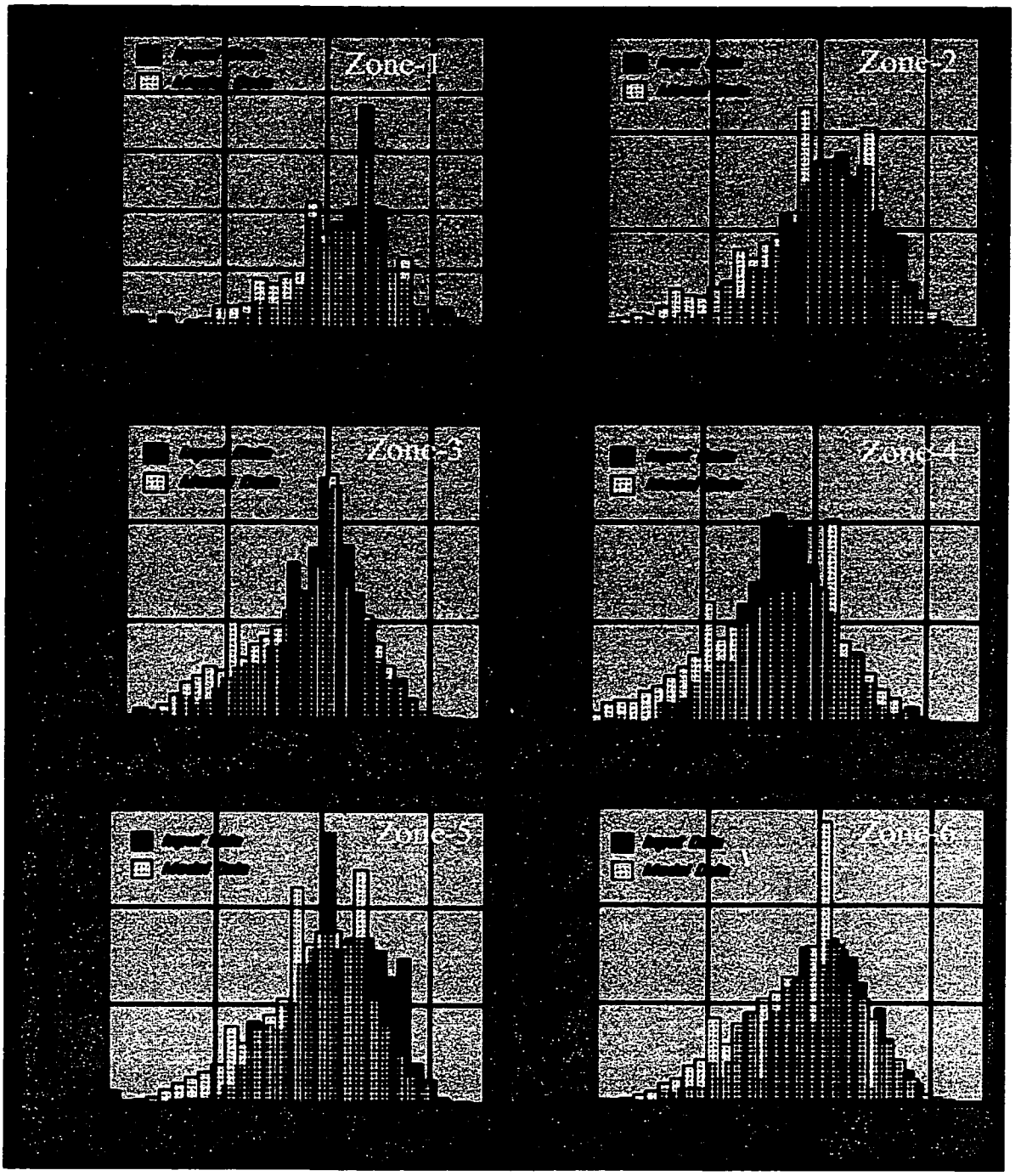

Figure 4.18: Comparison of histograms of observed and simulated porosity obtained from Sequential Gaussian Simulation Facies Based for reservoir zones 1 to 6

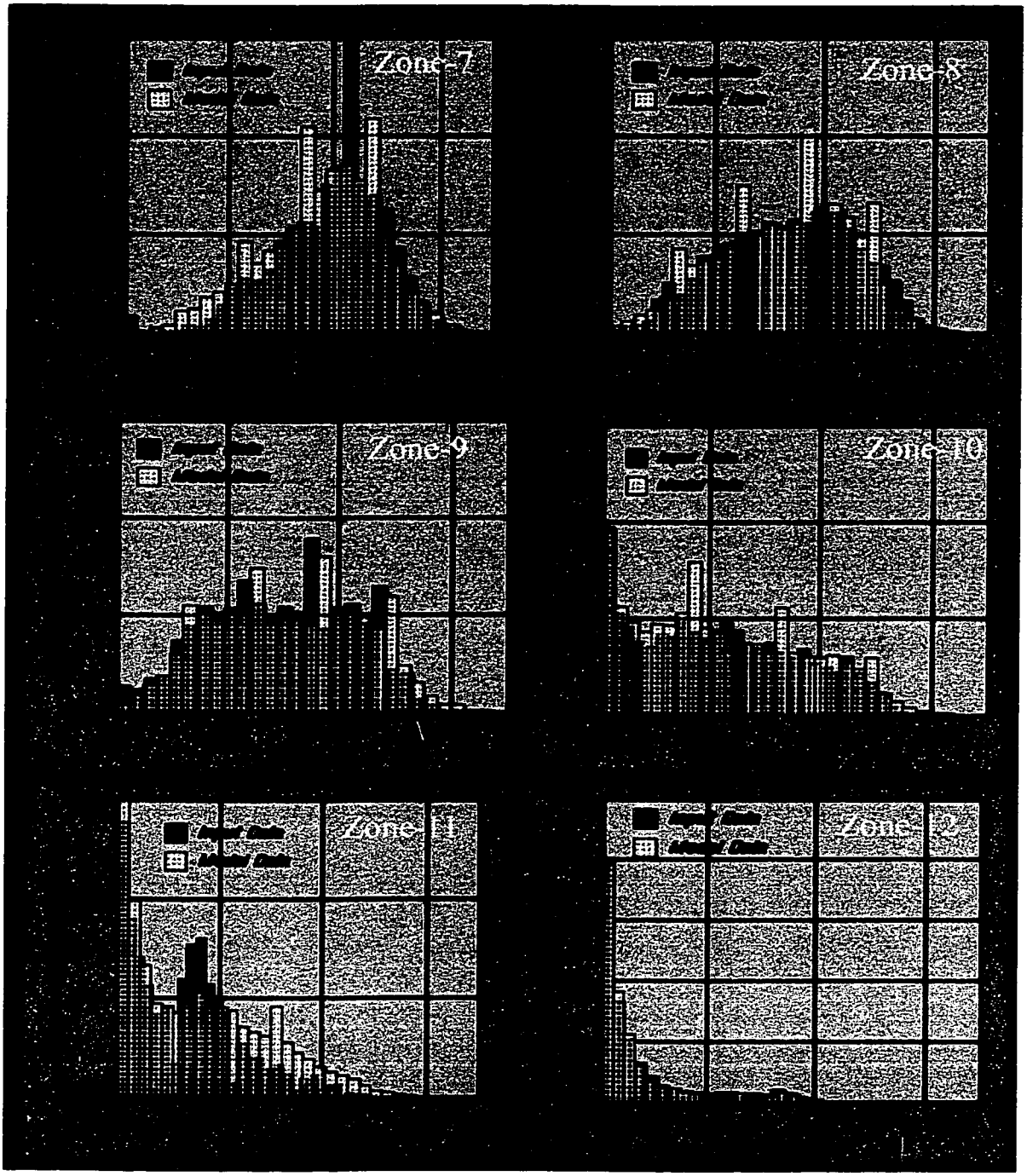

Figure 4.19: Comparison of histograms of observed and simulated porosity obtained from Sequential Gaussian Simulation Facies Based for reservoir zones 7 to 12

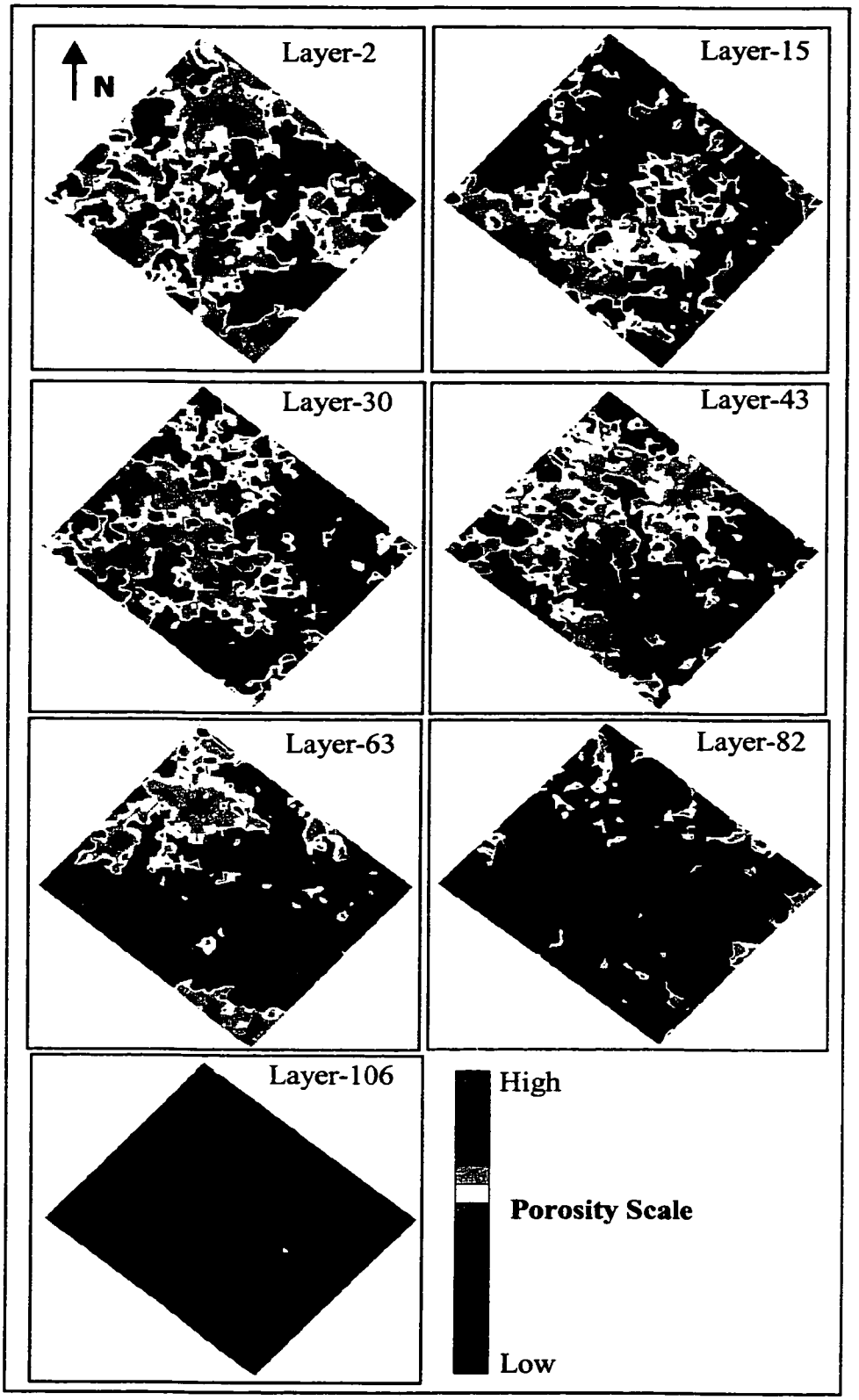

Figure 4.20: Different slices through the facies-based porosity model

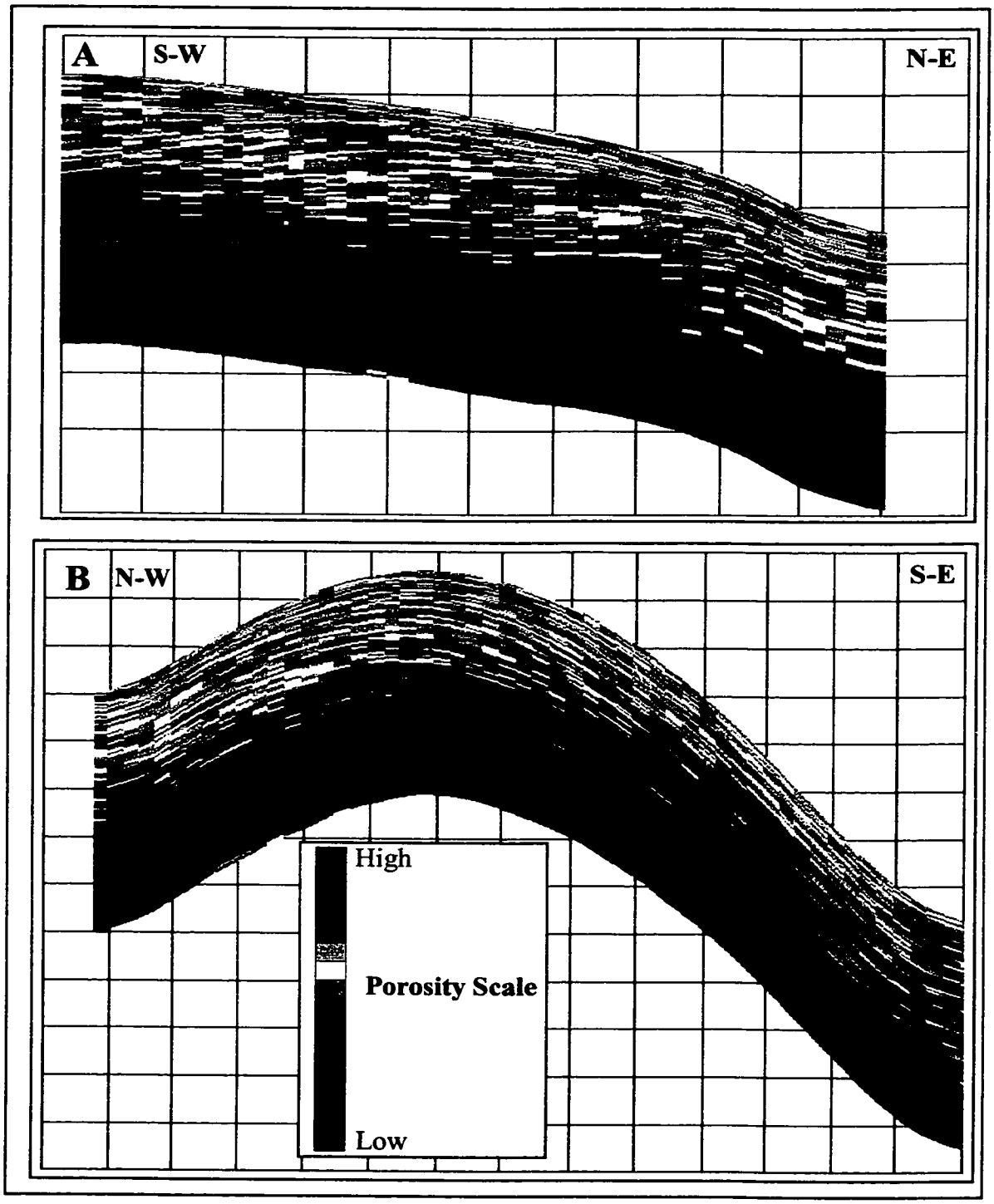

Figure 4.21: Cross section A and B across the facies based porosity model

Although this has been observed in the previous model, it is much clearer in this model. Also, this model tends to show less porosity in some layers, such as layer 15, as compared to the seismic controlled porosity model. Also in this model, the vertical layering of the reservoir is clearer than the previous two models. However, the overall spatial and vertical porosity trends are similar to the two previous models.

The next step is to compute the porosity traces for each well from each realization, compare it to the true porosity trace and calculate correlation coefficients. Table 4.3 shows the calculated correlation coefficients, and figure 4.22 displays their statistical distribution.

The best estimate has a correlation coefficient of 85%, and the lowest 26%. Three wells, namely B, C and H, have average correlation coefficients very similar to the wells only model, while five wells, namely A, D, E, G and I, showed a lower average correlation coefficient than the wells only model. Only two wells, namely F and J, showed a higher average correlation coefficient than that model. The overall accuracy of the seismic control model is better than in the case of the facies controlled model.

The decrease in accuracy in this model, compared with the two previous models, is due to the fact that the porosity is simulated based on the facies type at that location which is also an estimated quantity. In section 3.4 we have shown that each facies group has a distinct porosity distribution. Hence if there is an error in facies estimation it will lead to using an inappropriate porosity histogram that would cause inaccurate porosity estimation.

WELL	R1	R2	R3	R4	R5	R6	R7	R8	R9	R10	Average	Max	Min
A	52%	50%	57%	53%	58%	55%	48%	58%	53%	58%	54%	58%	48%
B	44%	44%	46%	44%	42%	48%	45%	43%	45%	52%	45%	52%	42%
C	84%	80%	78%	80%	82%	83%	82%	85%	80%	82%	82%	85%	78%
D	51%	51%	47%	50%	53%	47%	45%	53%	53%	50%	50%	53%	45%
E	61%	58%	62%	63%	65%	57%	58%	64%	63%	59%	61%	65%	57%
F	67%	77%	66%	66%	72%	78%	74%	68%	74%	77%	72%	78%	66%
G	36%	40%	52%	37%	42%	46%	33%	50%	50%	38%	42%	52%	33%
H	26%	30%	30%	33%	36%	27%	36%	29%	35%	42%	32%	42%	26%
I	71%	76%	75%	69%	77%	72%	74%	72%	75%	74%	74%	77%	69%
J	69%	64%	66%	63%	60%	68%	71%	63%	71%	66%	66%	71%	60%

Table 4.3: Correlation coefficients between the true porosities and the simulated porosities obtained from Sequential Gaussian Simulation Facies Based for the ten wells

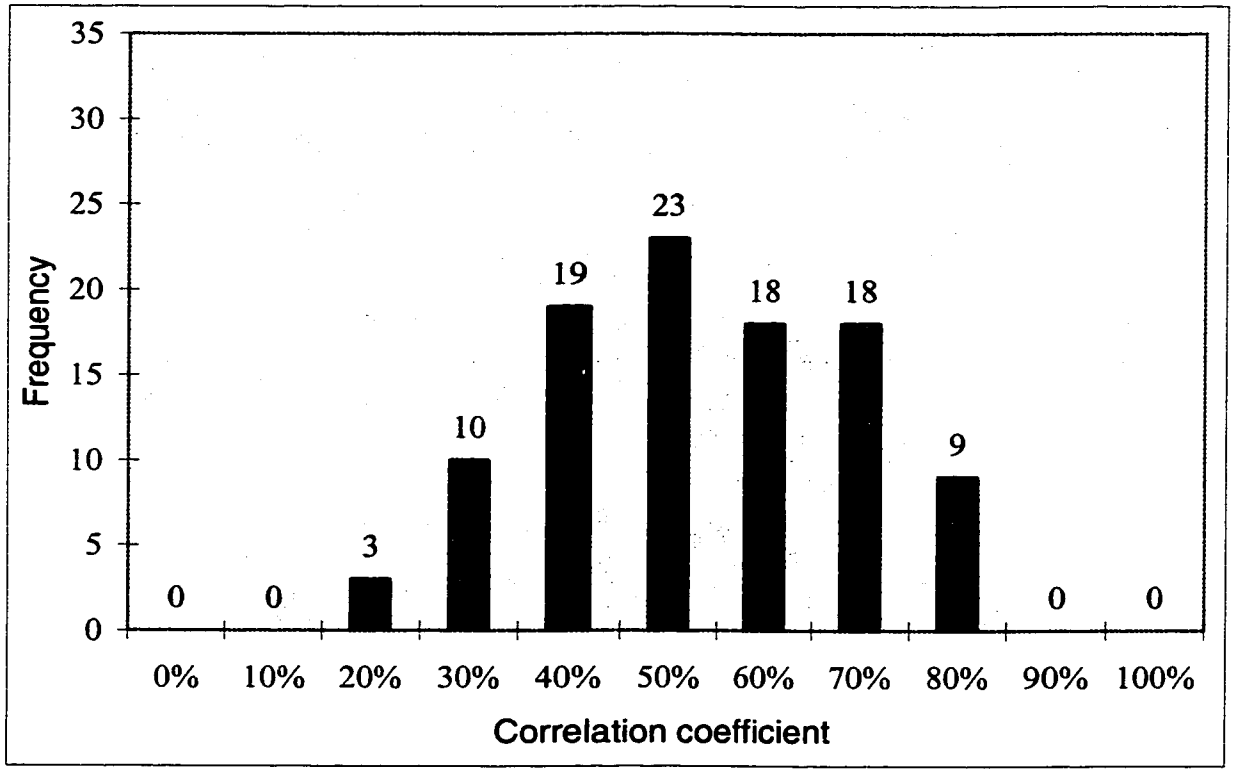

Figure 4.22 Distribution of the correlation coefficients between true and simulated porosity values obtained from Sequential Gaussian Simulation Facies Based for ten wells

4.3.4 Wells, Facies and Seismic Data Models

These porosity models are generated by integrating porosity from well logs along with facies and seismic data. The modeling algorithm uses porosity from well logs and integrates it with other data types by using sequential Gaussian simulation with Collocated Cokriging Facies Based (sGs_ Cok _FB). At each cell location in the model, the algorithm determines the facies present and uses porosity semivariogram, in addition to the seismic impedance to simulate a porosity value at that cell location.

The modeling workflow for this model is similar to the facies based porosity model, except that an impedance model is selected along with the correlation coefficient between porosity and impedance. As in the previous models, the same porosity semi-variograms and histograms are used in this model. The method is computationally intensive and it has the longest computer run time of all the techniques. Ten realizations have been generated by using this method.

As with previous models, the reliability of this model will be checked by comparing the histograms for input data and for simulated values (figures 4.23 and 4.24). The sGs_Cok_FB algorithm has preserved the statistical characteristics of the input data. The sGs_ Cok_ FB and the sGs_FB algorithms produced very similar statistics, which are slightly different from the sGs_Cok. This indicates that the results are more influenced by the facies model than the impedance model.

Figure 4.25 shows slices through the model, and figure 4.26 shows two cross sections. The model slices and the cross sections show porosity trends very similar to the previous three models.

Figure 4.23: Comparison of histograms for observed and simulated porosity values obtained by using facies and seismic data as constraint for porosity model for reservoir zones 1 to 6

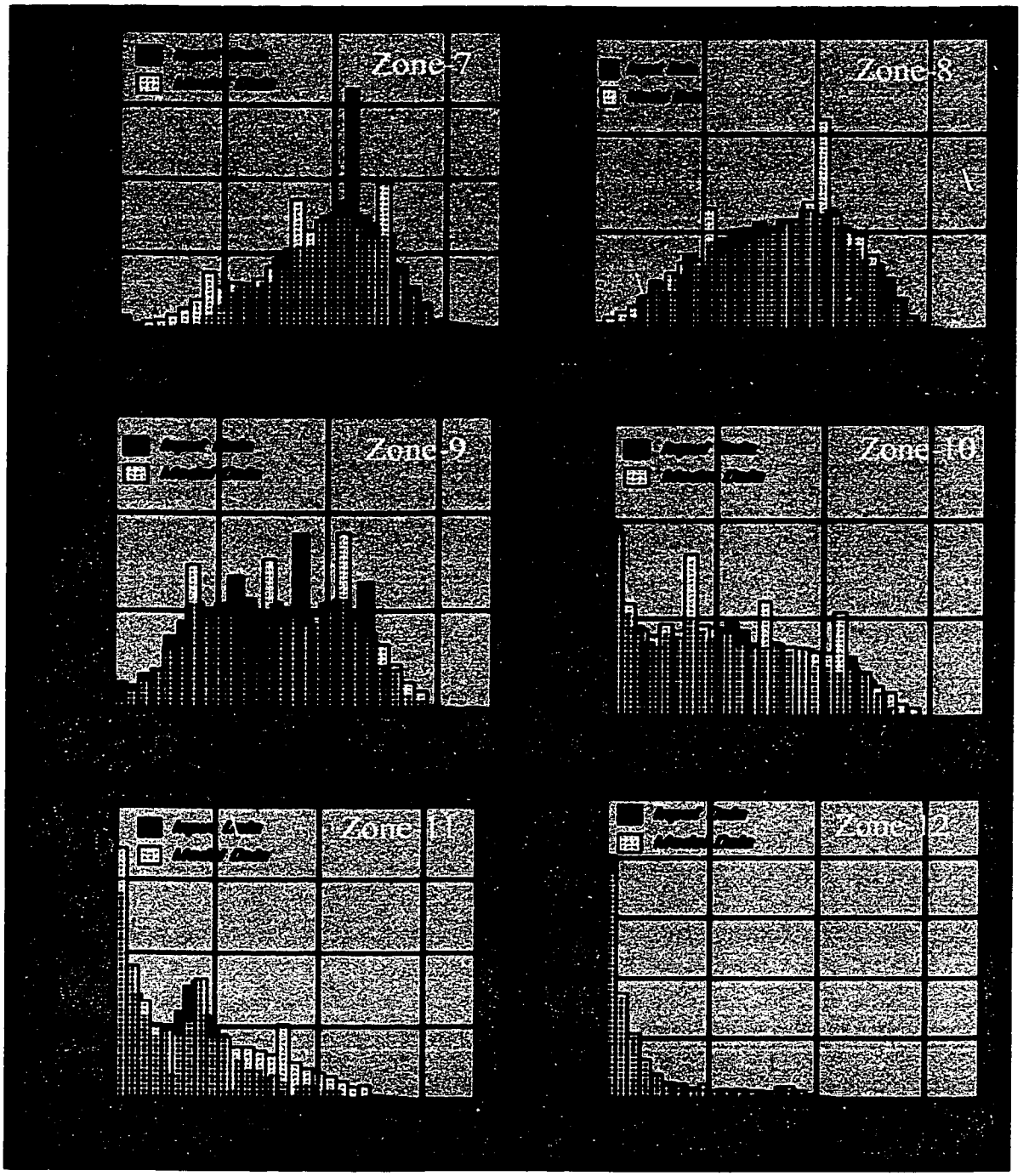

Figure 4.24: Comparison of histograms for observed and simulated porosity values obtained by using facies and seismic data as constraint for porosity model for reservoir zones 7 to 12

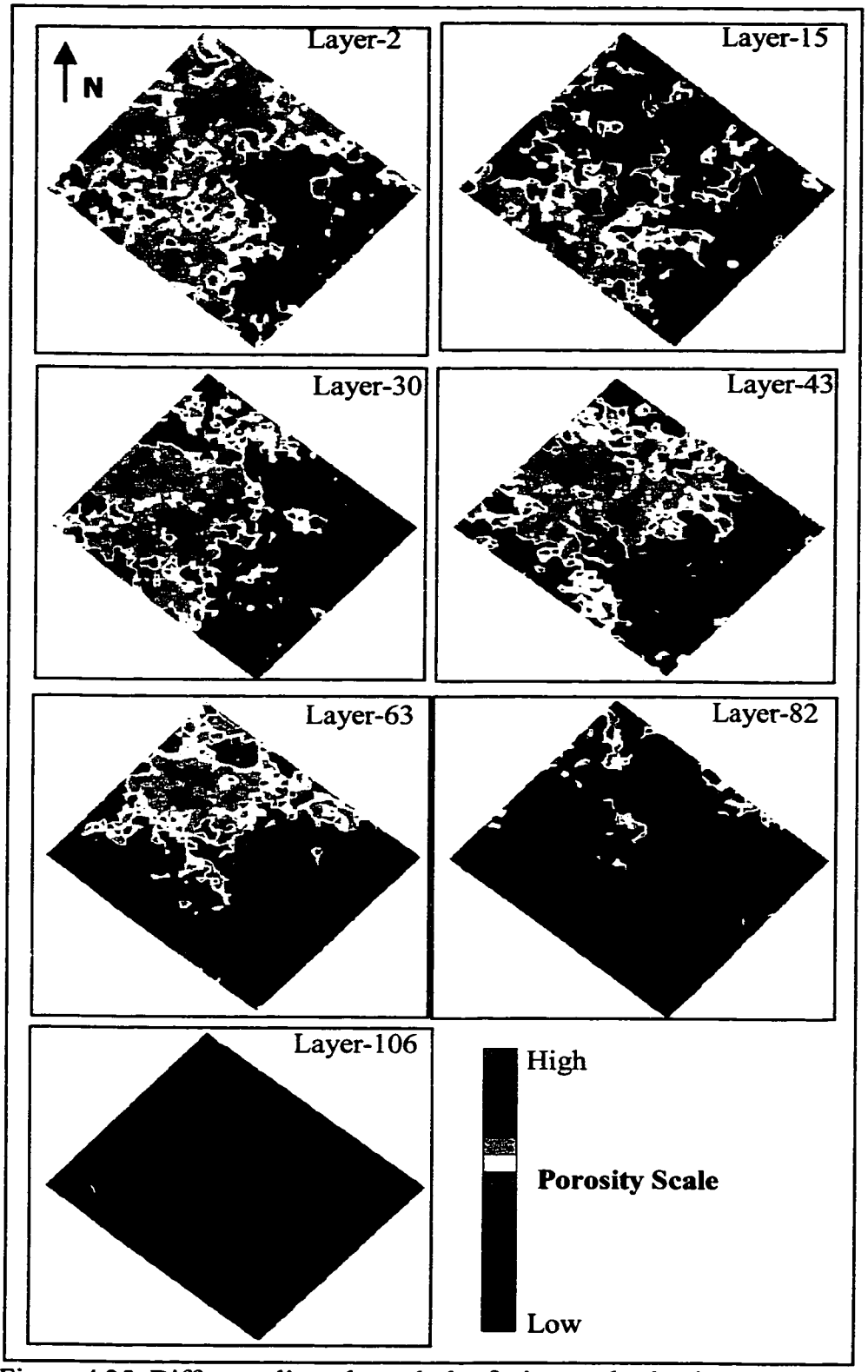

Figure 4.25: Different slices through the facies- and seismic- constrained porosity model

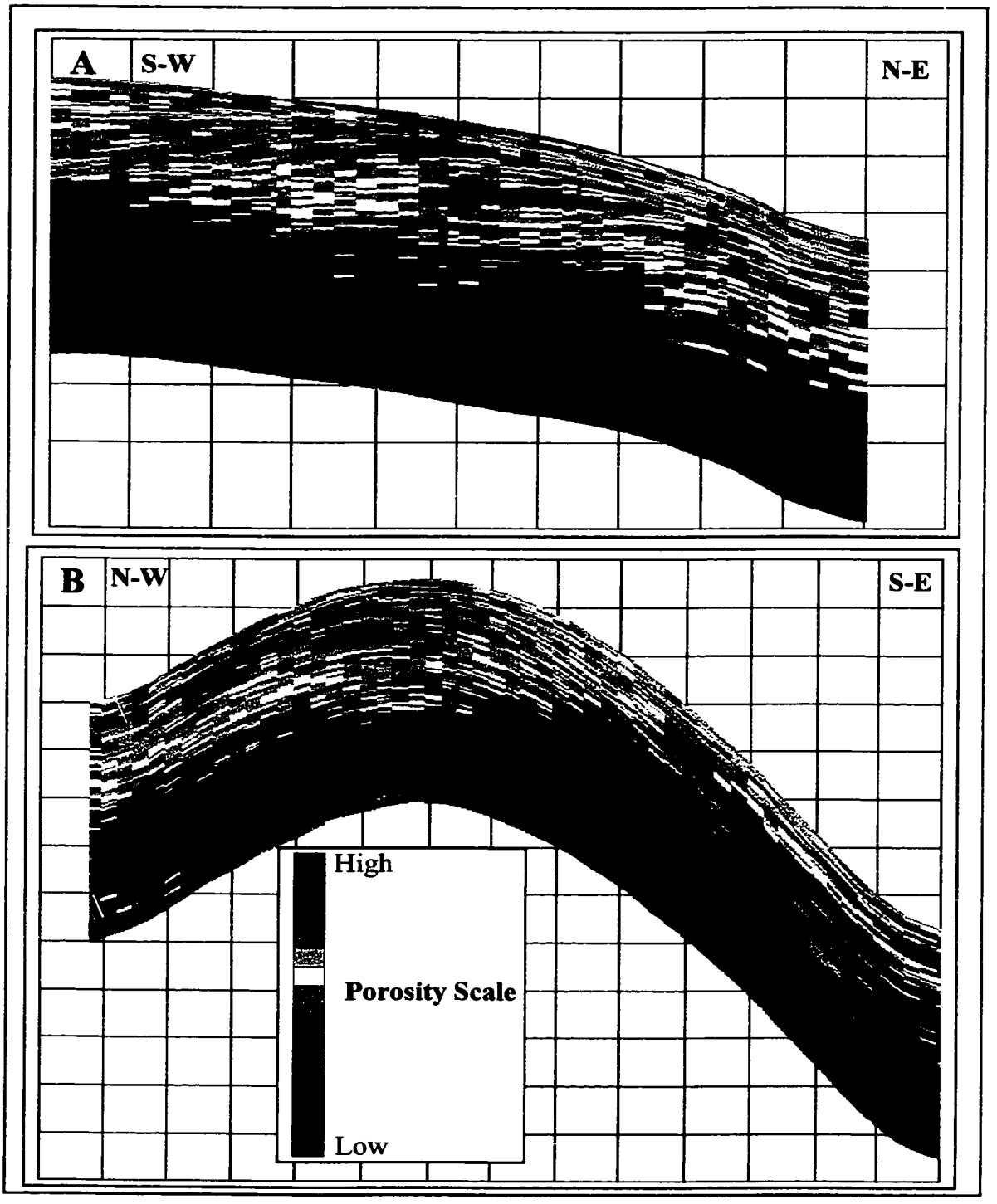

Figure 4.26: Cross section A and B through the facies- and seismic-constrained porosity model

Also, this model shows the fine vertical layering similar to the facies based model, which is the effect of using the facies model as a constraint. Moreover, it shows that porosity is more continuous here than in the wells only model and the facies based model, which reflects the effect of using the impedance model as soft data. This model seems to be better than the previous models in defining the vertical and lateral continuity of porosity.

Porosity traces for each well from each realization have been compared with the true porosity trace, and a correlation coefficient has been calculated. Table 4.4 shows the correlation coefficients between true and simulated porosity traces, and figure 4.27 displays its distribution.

The best estimate has a correlation coefficient of 86%, and the lowest has 35%. Three wells -C, F and H- have a very similar average correlation coefficient to the wells only model. Five wells, which are B, D, E, G and I, showed a lower average correlation coefficient than the wells only model and only two wells -A and J- showed higher average correlation coefficients than that model. This is very similar what has been observed in the facies controlled model, because the facies model is influencing the porosity distribution more than the impedance model. The overall accuracy, then, of the seismic control model is better than this model.

The accuracy of this model is better than the well only model and similar to the facies controlled, but it is less than that of the seismic controlled model. The reduction in accuracy is attributed to the error associated with the facies estimation as has been explained earlier.

WELL	R1	R2	R3	R4	R5	R6	R7	R8	R9	R10	Average	Max	Min
A	67%	65%	65%	61%	66%	66%	64%	61%	65%	60%	64%	67%	60%
B	44%	39%	38%	42%	43%	37%	41%	45%	43%	40%	41%	45%	37%
C	85%	82%	83%	84%	85%	85%	82%	86%	83%	83%	84%	86%	82%
D	54%	50%	60%	60%	53%	53%	55%	54%	55%	62%	56%	62%	50%
E	57%	59%	60%	60%	63%	57%	59%	63%	63%	60%	60%	63%	57%
F	69%	72%	69%	68%	72%	74%	71%	71%	72%	74%	71%	74%	68%
G	42%	44%	52%	43%	44%	45%	37%	52%	47%	44%	45%	52%	37%
H	38%	35%	39%	45%	44%	40%	43%	39%	38%	45%	41%	45%	35%
I	74%	73%	70%	72%	76%	71%	74%	76%	73%	75%	73%	76%	70%
J	66%	64%	66%	65%	66%	69%	69%	68%	65%	68%	67%	69%	64%

Table 4.4: Correlation coefficients between the true porosities and the simulated porosities obtained from the facies- and seismic-constrained porosity model for the ten wells

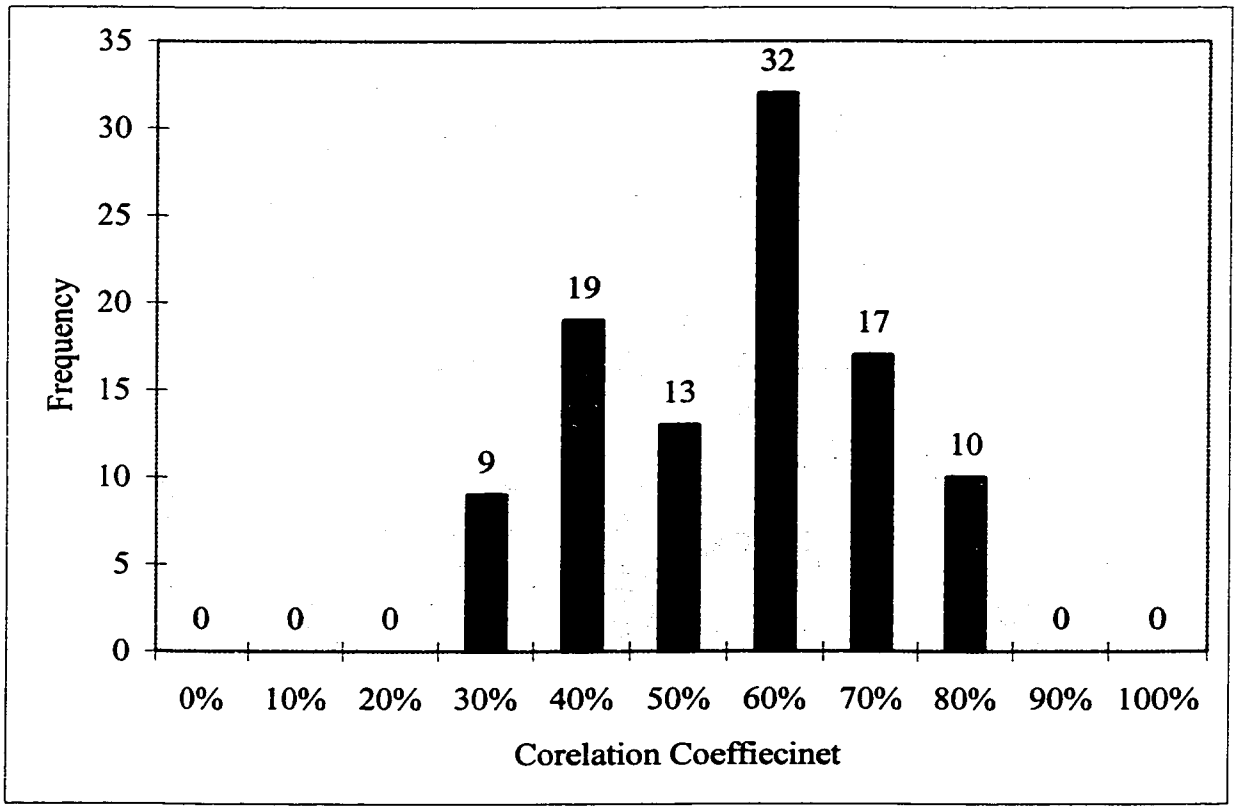

Figure 4.27 Distribution of the correlation coefficients between true and simulated porosity values obtained from the facies- and seismic-constrained model for the ten wells

CHAPTER 5

CONCLUSIONS AND RECOMENDATIONS

5.1 Summary

Statistical and spatial data analyses have been performed on the study data in order to verify data quality and look for trends. The analysis revealed that porosity distribution is closely related to depositional facies distribution for every reservoir zone. Also, there is a strong relation between porosity and seismic impedance. Facies analysis revealed that some facies could be grouped together based on the statistical analysis of geological and petrophysical properties, which would help in expediting the modeling work.

Vertical and directional grouped facies semi-variograms have been calculated for every reservoir zone. Vertical and directional porosity semi-variograms have also been calculated for every reservoir zone to be used in the modeling stage.

One facies model and four porosity models were generated using different geostatistical modeling methods. The facies model was generated by Sequential Indicator Simulation (SIS) algorithm. This facies model was used as a constraint in two porosity-modeling methods.

The first porosity model was generated by the Sequential Gaussian Simulation (sGs) algorithm using porosity logs from wells. The second model was generated by Sequential Gaussian Simulation with Collocated Cokriging (sGs_Cok) in which seismic impedance was used to condition the porosity model. The third was generated by Sequential Gaussian Simulation Facies Based (sGs_FB) where the facies model is used to condition the porosity model. The fourth was generated by Gaussian simulation with Collocated Cokriging Facies Based (sGs_ Cok _FB). This is a fully integrated model in which porosity from well logs was integrated with facies and seismic impedance. Ten realizations were generated for each porosity modeling method.

Qualitative and quantitative methods were used to validate each modeling method. The first step in the qualitative validation was to compare the histogram distribution of the simulated porosity values with that of the input data. The second step was to create model slices and cross sections to visualize the results and compare the models with each other.

In the quantitative validation step we checked model ability to predicate the porosity traces for the ten wells. These tens have not been used in the modeling steps.

Porosity traces for each well have been computed from each realization and compared to the true porosity trace. A correlation coefficient was calculated between the true and the simulated porosity trace to measure the accuracy as shown in Table 1.

WELL	sGs	sGs_Cok	sGs_FB	sGs_FB_Cok
A	63%	64%	63%	64%
B	46%	51%	45%	41%
C	82%	83%	82%	84%
D	70%	71%	71%	56%
E	77%	80%	61%	60%
F	67%	59%	72%	71%
G	62%	58%	42%	45%
H	28%	43%	32%	41%
I	80%	74%	74%	73%
J	58%	80%	66%	67%

Table 5.1: Average correlation coefficients between true porosity traces and simulated porosity traces derived from different modeling methods

The porosity models have similar porosity distribution; however, the facies based and the fully integrated porosity models showed better vertical layering than the other two models. This is due to the use of the facies model as constraint for porosity distribution. The accuracy of the seismic controlled model is better than all other models. The decrease in accuracy for facies based models is attributed to the error associated with facies estimation. Porosity from the wells only model has the lowest accuracy compared to the other models, which reinforce again the importance of using other types of data in porosity modeling.

5.2 Conclusions

Based on the modeling work and data analyses in this study, the main conclusions are as follow:

1. Statistical and spatial data analyses are an important step in modeling and sufficient time should be spent on them. The results of these analyses have a big impact on the accuracy of the model.
2. There is a strong relation between facies distribution and porosity distribution in Hanifa Reservoir in Berri Field. Reservoir zones that are dominated by grainstone rich facies tend to have high porosity and reservoir zones that are dominated by mudstones tend to have very low porosity.
3. The semi-variogram is a valuable tool in studying geological trends and carries their signature effect in the geostatistical model.
4. Spatial analyses revealed that facies and porosity in the Hanifa Reservoir are best represented by directional semi-variograms that have been calculated for every reservoir zone.
5. Integrating seismic impedance and facies data in porosity modeling will help to improve the overall model accuracy compared to the wells only porosity model.
6. The impact of data integration varies from one area to another depending on well density. Data integration will have a big impact in areas that have low sampling density.

7. Seismic impedance significantly improves the porosity model accuracy in sparse wells areas. This is because the seismic data are spatially densely sampled compared to wells.
8. Integrating facies in porosity models helps to preserve vertical and lateral reservoir heterogeneity. However, modeling facies based on well data and semi-variograms may lead to error in the facies model. This may result in decreased accuracy in the facies based porosity models. Facies maps should be used to constrain the facies model, especially in low-well control areas.
9. Comparison of simulated data with input data indicates that the modeling algorithms used were capable of reproducing the input data statistics, which increase the confidence in these algorithms.

5.3 Recommendations

Based on this study, the following are recommended:

1. Use streamline simulation methods to further study the value of data integration in modeling. The objective in using streamline is to check which model matches the best pressure and flow rate at each well. Streamline simulation methods have an advantage over the finite difference method simulator by being fast and they can handle high-resolution models. In addition to porosity models, permeability models and production data are needed to do this work.
2. Run 3-D Seismic surveys in the early field development stage when wells are widely spaced. The seismic data will help in improving the accuracy of porosity models and help in locating new wells.
3. Employ seismic impedance data, if available, to condition porosity models in future work.
4. Utilize facies maps to improve facies models in future work.

REFERENCES

Al-Salem, Ali Ahmed, 1996, Geostatistical Modeling of Arab-D Reservoir, Harmaliyah Field, Saudi Arabia, Master Thesis, KFUPM, Dhahran, Saudi Arabia, 213p.

Alsharhan, Abdulrhman S., Christopher G. Kendall, 1986, Precambrian to Jurassic Rocks of Arabian Gulf and Adjacent Areas: Their Facies, Depositional Setting, and Hydrocarbon Habitat, AAPG Bull. V-70, pp.977-1002.

Ayres, M. G., Bilal, M., Jones, R. W., Slentz, L. W., Tartir, M., Wilson, A. O., Hydrocarbon Habitat in Main Producing Areas, Saudi Arabia, AAPG Bull. V-66, pp.1-9.

Beydoun, Z. R., 1988, The Middle East: Regional Geology and Petroleum Resources, Scientific Press, U. K., 291p.

Blackbourn, Graham A., 1990, Cores and Core Logging For Geologists, Whittles Publishing Services, Caithness, U.K., 146p.

Chambers, Richard L., Zinger, Michael A., Kelly, Michael C., 1994, Constraining Geostatistical Reservoir Descriptions with 3-D Seismic Data to Reduce Uncertainty, AAPG Computer Application Geology, No. 3., pp. 143-157.

Choquette, P. W., Pray, L. C., 1970, Geologic Nomenclature and Classification of Porosity in Sedimentary Carbonate, AAPG Bull. V-54, pp.207-250.

Coombes, J., 1997, Handy Hints for Varography, Proc., AusIMM Ironmaking Resources and Reserves Conference, Perth, WA, pp.127-130.

Daly, C., Verly, G.W., 1994, Geostatistics for the Next Century, Kluwer Academic Publishers, Netherlands, pp.94-107.

Damsieth, Eivind and Omre, Henning, 1997, Geostatistical Approaches in Reservoir Evaluation, Journel of Petroleum Technology (JPT), May 1997, pp.498-501.

Edinburgh Petroleum Services Limited (EPS), 1998, Core Analysis Course notes, Dhahran, Saudi Arabia.

Fournier, F., 1995, Integration of 3D Seismic Data in Reservoir Stochastic Simulation: A Case Study, SPE Paper # 30564

Geostatistical Software Library (GSLIB), 1999, Short Course Notes, Stanford University, Stanford, CA, USA.

Goovaerts, Pierr, 1997, Geostatistics for Natural Resources Evaluation, Oxford University Press, New York, NY, USA, 483p.

Isaaks, E. and Srivastava, R., 1989, An Introduction to Applied Geostatistics, Oxford University Press, New York, NY, USA, 561p.

Journel, A.G. and Huijbregts, Ch. J., 1978, Mining Geostatistics, Academic Press, San Diego, CA, USA, 600p.

_____, 1994, Geostatistics and Reservoir Geology. AAPG Computer Application Geology, No. 3., pp.19-20.

Al-Khalifa, M. A., Makkawi, M., 2001, Reflection of Geology on Geostatistical Models: A Case Study, The First Saudi Science Collages Conference, paper# ES-1

Kompanick, G.S., Heil, R.J, Al-Shammari, Z.A. and Al-Shammery, M.J., 1993, Geological Modeling for Reservoir Simulation: Hanifa Reservoir, Berri Field, Saudi Arabia, SPE paper #25580.

McGuire, M.D., Kompanick, R.B., Markello, J. R., Stockton, M. L., Waite, L.E., Kompanik, G.S., Al-Shammery, M.J. and Al-Amoudi, M. O., 1993, Importance of Sequence Stratigraphic Concepts in Development of Reservoir Architecture in Upper Jurassic Grainstones, Hadriya and Hanifa Reservoirs, Saudi Arabia, SPE paper #25578.

Saudi Aramco, 1990, Jurassic Field Trip, Saudi Aramco short course notes.

_____, 1991, Integrated descriptions of the Hadriya and Hanifa reservoir, Berri Field, Saudi Arabia, unpublished Saudi Aramco Commissioned report, Mobil Research and Development Corporation and Mobil Exploration and Producing Services Inc.

_____, 2000, Hanifa Reservoir Modeling Project, Berri Field, Saudi Arabia, unpublished Saudi Aramco report.

Schlumberger, 1989, Log Interpretation Principles/Applications, Schlumberger Educational Services, Houston, TX, USA, pp. 155.

Selley, Richard C., 1985, Elements of Petroleum Geology, W. H. Freeman and Company, N.Y, USA, pp. 449

Stoneley, R., The Middle East Basin: a Summary Overview, Classic Petroleum Provinces, Geological Society Special Publication No. 50, pp. 293-298.

Al-Qassab, H. M, Fitzmaurice, J., Al-Ali, Z. A., Al-Khalifa, M. A., Aktas, G. A., Glover, P. W., 2000, Cross-Discipline Integration in Reservoir Modeling: The Impact on Fluid Flow Simulation and Reservoir Management, SPE paper# 62902.

Western Atlas, 1992, Introduction to Wireline Log Analysis, Western Atlas International, Inc., Houston, TX, USA, 312p.

Whittaker, Alun (Editor), 1985, Coring Operations, IHRDC, Publishers, Boston, MA, USA, 122p.

Wolf, D. J., Withers, K. D. and Burnaman, M. D., 1994, Integration of Well and Seismic Data Using Geostatistics. AAPG Computer Application Geology, No. 3, pp. 177-198.

Vejbaek, O. V and Rasmussen, K. B., 1996, Geostatistical Reservoir Characterization Using Inverted Seismic Data: Application to a Chalk Reservoir, Dan Field, Denmark, SPE paper# 35486.

Xu, Weanling, Tarn, T. T. Srivastava, R. M and Journel, A. G., 1992, Integrating Seismic Data in Reservoir Modeling: The Collocated Cokriging Alternative, SPE Paper # 24742.

APPENDICES

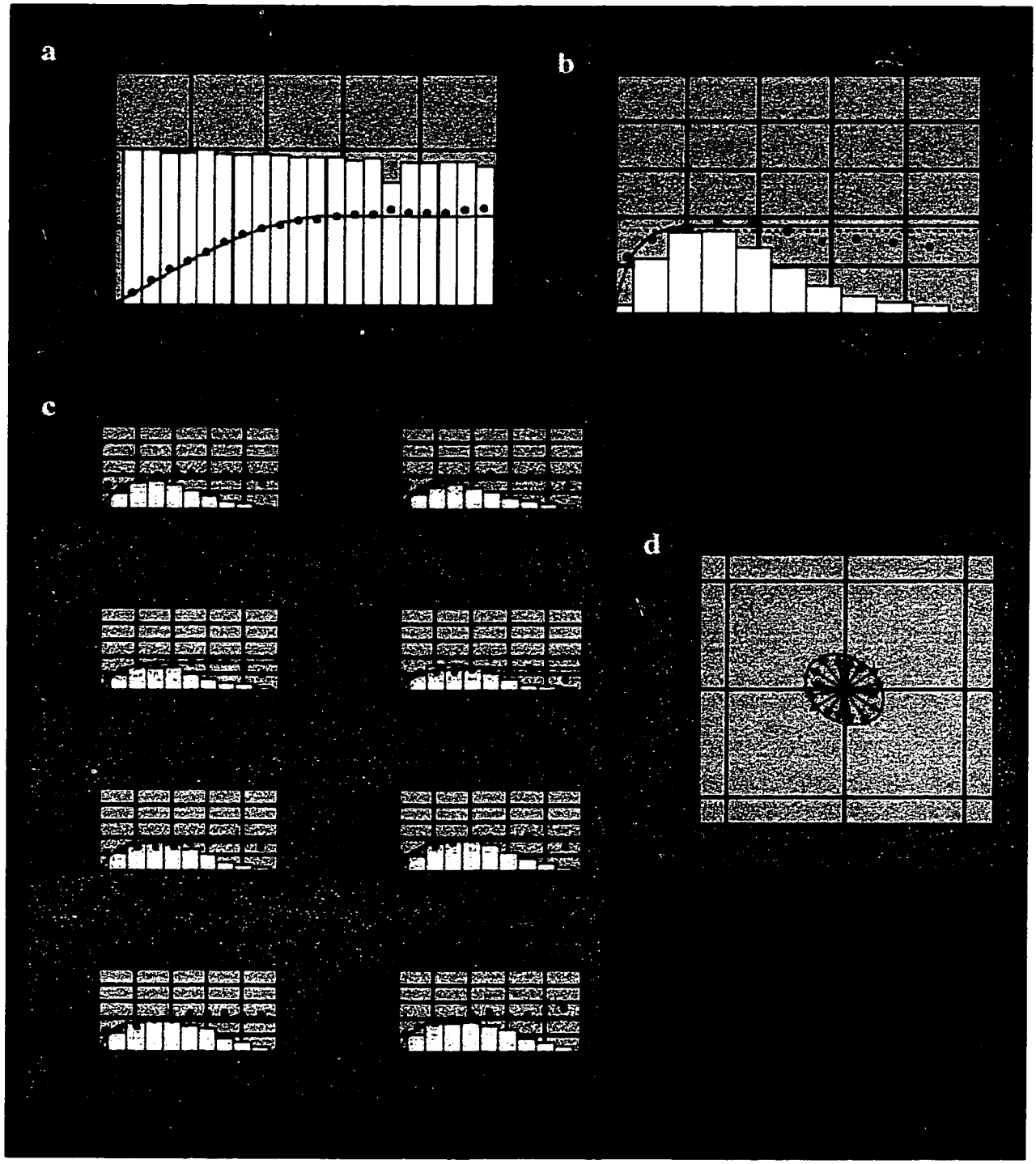

Figure A.1: Example for semi-variograms calculated for facies group 3, a-vertical, b-omnidirectional, c and d directional semi-variogram.

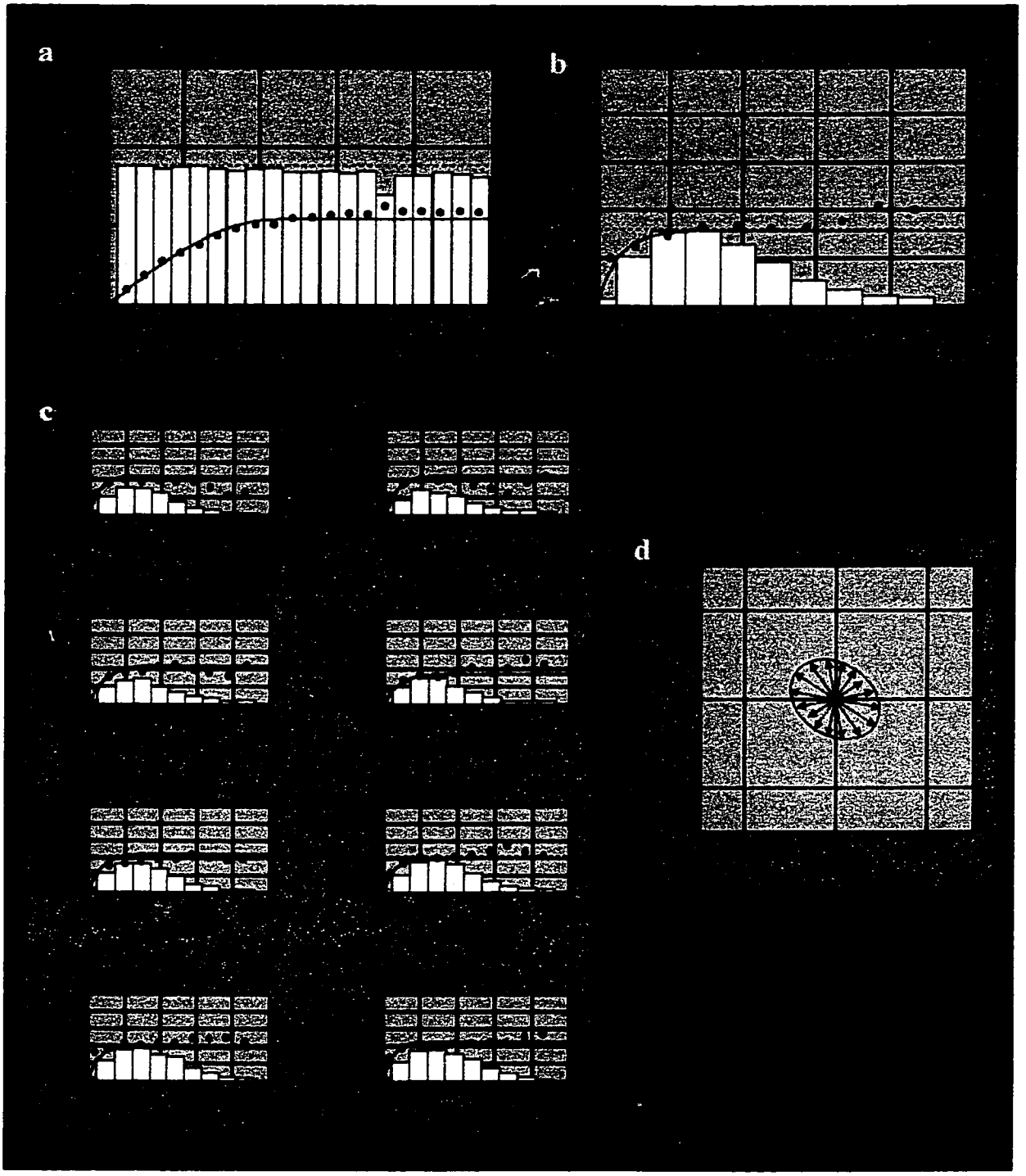

Figure A.2: Example for semi-variograms calculated for facies group 5, a-vertical, b-omnidirectional, c and d directional semi-variogram.

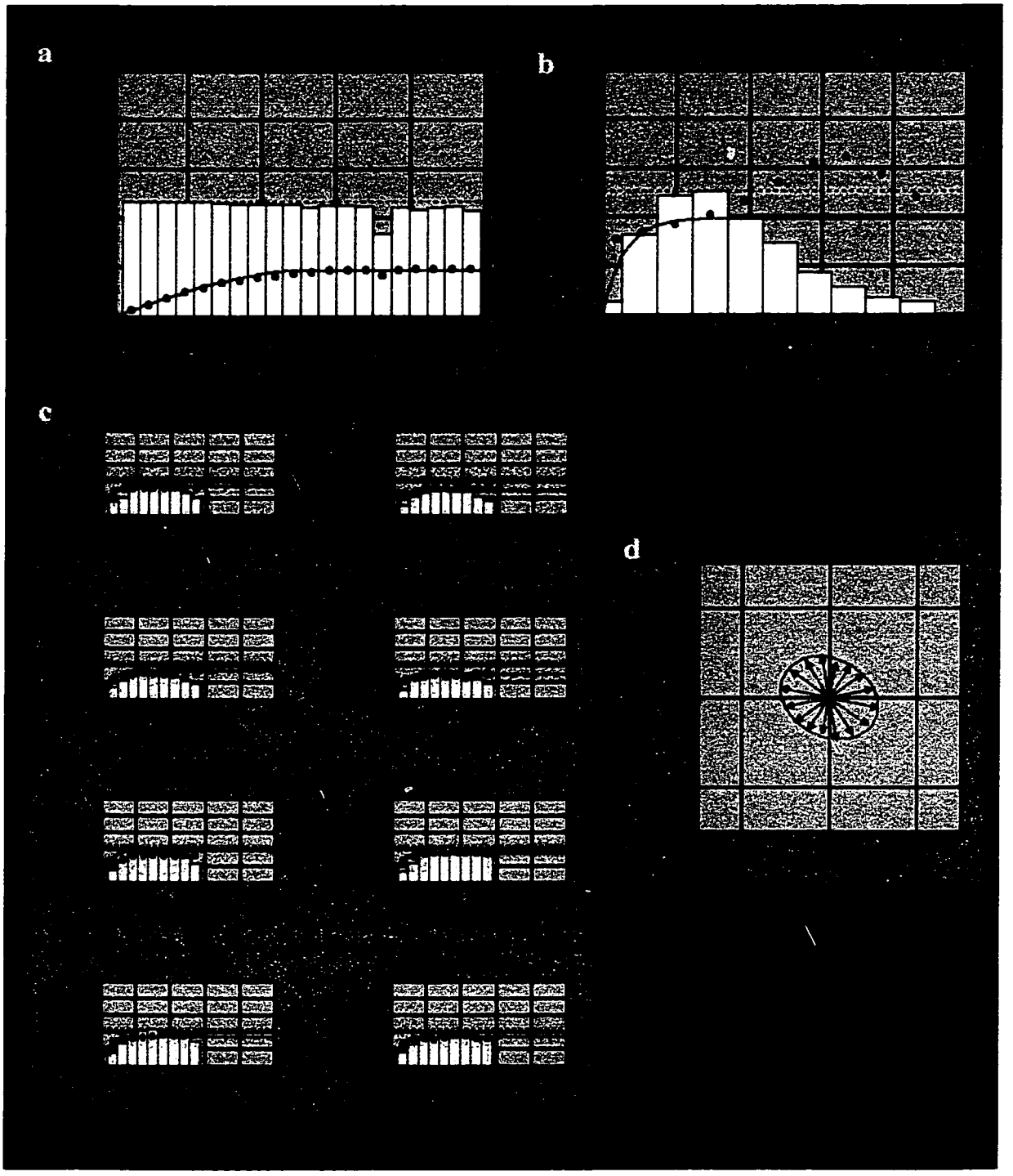

Figure A.3: Example for semi-variograms calculated for facies group 6, a-vertical, b-omnidirectional, c and d directional semi-variogram.

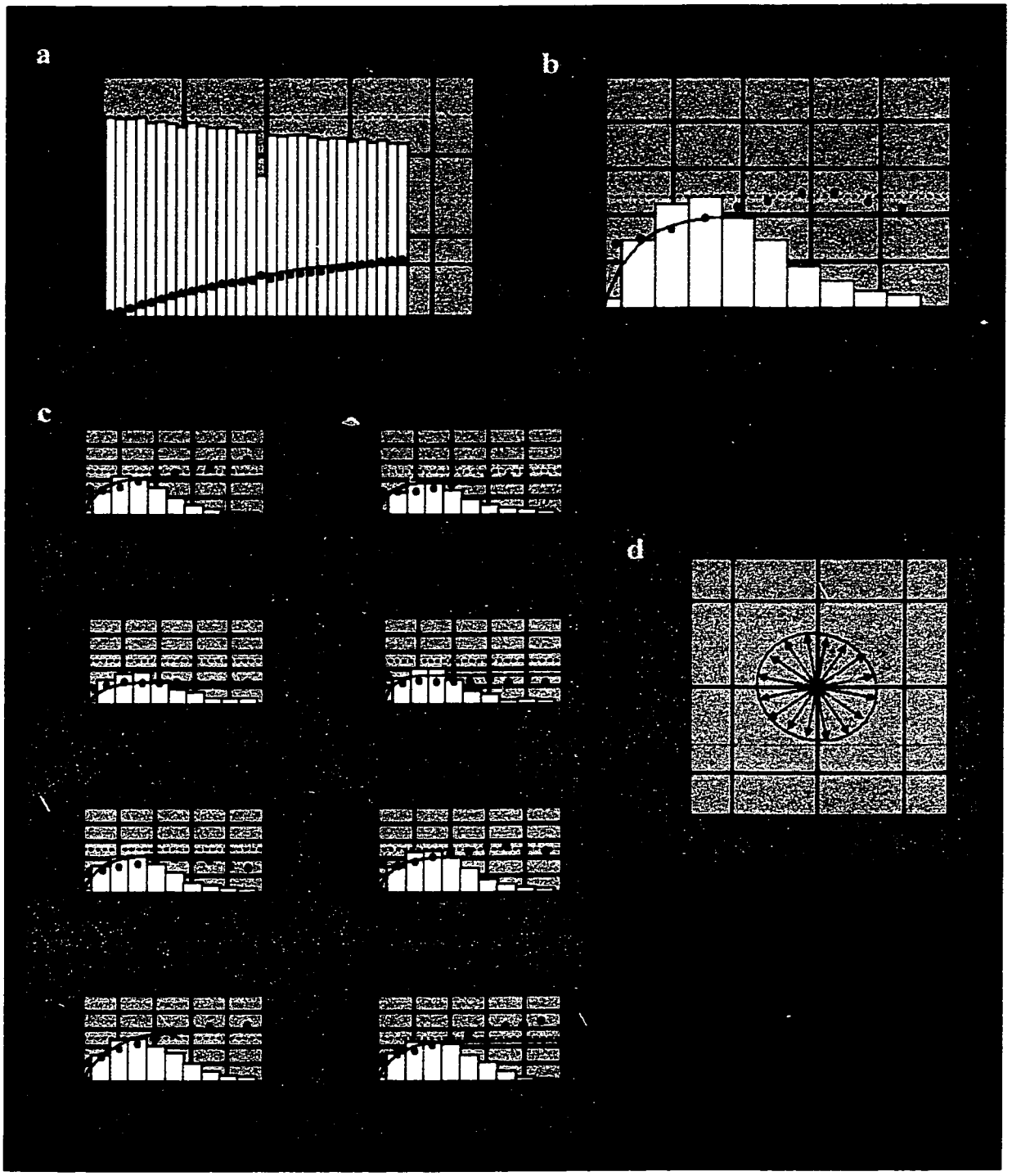

Figure A.4: Example for semi-variograms calculated for facies group 7, a-vertical, b-omnidirectional, c and d directional semi-variogram.

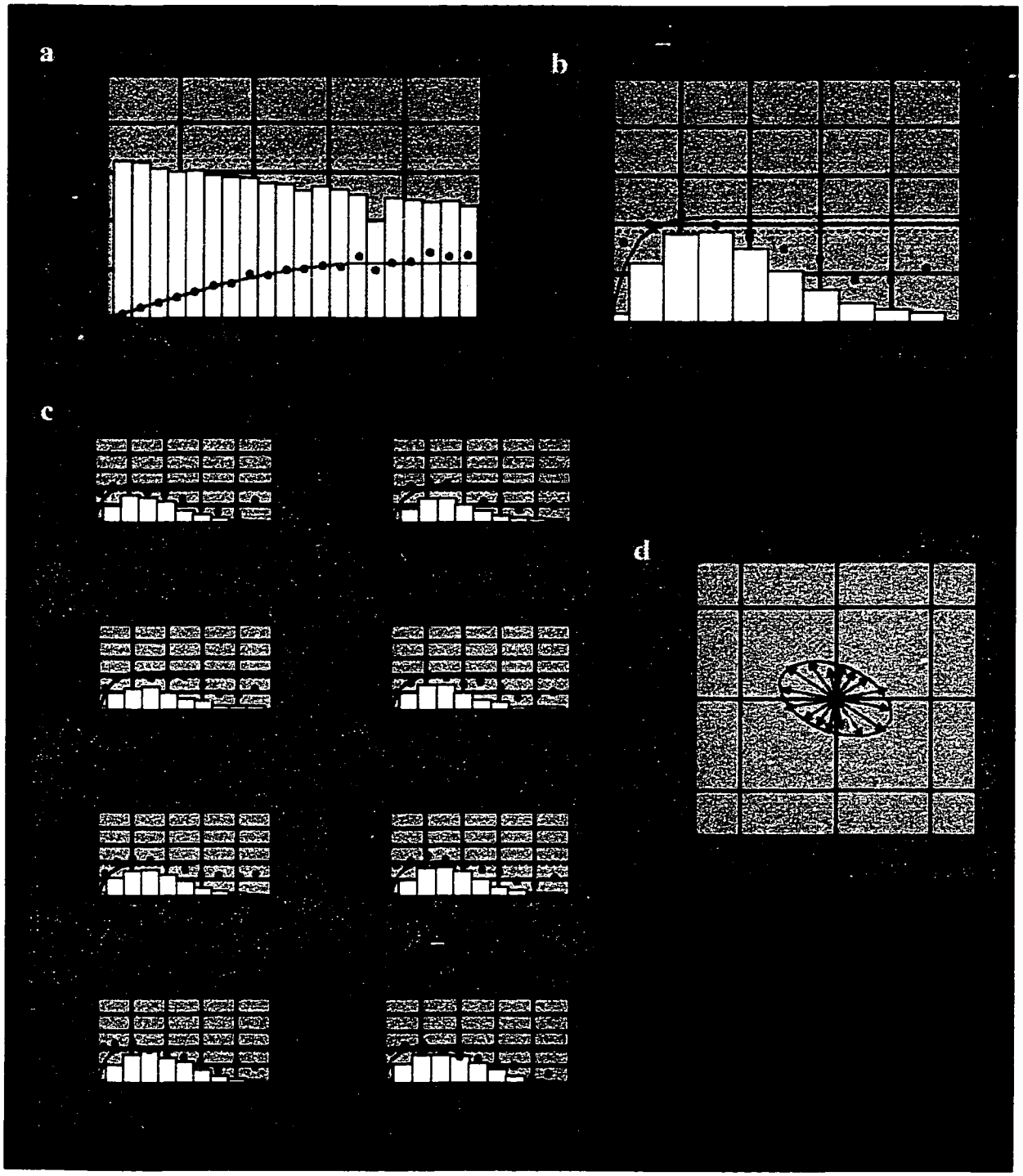

Figure A.5: Example for semi-variograms calculated for facies group 8, a-vertical, b-omnidirectional, c and d directional semi-variogram